

# **A CONTRIBUTION OF PRESSURE CONTROL AND ESTIMATION IN MINIMALLY INVASIVE SURGERY**

Dissertation to  
obtain the academic degree of Doctor of Engineering (Dr.-Ing.)

from the Faculty of Computer Science and Electrical Engineering  
at the University of Rostock

Submitted by:  
M.Eng. **Van Muot Nguyen**, born on 05-Jan-1975, in Dong Thap  
from Vietnam

**Rostock, 20.12.2019**



Dieses Werk ist lizenziert unter einer  
Creative Commons Namensnennung 4.0 International Lizenz.

### **Reviewers:**

Prof. Dr.-Ing. Torsten Jeinsch, University of Rostock, Faculty of Computer Science and  
Electrical Engineering, Institute of Automation.

Prof. Dr.-Ing. habil. Ping Zhang, Technical University of Kaiserslautern, Faculty of  
Electrical and Computer Engineering.

Prof. Dr.-Ing. habil. Olaf Simanski, Hochschule Wismar - University of Applied Sciences  
Technology, Faculty of Electrical Engineering and  
Computer Science.

**Date of submission:** 20.12.2019

**Date of defense:** 30.03.2020

## KURZFASSUNG

Die minimal-invasive Chirurgie spielt heute eine wichtige Rolle in nahezu allen medizinischen Bereichen. Sie ist als moderne Operationstechnik bekannt, die für den Patienten im Vergleich zu herkömmlichen Operationsmethoden wesentlich angenehmer ist. Trokare werden durch kleinste Einschnitte in den Körper eingeführt, um spezielle chirurgische Instrumente, faseroptische Systeme und unterstützende Instrumente im Operationsbereich für Visualisierung, Diagnose, Therapie und Reinigung zu applizieren. Diese Dissertation befasst sich mit der Interaktion zwischen einem Hardware-in-the-Loop-Simulator (HIL-Simulator) und dem applizierten Instrument, wobei eine Strategie zur Druckschätzung und -regelung mittels der Spülflüssigkeitsströme während der MIS entwickelt wurde.

Arthroskopie ist eine spezielle Applikation von MIS, bei dem Kochsalzlösung als Spülflüssigkeit im Operationsbereich verwendet wird. Die Phase der Verifikation und des Regelungsdesigns konnte aus Sicherheitsgründen nicht am realen Patienten vorgenommen werden, weshalb zunächst ein HIL-Simulator als Patientenmodell konzeptioniert werden musste. Der Simulator muss in geeigneter Weise die Druckausdehnung in einem geschlossenen Bereich durch die Regelung der Flüssigkeitsströme darstellen. Bei der Arthroskopie wird die Spülflüssigkeit auch verwendet, um den Operationsbereich zu reinigen und damit dem Chirurgen über den Monitor eine gute Sicht zu bieten. Bei zuviel Flüssigkeit und damit Überdehnung des Gewebes kann es jedoch zu einer Gefährdung angrenzender Körperareale kommen. Ist der Druck für die Flächenexpansion niedriger als der Blutdruck, kommt es zu Blutungen. Daher ist es notwendig, die Spülflüssigkeitsströme zu regeln, um den Druck im Operationsbereich stabil auf dem Zielwert zu halten. Dieser Zieldruck hängt vom individuellen Blutdruck eines Patienten ab. In dieser Arbeit wurde das System der MIS mit einem physikalischen Modell des Kniegelenks im HIL-Simulator für Echtzeit-Experimente zur Kniearthroskopie simuliert. Sogenannte Doppelrollenpumpen (DRP) wurden verwendet, um die Spülflüssigkeiten ein- und abzuleiten. Über Gleichstrommotoren wurde der Fluss in das bzw. aus dem Operationsfeld reguliert. Der Abfluss kann bei Bedarf von dem Chirurgen angepasst werden. Der Druck des Flüssigkeitszuflusses wurde im Kniegelenkmodell automatisch in Relation zum Abfluss geregelt.

Für die Strategie der Druckregelung und -überwachung wurde ein Proportional-Integral-Regler (PI-Regler) entwickelt, der auf der Methode des symmetrischen Optimums (SO) basiert. Bei der Implementierung des nichtlinearen Prozesses der Kniearthroskopie wurde das Anti-Windup

berücksichtigt. Darüber hinaus wurde ein Überwachungsalgorithmus entwickelt, um unerwünschter Druckstörungen durch die Kniebeugung zu vermeiden.

Für die Druckschätzung im Kniemodell während der MIS wurden drei Arten von Beobachtern für die Druckzustandsschätzung untersucht: der Luenberger Observer, der klassische Kalman-Filter und der erweiterte Kalman-Filter. Der geschätzte Druckzustand spielte eine Schlüsselrolle für die Druckregelung im Operationsbereich ohne direkte Messung.

Aus den Ergebnissen der Modellierung sowie den Echtzeit-Simulations-Experimenten ging hervor, dass Regler und Supervisor auch bei Störungen stabil arbeiten. In einem Vergleich der Schätzergebnisse der drei Beobachter erwies sich der erweiterte Kalman-Filter als am besten geeignet. Dessen geschätzter Druckzustand wurde erfolgreich in der Regelung des nichtlinearen MIS-Systems appliziert.

## ABSTRACT

Companioning with the development of science and technology, the minimally invasive surgery (MIS) has taken today an important role in all medical fields. It is known as a modernized surgical technique that offers patients more convenience compared to traditional surgical methods. By using trocars and specialized instruments through small incisions into the body, the injured area can be diagnosed and treated effectively. In arthroscopy, rinsing fluid is used for visualization and expansion of the operational area. During the stage of verification and control design, the investigation with real patients is not allowed for safety reasons. Therefore, the aim of this research is to implement a suitable hardware-in-the-loop (HIL) simulator to develop a controller for the pressure expansion within a closed surgical area by controlling the flows of rinsing fluid. Methods of pressure estimation were proposed as an alternative to pressure sensor usage.

The HIL-Simulator is imitating some physiological states during MIS. Particular in the knee arthroscopy, the pressure in the knee joint model was realized via actuators and physical interface. Double roller pump (DRP) was used as a medical therapy device to control the pressure in the surgical area by the flow of the rinsing fluid, which offers both a suitable expansion and a clear visibility monitored on the screen. In case of over-expansion of the surgical area, it can be risk to adjacent tissue areas if the fluid flows into the tissues or blood vessels. Otherwise, when the pressure is lower than the actual blood pressure, hemorrhages can occur. Therefore, it is necessary to control the flows of rinsing fluid in order to keep pressure in the surgical area stable within the desired value. This desired pressure depends on the individual blood pressure of each patient. In this thesis, the system of MIS was simulated with a physical model of the knee joint in the HIL-Simulator for real-time experiments of the knee arthroscopy. One DRP each together with a DC motor was used for the flow into and out of the operation field. Additionally, the outflow could be adjusted by a surgeon whenever needed. The inflow of fluid was controlled for the desired pressure in the knee joint model automatically regarding the outflow.

For the strategy of pressure controlling and supervising, proportional-integral controller (PI controller) was designed based on the symmetric optimum (SO) method. During the implementation of this nonlinear process of knee arthroscopy, the appearance of the wind-up phenomenon was also paid attention to deal with the anti-wind-up algorithm. In addition, to avoid some situations of unwanted pressure disturbances from the knee flexions, a supervisory algorithm was also designed in order to monitor and eliminate these cases of pressure disturbances.

For the solution of pressure estimation in the knee model during MIS, some observer methods were applied. Because the controlled pressure in the operational region is not allowed to measure directly to the real patient due to some reasons such as the risks to the patient, the high cost of the pressure sensor and so on. Therefore the research was performed with three types of observers for the pressure state estimation. Those are Luenberger observer, basic Kalman filter, and extended Kalman filter. The estimated pressure state in the surgical area played a key role in providing feedback data to the controller of the system.

From the results in modelling as well as in real-time simulator experiments, it indicated that the designed controller and supervisor worked stably within cases of disturbances. Furthermore, by comparing the estimate results among the three cases of observers, the best estimate state of pressure from the extended Kalman filter was interconnected successfully to the controller for the replacement of the feedback pressure sensor of the nonlinear controlled system of MIS.

## ACKNOWLEDGEMENTS

During my research time here at the Institute of Automation, Faculty of Computer Science and Electrical Engineering, University of Rostock, I have got lots of precious and helpful supports from many people that I might not express to all from my poor words.

Firstly, I would like to express special thanks to my advisor, Prof. Dr.-Ing. Torsten Jeinsch for his valuable advice and powerful supports on my study. I am greatly thankful to Dr.-Ing. Wolfgang Drewelow for the open-minded and generous guidances from his experience and knowledge. I am also deeply grateful to the memorial professor Dr. rer. nat. Dr.-Ing. habil. Dr. h. c. Bernhard Lampe who gave me the first steps and his worthy guide from my starting time of research. Many truthful thanks send to M.Sc. Alexander Benkmann and M.Sc. Eike Christian Smolinski for their supports and useful discussions on experience and knowledge. I would also like to thank Frau. Dr.-Ing. Agnes Schubert, Dr.-Ing Björn Kolewe, M.Sc Alexander Schöley, Dipl.-Ing. Martin Kurowski, Frau Julia Lau and all friendly staffs at the Institute of Automation, Faculty of Computer Science and Electrical Engineering, University of Rostock for help me and providing useful information.

Secondly, I would like to present my great gratefulness to Prof. Dr. Nguyen Chi Ngon, Dr. Vo Minh Tri, and M.Sc Doan Hoa Minh for all their enthusiastic supports to my study. My sincere gratitude is sent to all my colleagues at the Department of Automation technology, college of Engineering Technology, Can Tho University for the helps and encouragements. And surely, I want to send my thankfulness to the Ministry of Education and Training, International Cooperation Department in Vietnam as well as the organization of Deutscher Akademische Austauschdienst (DAAD), and AFluCoMIS project (numbered 13GW0164B and managed by the Project Management Agency VDI Technologiezentrum GmbH) in Germany for financial supports to my study.

Additionally, my honest acknowledgment comes to Dr. Nguyen Thanh Lich, Dr. Phung Van Trang, and all of my friends who have given interesting ideas and useful discussions; especially thanks to Dr. Do Vinh Quang who has helped and encouraged me so much since the early days arriving to Rostock.

Last but not least, I want to say my great thanks to my lovely family, especially to my wife Nguyen Thi Bich Thuyen and my son Nguyen Phuoc Vinh for all their faithful loves and honest encouragements to me. Their everlasting loves always give me more energy and motivation to complete my work of research here at the University of Rostock.





# TABLE OF CONTENTS

KURZFASSUNG .....	iii
ABSTRACT.....	v
ACKNOWLEDGEMENTS.....	vii
TABLE OF CONTENTS.....	ix
NOMENCLATURE .....	xiii
1 INTRODUCTION .....	1
1.1 State of the art .....	1
1.2 Motivation.....	3
1.3 Objectives .....	5
1.4 Materials .....	7
1.5 Outline of the thesis .....	9
2 OVERVIEW AND MODELLING OF THE MIS SYSTEM.....	11
2.1 Introduction.....	11
2.2 System overview of Minimally invasive surgery .....	12
2.3 Modelling of the process in MIS .....	14
2.3.1 Modelling of the motors .....	15
2.3.2 Modelling of the double roller pump.....	17
2.3.3 Modelling of the tubes .....	19
2.3.4 Modelling of the operation area.....	22
2.3.5 Influence of turbulent flow to the pressure change in the tubes .....	24
2.3.6 Modelling of disturbances from the knee angle changes.....	26
2.3.7 State space presentation of the knee model .....	28
2.4 Hardware interfaces in MIS .....	31
2.4.1 Input/Output hardware interface as a target computer.....	31
2.4.2 Hardware-in-the-Loop simulator .....	33

2.5 Summary .....	39
3 CONTROLLER DESIGN AND SUPERVISOR STRATEGY.....	41
3.1 Introduction.....	41
3.2 PI controller based on Symmetric Optimum method.....	42
3.2.1 Analytical case of $37^\circ$ in phase margin.....	47
3.2.2 Analytical case of $60^\circ$ in phase margin.....	48
3.2.3 Analytical case of $78^\circ$ in phase margin.....	49
3.3 Anti-windup algorithm in PI controller .....	52
3.3.1 Conditional integration .....	52
3.3.2 Anti-windup tracking by the integrating time.....	53
3.3.3 Back-calculation and tracking by the time constant .....	53
3.4 Inner disturbance controller for the changes of the knee flexion.....	54
3.4.1 Using separate PI_SO controller for the inner disturbance elimination .....	54
3.4.2 Using empirical Proportional controller .....	55
3.5 Simulation results of pressure control.....	55
3.5.1 Simulation results of controller without supervisor.....	56
3.5.2 Simulation results of controller with the supervisor of the knee flexion disturbances ....	56
3.6 Real-time device simulator results .....	57
3.6.1 Experimental results of controller without supervisor.....	58
3.6.2 Experimental results of controller with supervisor of the knee flexions .....	58
3.7 Summary .....	59
4 PRESSURE ESTIMATION IN MINIMALLY INVASIVE SURGERY .....	61
4.1 Introduction.....	61
4.2 Observer methods for pressure estimation in MIS.....	63
4.2.1 Luenberger observer .....	63
4.2.2 Basic Kalman filter .....	66
4.2.3 Extended Kalman filter .....	73
4.3 Simulation results.....	75
4.3.1 Simulation results with Luenberger observer .....	76

4.3.2 Simulation results with basic Kalman filter.....	78
4.3.3 Simulation results with extended Kalman filter .....	79
4.3.4 Simulation results with combined state estimator .....	82
4.4 Real-time simulator results .....	83
4.4.1 Real-time results with Luenberger observer .....	83
4.4.2 Real-time results with basic Kalman filter .....	84
4.4.3 Real-time results with extended Kalman filter .....	85
4.4.4 Real-time result in combination of the estimate state to the controlled process.....	86
4.5 Discussion of estimate methods.....	86
4.6 Summary .....	87
5 CONCLUSIONS AND FURTHER WORK .....	89
5.1 Conclusions.....	89
5.2 Further work .....	90
APPENDIX A.....	93
A.1 Results of controller design in simulation .....	93
A.1.1 Simulation of pressure control without disturbances.....	93
A.1.2 Simulation with supervisory algorithm of the knee flexion disturbances.....	95
A.2 Experimental results of controller design in real-time device simulator .....	98
A.2.1 Experimental results of controller without supervisor of disturbances .....	98
A.2.2 Experimental results of supervised controller with the knee flexion disturbances.....	101
LIST OF FIGURES .....	105
LIST OF TABLES.....	109
REFERENCES .....	111
THESES.....	117
LIST OF PUBLICATIONS .....	119
BIOGRAPHY .....	121
DECLARATION.....	123



# NOMENCLATURE

## Abbreviations

ADC	<u>A</u> nalog to <u>d</u> igital <u>c</u> onverter
BNC	<u>B</u> ayonet <u>N</u> eill- <u>C</u> oncelman connector
BP	<u>B</u> lood <u>p</u> ressure
CAN	<u>C</u> ontroller <u>A</u> rea <u>N</u> etwork
CO <sub>2</sub>	<u>C</u> arbon <u>d</u> ioxide
DAC	<u>D</u> igital to <u>a</u> nalog <u>c</u> onverter
DRP	<u>D</u> ouble <u>r</u> oller <u>p</u> ump
D-sub	<u>D</u> - <u>S</u> ubminiature (D denotes the shell size of the connector)
FPGA	<u>F</u> ield- <u>p</u> rogrammable gate <u>a</u> rray
GM	<u>G</u> ain <u>m</u> argin
HIL	<u>H</u> ardware- <u>i</u> n-the- <u>L</u> oop
I/O	<u>I</u> nput / <u>O</u> utput
MIS	<u>M</u> inimally <u>i</u> nvasive <u>s</u> urgery
OA	<u>O</u> peration <u>a</u> rea
PC	<u>P</u> ersonal <u>c</u> omputer
PM	<u>P</u> hase <u>m</u> argin
PI_SO	<u>P</u> roportional- <u>I</u> ntegrated controller based on <u>S</u> ymmetric <u>O</u> ptimum
RTI	<u>R</u> eal- <u>t</u> ime <u>i</u> nterface
SASP	<u>S</u> ub <u>a</u> cromial <u>s</u> pace <u>p</u> ressure
SBP	<u>S</u> ystolic <u>b</u> lood <u>p</u> ressure
USB	<u>U</u> niversal <u>s</u> erial <u>b</u> us
W.O.M	<u>W</u> orld <u>o</u> f <u>M</u> edicine GmbH

## Denotations

<i>Symbol</i>	<i>Meaning</i>
$d$	Disturbance signal
$e, p_e$	Error signal, pressure error
$u, \Delta u$	Control signals
$ref$	Reference signal
$p_{ref}, p_{knee}, p_{hil}$	Reference pressure, pressure of the knee, pressure of the HIL-simulator
$x, \hat{x}, \hat{p}_{knee}$	State variable vector, estimated state vector, estimated pressure variable
$y, \hat{y}, \hat{p}_1$	Output signal, observed state/signal, observed pressure variable
$\dot{x}$	First order differential expression of the state vector $x$
$M1, M2$	Motor 1, Motor 2
$u_1, u_2$	Signals to the motors M1, M2 (in voltage)
$n_1, n_2$	Rotational speeds of the motors M1, M2 (in revolutions per second)
$p_0, p_a$	Ambient pressure
$p_{ac}$	Pressure from the accumulator of the air compressor
$p_1, p_2$	Pressure at the pump1, pressure at the pump2 of the DRP
$Q_{p1}, Q_{p2}$	Flow of fluid at the pump1, flow of fluid at the pump2
$Q_{in}, Q_{out}$	Flow of fluid into the operation area, flow of fluid out of the operation area
$Q_{sum}$	Difference of flows between the inflow and the outflow
$Q_{err}$	Error of total flow lost in the operation area
$Q_{dep}, Q_{hae}$	Flow of fluid depletion, flow of haemorrhage in the operation area
$\Delta Q_1, \Delta Q_2$	Error of flow between $Q_{p1}$ and $Q_{in}$ , error of flow between $Q_{out}$ and $Q_{p2}$
$R_1, R_2, Re$	Static resistances of the flow in tube1, in tube2, Reynolds number
$R_c, R_{air}$	Gas constant, air constant
$T_c, T_{air}$	Gas temperature, air temperature
$\Delta p_1, \Delta p_2$	Error of pressure between $p_1$ and $p_{knee}$ , error of pressure between $p_{knee}$ and $p_2$
$f(), g()$	Representation of the nonlinear functions
$A, B, C, D$	Matrices used in state space expressions
$C_{tube}$	Capacity of the tube for transferring fluid
$C_{knee}$	Capacity of the knee model
$T_d, \tau$	Dead time, delay time
$T_M, K_M$	Time constant, static gain of the motor M
$V_f, V_{gas}, V_{air}$	Volume of fluid, volume of gas, volume of air
$V_{pd}, V_{pipe}$	Volume of the piston drive, volume of the pipe between piston and reservoir

<i>Symbol</i>	<i>Meaning</i>
$m, m_{\text{gas}}, m_{\text{air}}$	mass of gas, mass of air
$K$	Gain constant of the linearized process
$Q_{lp}$	Flow of the liquid pump actuator
$F_m, F_p$	driving force on the piston, acting force on the piston of the air pump
$A_p$	piston surface
$U_m$	Voltage to the motor drive of the air pump
$U_v, u_{val} (u_{\text{valve}})$	Voltage signal to the bidirectional controllable electric valve
$\alpha$	Rotation factor of the piston motor,
$k_{\text{pitch}}$	Spindle pitch of the piston
$a_1$	Proportional factor
$A_a, b_a, c_a$	Flow cross-section, critical pressure ratio, pneumatic conductance of the valve
$A_{\text{max}}$	Maximum opened cross-section of the valve
$p_{v1}, p_{v2}$	Pressure before and behind the valve
$K_P, K_I, K_D$	Proportional gain, integral gain, derivative gain
$T_I (T_N), T_D$	Integral time, derivative time
$\omega_n (\omega_0), \omega_c$	Undamped natural frequency, crossover frequency
$\zeta, \zeta, \xi$	Damping ratio, damping coefficient, damping factor
$V_i$	Fluid velocity
$\lambda_f, k_s$	Friction factor, roughness factor
$\rho$	Density of fluid
$\beta$	Flow resistance
$\psi$	Dynamic element of wave-induced motion
$\phi_R$	Phase margin
$\epsilon$	Noise signal from the process
$v$	Noise signal from the output measurement
$vI$	Additional factor from the computed Kalman gain
$L, K_e, K_k$	Symbols of the observer gain vectors
$Q$	Process noise covariance matrix
$R$	Measurement noise covariance matrix
$P, P_k$	State variables covariance matrix
$\lambda$	Eigenvalue of characteristics equation
$\lambda^*$	Eigenvalue of desired characteristics equation





# 1 INTRODUCTION

This chapter presents a general introduction of the research including the state of the art and existing problems for the motivation. Additionally, it is focused on the objectives of the thesis in general ideas. Some materials and methods are summarized with the concepts and the needs for solving problems. And the outline of the thesis is figured out briefly by the end of the chapter.

## 1.1 State of the art

The development of modern medicine technology has become more important to the patient's healthcare and diagnostic. It has been continuously improved to a higher standard of a clinical expertise not only in developed countries [1] but also in developing countries. Minimally invasive surgery (MIS) is an advanced surgical technique which has been applied widely to most of nations. By using specialized instruments in operation with small incisions, the process of MIS offers many benefits compared to traditional open surgery method. Indeed, the trauma is reduced and therefore the wounds are healed faster during a short time of post-operative care (short recovery time). In addition, the risk of infections shall be minimized by using MIS.

Beside many of other important procedures during MIS, a crucial role which can not be ignored is to remain visualization with a clear working space in the closed operation area (OA). This can be performed by the support of medical therapy device for keeping a suitable expansion inside the surgical area. Depending on the area of the operation to be cured or diagnosed, an expansion can be maintained by insufflating gas (CO<sub>2</sub>, Helium) or flushing fluid through the tubes into the OA. From the citations [2], [3], [4], in laparoscopy cases for example with the abdomen or the uterus, gas is used to insufflate into the OA. On the other hand, in the cases of arthroscopy, rinsing fluid is used for flushing in the areas like the knee joint, shoulder, ankle, hip, wrist, or elbow [5], [6], [7], [8]. The main purpose is that a certain amount of gas or rinsing fluid needs to be controlled getting into the surgical area in order to remain a suitable pressure for the expansion and visibility during MIS.

Arthroscopy is a kind of minimally invasive surgery which is used for the joints. A tiny camera with a fiber optic cable is inserted via a trocar through a small incision for imaging. Other specialized instruments are placed through other small incisions to evaluate and repair the injured joint area [9]. Figure 1.1 is an overview of the knee arthroscopy [10]. For a clear vision to the camera, the surgical area needs to be obtained as a clear space.

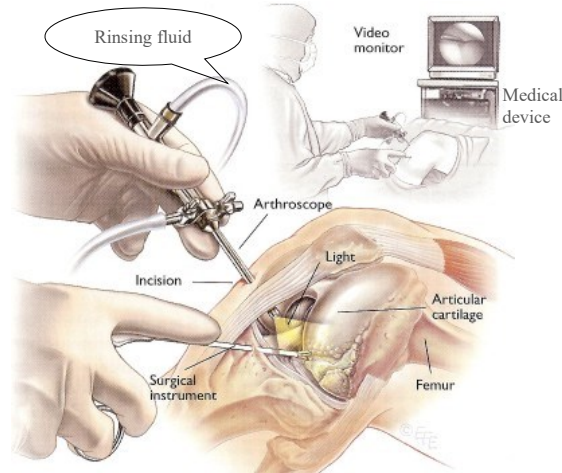


*Fig. 1.1 An overview of the knee arthroscopy [10]*

In arthroscopy, there are some existing methods to control the rinsing fluid for the visibility and expansion. According to the authors from [5] and [6], methods of gravity flow systems and pump systems have been commonly used since the middle of 20<sup>th</sup> century. Via the control of rinsing fluid flows, the pressure in the operation area could be controlled for an appropriate expansion.

Firstly, gravity flow method was used with a fluid bag positioned at a higher elevation than the surgical area for the fluid insufflation (see in Fig. 1.2). The inflow as well as the outflow of fluid could be adjusted manually. This simple method is based mostly on the Earth gravity to create the pressure to the fluid flow.

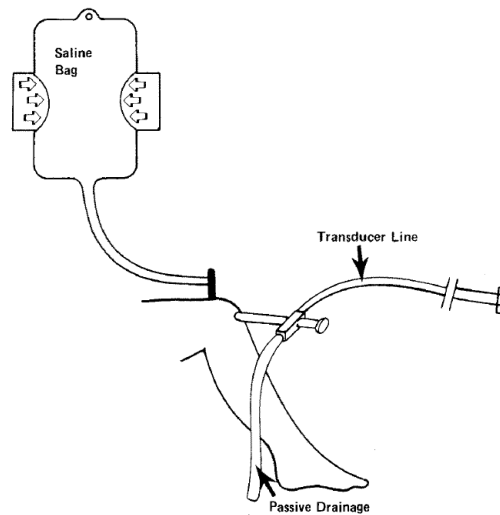


*Fig. 1.2 A simple schematic representation of the knee arthroscopy [11]*

Secondly, some methods of automated pump systems have been used and developed since the 1970s [5]. As another option from method of gravity flow, the usage of the pump systems has two

stages in the development progress. Initially on the first stage, by utilizing the single pump systems, the pressure in the operation area was maintained by controlling the inflow only. Then on the second stage, the automated pump systems were developed to remain the pressure by controlling the inflow and the outflow. But the inflow was controlled independently to the outflow. Furthermore, another investigation from [12] showed the comparison of pressure control alone versus pressure and flow control (but separately) for the visibility. The results proved that using the pumps which separately control the pressure and the flow gave a better visualization than the case of only pressure control. However, those methods might still exist some error or slow response of pressure compared to the desired value. Therefore, the usage of medical device called double roller pump (DRP) for controlling pressure via the control of fluid flows has been a positive selection for the development of the automatic pump systems from the author's investigation in [13], [14].

## **1.2 Motivation**

For the goal of offering a contribution of the research to the development of the medical device applications in the MIS, the author has especially mentioned to the subject of arthroscopy as an example of MIS. The motivation is to acknowledge the existence of currently problematic situations that should be carried out and improved. From the states of the art presented above, there exists some advantages as well as disadvantages while using the methods of flushing fluid for a suitable expansion and a clear visibility in the closed operation area.

Firstly, the utilization of gravity flow method gives some advantages such as the simplification in performance; saving cost for the pump system. However, the method meets the problems of: slow time of response; over flow or under flow situations from the manual adjustments with inaccurate pressure control. The adjustments on the height of the fluid bag and the valve opened level are all manipulated based on the observation directly from a doctor or a surgeon. This might affect to the bad quality of visualization and lead to the risk of patient because of the high pressure inside the operation area. With those limitations, the motivation is how to improve the control strategy for a high precision in pressure control automatically, and reduce the time of response for the safety of the patients during MIS.

Secondly, In the stage of using automatic pump systems, some steps of development have been approached for the pressure preservation. The first step was the usage of single pump system method for controlling only the inflow of fluid. In this case, the pressure in the surgical region was controlled via the inflow of rinsing fluid. The gain from this case is that the pressure is supervised and controlled to the desired value automatically. This results to more accurate control compared to the gravity flow method. But this method of single pump can cause the problem from outflow

control when needed. Then the outflow can only be taken out manually but untimely. This might lead to a danger of increasing pressure rapidly in the OA. In the second step, the pump system has been developed by utilizing two single pumps in order to control the inflow and the outflow independently. As an advantageous point, this solution of two pump system can deal with the problem of danger from a high pressure increased rapidly inside the surgical area. However, this solution is still not an optimal method in pressure control because of the independence between the controls of inflow and outflow. So the settling time or response time is still not improved. Because both inflow and outflow of rinsing fluid have the influence to the actual pressure in the OA. In some case, the blood pressure (BP) in the part of body is not stable. Therefore the pressure in the working space of MIS needs to be controlled and responded quickly to adapt to the change of blood pressure. This solution is also to avoid situations of fluid depletion (when the pressure in the working space is higher than the BP) or haemorrhages (when the pressure in the working space is lower than the BP). From those drawbacks of using automatic pump systems in controlling flows, another idea for motivation in this research is using another type of pump such as a double roller pump to solve the existed problems during MIS. This illustrates an improvement of the medical device control strategy for a higher quality development of instruments in MIS. When using DRP as an automated pump system developed for the flows control and the desired pressure automatically, there is no need for a surgeon to change the height of the fluid bag or adjust the outflow valves manually.

Thirdly, during in the stage of investigation and controller design for evaluation and validation, real-time experiments on the real patients are not allowed because of the patient's safety. Therefore an essential think for the motivation which needs to be realized is the construction of the Hardware-in-the-Loop (HIL) simulator for the replacement of the real patient body. The constructed HIL-Simulator should be programmed to behave and produce some physiological states like the behaviour of the human body. This integrated simulator module is really important and useful for the realization of actuators as well as physical interface in experiments.

Additionally, while solving the problems of pressure control via the control of fluid flows, it is important to get a feedback data from the actual pressure in the operation area to the controller. The matter of fact is that the actual pressure is not allowed to measure directly because of the risks to the patient during MIS. Together with the controller design, therefore an estimator of pressure state should also be implemented as a feasibility in this research. This method produces the state of estimated pressure to replace the feedback data of unmeasurable pressure in the OA. In order to estimate the unmeasurable pressure in this case, it is worthy to observe a measurable data at another place such as the pressure at the DRP. This observer can be performed completely by making use of available pressure sensors at the DRP.

In the knee arthroscopy especially, there are some possibilities of disturbances that can make the pressure in the knee change significantly from the reaction of the patient during MIS. These possibilities are the flexions from the knee joint. According to the investigations in [11], [15], and [16], the change of pressure in the knee joint is not only depended on the knee angles but also depended on the volume of rinsing fluid inside the knee during arthroscopy. Figure. 1.3 shows the relationship between the volume of fluid injected and the pressure while changing the angle of the knee [16]. Those changes need also be concerned in the cases of supervisor and control strategy.

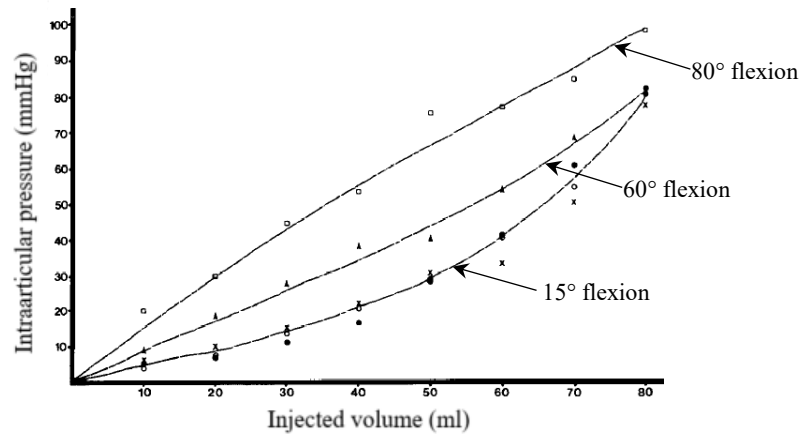


*Fig. 1.3 Graph of pressure-volume relationship with the knee flexion angles 15°, 60°, 80° [16]*

### 1.3 Objectives

Basing on the state of the art and motivations presented, the author aims to research and share the contribution of pressure control and estimation in Minimally invasive surgery. The objectives of the thesis include the following points:

The first objective is constructing a system for modelling the process of the knee arthroscopy. This includes both modelling system on Simulink and building the HIL-Simulator for the MIS process. The equipments in the Medicine laboratory are supported by the Institute of Automation, Faculty of Computer science and Electrical engineering, University of Rostock. Via the project AFluCoMIS, medical devices and specialized instruments related to the MIS are sponsored by W.O.M. - World of Medicine GmbH - Berlin, Germany. The constructed system is useful for the members in our group of medical engineering research. Because of being on the stage of verification and evaluation, the modelling system with the HIL-Simulator is required to concrete for the replacement of the real patient in experiments. This is to avoid undesirable injuries before the stage implementing to the real patient.

The second objective is controller design of the pressure in the operation area via controlling the flows of rinsing fluid. This should be performed by utilizing the double roller pump. During MIS, the actual pressure for expansion inside the part of body is unmeasurable. However, our research is currently on the period of evaluation. Therefore the experiments on the real patients are not allowed. The constructed modelling for real-time simulator is used to replace the real patient. The controlled process should be identified and linearized from the experiment data. And a pressure sensor can be temporary used in this stage of research to measure pressure currently for the feedback data supporting to the controller design to be tested.

The third objective in this thesis is implementing different types of observer algorithms in order to estimate the state of pressure in the surgical area. Furthermore, the best result of estimation from the observers is really valuable for the replacement of unmeasurable data of actual pressure in the surgical area.

Some other possibilities like the knee flexions might be occurred as some situations of disturbances during MIS. Those situations should also be supervised and adaptive controlled for evaluating the quality and stability of the system generally. This performance is also an additional objective that should be done for the tested cases of the knee arthroscopy.

In short, the goals of the dissertation can be summarized as following approachments:

- *Studying on the basic of minimally invasive surgery procerdures.*
- *Building theoretical mathematical equations of the related components for the process of MIS, typically in the knee arthroscopy.*
- *Modelling the system on computer using MATLAB/Simulink and Functions for the simulation.*
- *Identifying the process of the system for a strategy of controller design.*
- *Modelling and identifying the effect of the disturbance possibilities of the process.*
- *Constructing the system with the HIL-Simulator for the real-time experiments.*
- *Setting up the hardware interface modules for the connection between the computerized software model and the actuators of the HIL-Simulator.*
- *Designing a closed loop controlled system using PI controller based on Symmetric optimum algorithm (PI\_SO controller).*
- *Solving the problem of windup phenomenon by an anti-windup algorithm in nonlinear process.*
- *Supervising some cases of the knee flexions as disturbances of the process.*

- *Developing a supervisory algorithm and updating parameters of the PI controller for the adaptation from the knee flexion disturbances.*
- *Designing pressure estimators using observer methods for evaluating the quality of estimated pressure in the knee arthroscopy.*
- *Implementing and combining the best estimator to the closed loop controlled system for the replacement of the unmeasurable pressure in the knee joint model.*
- *Simulating the whole controlled system on computer (MATLAB / Simulink)*
- *Executing and evaluating the whole controlled system in real-time device simulator.*

## 1.4 Materials

To deal with the objectives given out, some materials and methods were proposed. A general description of the whole controlled system is indicated in Fig. 1.4.

One of the essential materials supporting for modelling system is MATLAB/Simulink on computer. In addition, for the realization from modelling to real-time experiments, it is important to build up the HIL-Simulator to reconstruct some states of the surgical area for the replacement of operation on the real patient. Besides this, it is necessary to set up an interface module in order to communicate between the digital signals from computer and the analog signals of the actuators. In this research, the product of dSPACE hardware interface was utilized for both digital to analog converter (DAC) and analog to digital converter (ADC) for the communication between the devices.

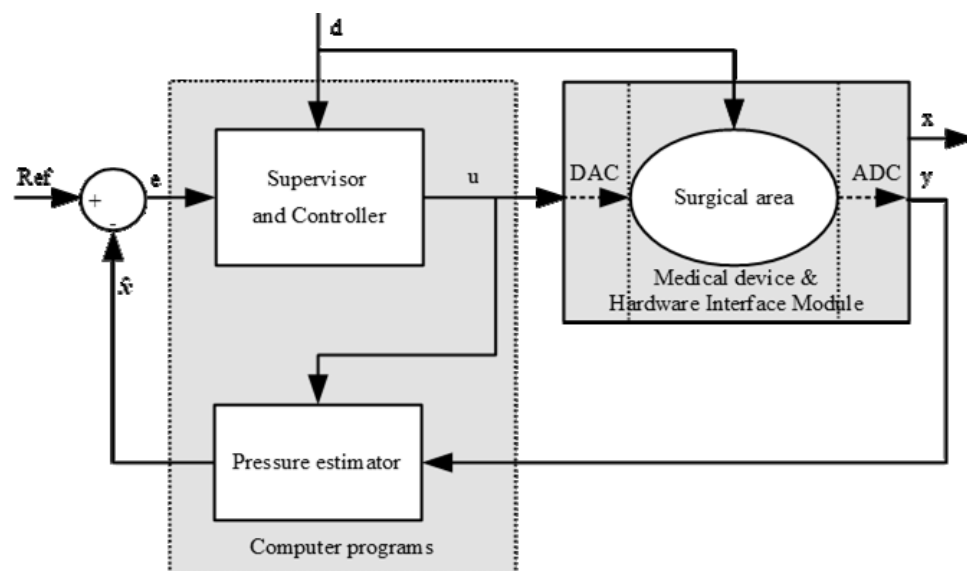


*Fig. 1.4 An overview of the whole controlled system*

Together with the construction of real-time device simulator system shown in Fig. 1.4, the other two main objectives of controller design and estimator for the desired pressure are also crucial in this thesis. Via the medical device and hardware interface module, the pressure in the *surgical area* is estimated and controlled continuously during MIS.

The *supervisor and controller* block needs be designed in order to remain a stable value of pressure in the surgical area whenever there are some changes from the inputs of error  $e$  and disturbance  $d$ . The disturbance signal  $d$  could be created from any change of liquid outflow from the OA; or it could be created from any reaction like a sudden change of the unwanted knee flexion. Signal  $e$  is the error between the desired pressure  $Ref$  and the estimated value  $\hat{x}$ . The signal  $x$  represents to the actual state of pressure in the OA. The signal  $y$  denotes an output expression for the observation state of the estimator. And  $u$  is defined as the control signal of the process of MIS as well as the input data of the estimator. For controller design, the modelled process of the knee arthroscopy should be identified and linearized from the experiment data. Based on the response of the process to be identified, a PID controller shall be designed to obtain and maintain the pressure in the OA stably. In most of nonlinear processes like the process in this research, the pressure in a closed area might change rapidly while the actuators for the fluid flows are changed. This leads to the wind-up phenomenon. Hence, an anti wind-up algorithm is necessary to be performed to avoid the overload to the controller. On the other hand, a supervisory algorithm is proposed to detect some changes from the disturbance actions for the adaptation in controlling system. So, the parameters of the controller should be designed from the results of the supervisor.

The estimated pressure  $\hat{x}$  from the block of *pressure estimator* should be closely like the pressure in the surgical area. In Simulink as well as in real-time device experiments, some methods of estimation are investigated for comparing the results. These methods include Luenberger, basic Kalman filter and extended Kalman filter algorithms of estimation. The best estimated result should be a valid data in replacing unmeasurable pressure of the surgical area.

Interaction between the medical device and the HIL-Simulator module present the realization of the programs and tools installed from the computer connecting to the knee joint model via the actuators. The medical device which was proposed to use for the investigation is DRP. Structure of the DRP is described more details in Chapter 2. From controlling the speed of the motors at the DRP, the flows of fluid are therefore controlled via the roller wheels of DRP. On the other side, the hardware interface module of dSPACE product works in both two functions of DAC and ADC convertors. These components are necessary in communication from the computer programs to the actuators of the HIL-simulator.



## **1.5 Outline of the thesis**

The first Introduction chapter of the thesis has just been presented with an overview in brief state of the art, motivations and problems which need to be solved. Then objectives and ideas on the methods dealing with the problems were also given out. Chapter 2 summarizes some related fundamentals in theory and system modelling. In this chapter, a general information of system overview in MIS is described for identifying, modelling of the process in simulation and real device simulator. Medical devices and hardware interface module as well as HIL-Simulator are also introduced. In addition, concepts of controller and supervisor design and the related results are arranged in chapter 3. The PI controller based on Symmetric optimum (SO) method is proposed. Supervisory algorithm is added to correct the controller parameters. Some cases of disturbance on the knee flexions are proposed for the adaptation of the controlled system. The results on Simulink and on real-time device simulator in different cases are shown for comparison and evaluation. Furthermore, chapter 4 provides estimation methods and the results from implemented methods on both Simulink and real-time simulator. These implemented methods are Luenberger observer, Kalman filter, and extended Kalman filter. The best estimator is used to combine with the closed sensorless controlled process. Chapter 5 concludes the whole thesis and gives some ideas for further work. And final sections of Appendix and Reference show some notifications and various scientific contributions referred in this dissertation.



## **2 OVERVIEW AND MODELLING OF THE MIS SYSTEM**

This chapter content is arranged with general background in MIS and modelling of the MIS system in mathematical equations. This is a basic demonstration in constructing a model of a process. After the first section of introduction in this chapter, an overview of the minimally invasive surgery is described with the medical therapy devices supported. Then the process of the knee arthroscopy and related components are modelled for simulation. A nonlinear state space presentation of the operation area is then performed. Additionally, general descriptions of the hardware interface modules construction are also briefly introduced. These modules are the Input/Output hardware interface MicroLabBox from dSPACE products and the HIL-Simulator of MIS.

### **2.1 Introduction**

In minimally invasive surgery, some important procedures need to be obtained not only professionally but also accurately. Arthroscopic surgery of MIS involves the performance of visualization inside the problematic area with the a tiny camera and fiber optical system. To have a clear vision, the area should be filled with some saline fluid and the camera is placed in the area via trocar with a small incision. Most of orthopaedic surgeons use arthroscopy method to treat variety of problems, including: joint infections and inflammation, removal of loose parts or tissues, and ligament reconstructions [17]. In the knee arthroscopy for example (see in Fig. 2.1), beside using specialized instruments for diagnostics and treatment, one more significal requirement of MIS is how to keep the operation area clear and visible during surgery. This should be performed by the support of medical therapy device in pressure control via controlling the rinsing fluid flows. As mentioned in Chapter 1, some methods for the pressure expansion were introduced. The motivation of the research is to develop the method of pressure control in the closed area to the desired value precisely by utilizing the medical device of DRP. By controlling the DRP, rinsing fluid is flushed in the closed surgical area for a suitable expansion of pressure based on the reference of BP from the patient. This aims to reduce the inconveniences of inaccuracy and slow response of pressure control from the former methods. Moreover, the goal gives a further effect of elimination of fluid depletion or haemorrhage situations in the parts of body. And the control of flushing fluid in and out continuously offers a clean area for a better visualization.

Double roller pump is one of medical therapy devices which were supported to the Institute of Automation, University of Rostock by the company W.O.M. GmbH (Berlin - Germany) via the project AFluCoMIS. The improvement of pressure control via controlling the flows of fluid during

MIS by using DRP is really beneficial while the pressure in the operation area can be controlled stably at anytime according to any change of the outflow. Indeed, this can be performed when the inflow of fluid is controlled automatically depending on the outflow of fluid. And the outflow can be activated and changed from the surgeon (whenever if the fluid in the surgical field is messy).



*Fig. 2.1 An example of the knee arthroscopy in minimally invasive surgery [18]*

To deal with the system modelling in simulation and controller design, it is necessary to construct mathematical equations based on theoretical fundamentals. Before going to the section of modelling process, an overview of the system in MIS is depicted in section 2.2.

## 2.2 System overview of Minimally invasive surgery

Figure 2.2 depicts an overview of the system in MIS in a simplified graph [7], [14].

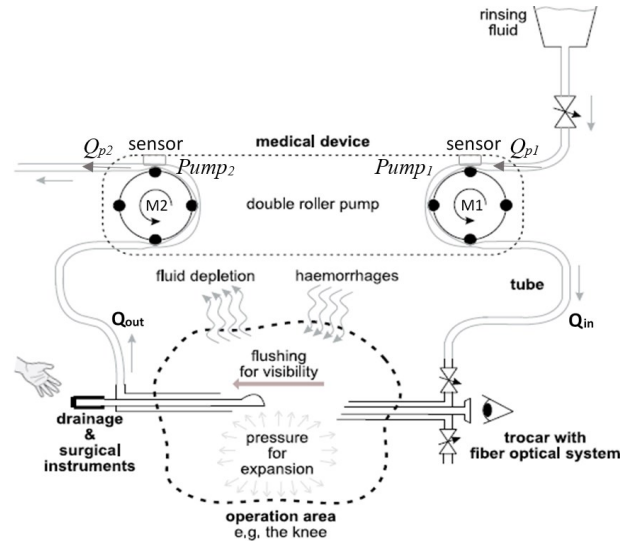


*Fig. 2.2 An overview of the system in minimally invasive surgery [7], [14]*

The operation area in Fig. 2.2 represents to the knee joint of the patient in the knee arthroscopy. Via some trocars, the tubes and other medical instruments are reached into the OA. In order to remain a suitable pressure for expansion in the knee joint, rinsing fluid flows control is chosen for this purpose. Depending to the currently outflow data ( $Q_{out}$ ) which can be ready set up or changed by the surgeon, the inflow of fluid ( $Q_{in}$ ) needs to be controlled automatically respectively. Indeed, maintaining a suitable pressure in the OA is important for procedures of MIS. If the pressure in the surgical region is higher than the blood pressure at the operation area, it can be damage to the part of body by causing the situation of fluid depletion to the tissue. Otherwise, when the OA pressure is lower than the required value, it might have not enough clear space for the visibility. This also leads to the result of haemorrhages into the OA.

The double roller pump (including *pump1* and *pump2*) shown in Fig. 2.2 is used to control the flows of fluid  $Q_{in}$  and  $Q_{out}$ . It is structured by the two DC motors (marked by  $M1$  and  $M2$ ) and two roller wheels plates positioned on the shafts of the two motors. The roller wheels on each rotated motor cause the change of pressure inside the soft and flexible plastic pipe fixed around the wheels. This change of pressure on each roller pump creates the change of fluid flow inside the tube connecting to the operation area. Additionally, a beneficial thing of using the DRP is that on each roller pump, there exists a fixed pressure sensor for pressure measurement at the pump. In this thesis, the motor  $M1$  of the *pump1* is assigned to control only one direction of fluid flow into the operation area; and the motor  $M2$  of the *pump2* is allocated only for the activation of the fluid outflow from the operation area. The outflow can be set up to a fixed value. Sometime this value can be changed and considered as a disturbance in the working space of the MIS. This change makes influence to the change of pressure in the surgical area. With any sudden change of pressure in the area, the inflow of fluid must be supervised and controlled automatically in order to maintain the desired pressure during MIS.

The desired pressure value might be varied from different types of patients; and it depends on the blood pressure at the particular part of body in MIS. Unfortunately, the systolic blood pressure (SBP) can be only measured relatively by some part of the body near to the heart, like by the left arm of the patient. Therefore, according to the study of arthroscopy from the group of research [19] in 1995, the authors provided the measurement data on the survey of twenty two consecutive patients in evaluating a suitable subacromial space pressure (SASP). They suggested that, on average, maintaining a relative pressure value of SASP in arthroscopy at about 49mmHg lower than the SBP would prevent bleeding and permit a good visualization. On the other cites of [5], [8], [20] and [21], the minimum of pressure in the knee arthroscopy was proposed at 28mmHg; and the acceptable range of SASP was suggested from 30mmHg to 60mmHg, depending on the specific SBP of the patient. This range is approximate in Pascal unit (Pa) from 4000Pa to 8000Pa

(1mmHg  $\approx$  133.32Pa). Even in some cases with tourniquet or without tourniquet, the pressure level at some various joints was proposed differently in Table 2.1 [5].

*Table 2.1 Proposed pressure level with and without tourniquet in various joints [5].*

Joint type	With tourniquet (in mmHg)	Without tourniquet (in mmHg)
Shoulder	-	50 - 60
Acromioplasty	-	50 - 60
<b>Knee joint</b>	<b>30 - 35</b>	<b>65</b>
Wrist	30 - 40	65
Elbow, ankle	30 - 40	65
Hip	40 - 45	65

### 2.3 Modelling of the process in MIS

From the simplification of the knee arthroscopy in Fig 2.2, it is clear that the pressure in the knee can be controlled by controlling the inflow regarding to the outflow currently. This is performed by controlling the rotation speeds of the motors at the DRP. Normally, the outflow is set equally to a constant during the time of MIS. Sometimes, this constant might be changed according to specific situations in the part of body. Hence, the pressure can be controlled based on the controlled speed of the motor  $M1$  regarding to the speed of the motor  $M2$ . Plastic tubes are used to transfer the fluid into and out of the operation area. The block diagram for modelling of the process has been developed with the signals and blocks indicated in Fig. 2.3. In this figure, the first dark grey block ‘Line in’ including the motor  $M1$ ,  $pump1$  and  $tube1$  is represented to the direction of inflow to the surgical area. The second dark grey block of ‘Line out’ with the motor  $M2$ ,  $pump2$  and  $tube2$  symbolizes the outflow direction from the surgical area. The inverse direction of flow is assigned by the minus sign “-”. Both these two blocks have the same structure and materials. The input of the process which need to be controlled is  $u_1$  signal connected to the motor  $M1$ , whereas  $u_2$  signal is connected to the motor  $M2$  and it is considered as an extra input (a kind of input disturbance while changing the outflow) of the process. The output of the process is the pressure of the operation area called  $p_{knee}$ . In the whole controlled system, the pressure  $p_{knee}$  should be maintained close to the desired value of  $p_{ref}$ . The input  $pe$  of the controller block is the pressure error between  $p_{ref}$  and  $p_{knee}$ . The output from the controller  $\Delta u$  and the signal of  $u_2$  are summed for supervising and producing the control signal  $u_1$  to the motor  $M1$ . In this section, the author presents the principal mathematical equations for modelling the main parts of the process in MIS: the motors, pumps, tubes and the operation area.

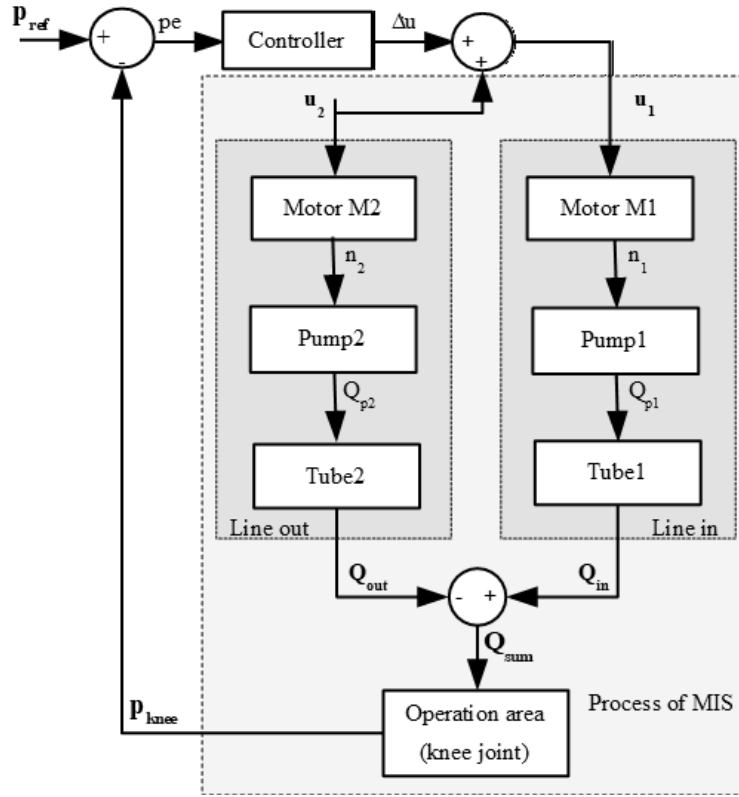


*Fig. 2.3 Block diagram and signals for modelling of process in minimally invasive surgery*

### 2.3.1 Modelling of the motors

The two motors *M1* and *M2* used in the blocks ‘Line in’ and ‘Line out’ have the same type of GR63-55. Figure 2.4 is an overview of this motor type. The parameters of the motors are shown in Table 2.2 [22]. The control voltage range of these brushed DC motors is from 0 to 5 volt. The flow of fluid is mostly depended on the rotation speed of the motor with the roller wheels plate fixed on the shaft of the motor.



*Fig. 2.4 Overview of the brushed DC motor GR63-55*

Table 2.2 Parameters of the motor GR63-55 [22].

Parameter	Unit	Value
Nominal voltage	V	24
Nominal current	A	4.9
Nominal torque	Ncm	27
Nominal speed	rpm	3350
Friction torque at no load	Ncm	2
Peak stall torque	Ncm	257
No load speed	rpm	3650
Maximum output power	W	245
Nominal power	W	94.7
Torque constant	Ncm/A	6.4
Terminal resistance	Ohm	0.6
Terminal inductance	mH	1.5
Starting current	A	40
No load current	A	0.4
Demagnetisation current	A	33
Rotor inertia	gcm <sup>2</sup>	750
Weight	kg	1.7

From the operation of the motor in experiment, the relationship between the input control voltage ( $u_i$ ) and the numbers of revolution per second of the motor (symbolized by  $n_i$ ) is formed in (2.1).

$$n_i(t) = f(u_i(t)); (i = 1, 2) \quad (2.1)$$

At each revolution of the motor, it is encoded with 1000 pulses. Therefore, the revolution  $n_i$  can be determined by providing the input voltage  $u_i$ . From experiments, the static gain data of the motor is determined approximately in Fig. 2.5. And dynamic response of the motor is indicated in dark yellow signal of Fig. 2.6.

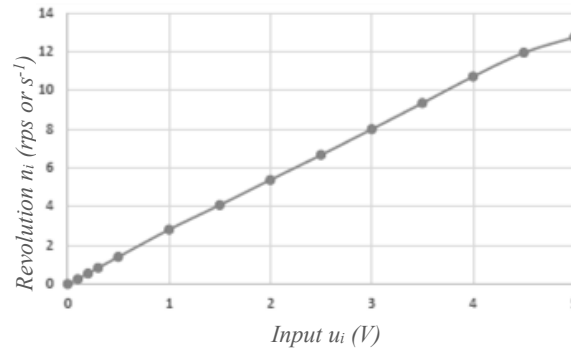


Fig. 2.5 Response of revolution regarding to the input voltage



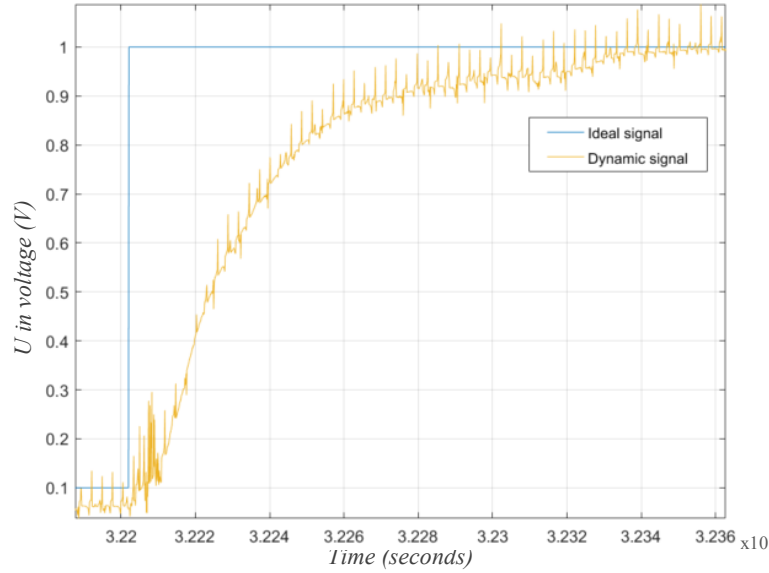


Fig. 2.6 Dynamic response of the motor

From Fig 2.6, it is interesting to note that the dynamic behavior of the motor is considered to the transfer function type  $P-TI$  with a small dead time of  $T_d$ . Hence, the transfer function of the motor  $G_M(s)$  can be formed in (2.2) for motor modelling.

$$G_M(s) = e^{-T_d s} \cdot \frac{K_M}{T_M s + 1} \quad (2.2)$$

whereas:  $T_d = 0.006$  (s) is dead time;  $T_M = 0.038$  (s) is time constant; and  $K_M = 2.5$  ( $s^{-1}/V$ ) is the static gain of the motor from experiment.

In some cases, because the dead time  $T_d$  is too small compared to the time constant  $T_M$ , therefore  $T_d$  can be approximated to zero.

### 2.3.2 Modelling of the double roller pump

Double roller pump is placed to produce the pressure change in the tubes for the fluid flows. This is a kind of peristaltic pump which is basically described in Fig 2.7 [23], where the blue part is represented to the fluid being transferred by the roller pump. Each roller pump is fixed to the shaft of the motor and bounded by a soft flexible segment of the plastic tube. The tube is presented more details in section 2.3.3. In the process of MIS, each roller pump of the DRP is responsible for one direction of the fluid flow. One pump creates the direction of fluid flow into the surgical area. The other pump produces the direction of outflow from the area. The pressure at each pump is currently measured by the available pressure sensor fixed in each tube. By producing pressures from the rotation speed of the motors, the fluid flows in the tubes can be controlled definitely.

The complete structure of the DRP fixed with the two motors and two tubes is shown in Fig. 2.8.

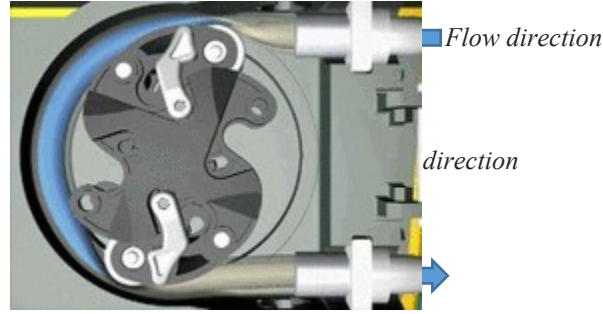


*Fig. 2.7 Basic function of a peristaltic pump for flowing fluid [23]*

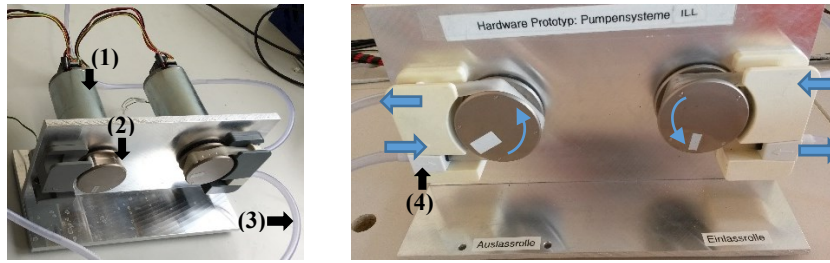


*Fig. 2.8 Overview of the DRP: 1. Motor; 2. Roller wheel; 3. Plastic tube; 4. Pressure sensor*

At each revolution of the motor, series of fluid ‘package’ are transferred inside the tube by the roller pump. This means that from the actual speed of the motor  $n_i$ , the pump converts a certain flow through the tube at the pump called  $Q_{pi}$ . When the speed is a constant, then the flow  $Q_{pi}$  is also equal to a constant relatively after a period of time.

$$Q_{pi} = \frac{dV_f}{dt} ; (V_f: \text{volume of fluid}) \quad (2.3)$$

With the maximum speed of the motor  $n_i$  about  $12s^{-1}$ , the flow at the pump  $Q_{pi}$  can reach to the maximum value of  $22ml/s$  approximately. The relationship between  $Q_{pi}$  and  $n_i$  is indicated in Fig. 2.9. The flow area within the speed from 0 to  $4s^{-1}$  is nearly linear, and the other area is nonlinear.

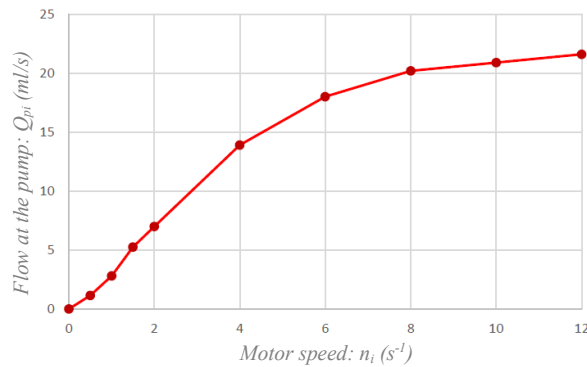


*Fig. 2.9 Relationship between the motor speed  $n_i$  and the flow at the pump  $Q_{pi}$*

Assuming that the rotation speed of the motor  $M1$  on the right is defined as  $n_1$ ; and  $n_2$  is the rotation speed of the motor  $M2$  on the left. Equations of flows at the DRP ( $Q_{p1}$  and  $Q_{p2}$ ) are formed in (2.4) and (2.5).

$$Q_{p1}(t) = f(n_1(t)) \quad (2.4)$$

$$Q_{p2}(t) = f(n_2(t)) \quad (2.5)$$

From the parameters shown in Fig. 2.9, a lookup table was established for modelling of the double roller pump.

### 2.3.3 Modelling of the tubes

There are two long plastic tubes separately connected from the trocar in operation area passing over each pump of the DRP for the flows transportation. One tube is used for the inflow transferring, and the other tube is used for the outflow from the operation area. Fig. 2.10 shows a typical plastic tube being used with the trocar in MIS. The soft and flexible segment (marked by number 3 in the figure) of the tube is bound tightly together with the roller wheels of the pump.

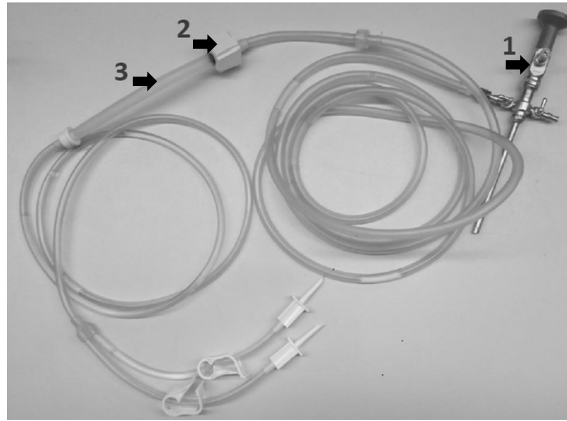


*Fig. 2.10 The tube for fluid transfer: 1. Trocar; 2. Pressure sensor; 3. Flexible part*

Because the whole plastic tube is an elastomeric type, therefore there exists not only a hydraulic resistance but also a hydraulic capacity of the tube. The tube expands partly and stores a small part of volume flow when there is a pressure acts on the tube. But this does not happen in the trocar which is made from steel materials. This really causes the problem on mathematical description clearly in theory about the relationship between the volume flow and the pressure at the pump. Indeed, this drop of static pressure in the trocar creates a difference between the pressure at the pump and the pressure at the operation area. This difference of pressure through the tube ( $\Delta p_s$ ) can be determined in experiments by measuring the pressure at the pump with the varied parameters of volume flows through the hose, while the pressure in the model of the operation area is prevailed to the ambient pressure. The results of measurement are illustrated in Fig. 2.11.

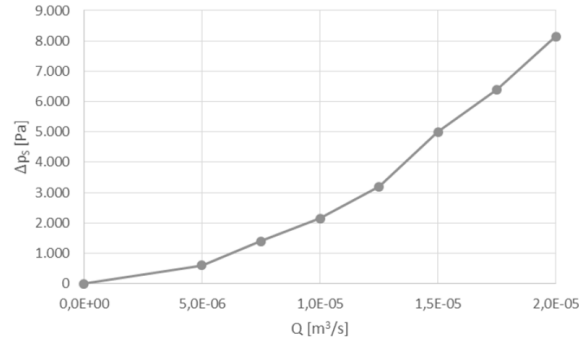


*Fig. 2.11 The pressure drop through the operation area depending on the flow at the pump*

It is clear that the behavior of the pressure change regarding to the flow of fluid is a form of exponential function, or a nonlinear expression.

On another side, Fig. 2.12 shows the measurement data of flow at the end of the tube (close to the operation area) in the relationships of various voltages and motor speed parameters. It can be seen that there is some error of flow between the data in Fig. 2.12 and the data in Fig. 2.9 because of the resistance and hydraulic capacity existence along the tube. The maximum flow in Fig.2.12 is limited about 16ml/s (in maximum speed of motor) while the maximum flow in Fig.2.9 is 22ml/s.

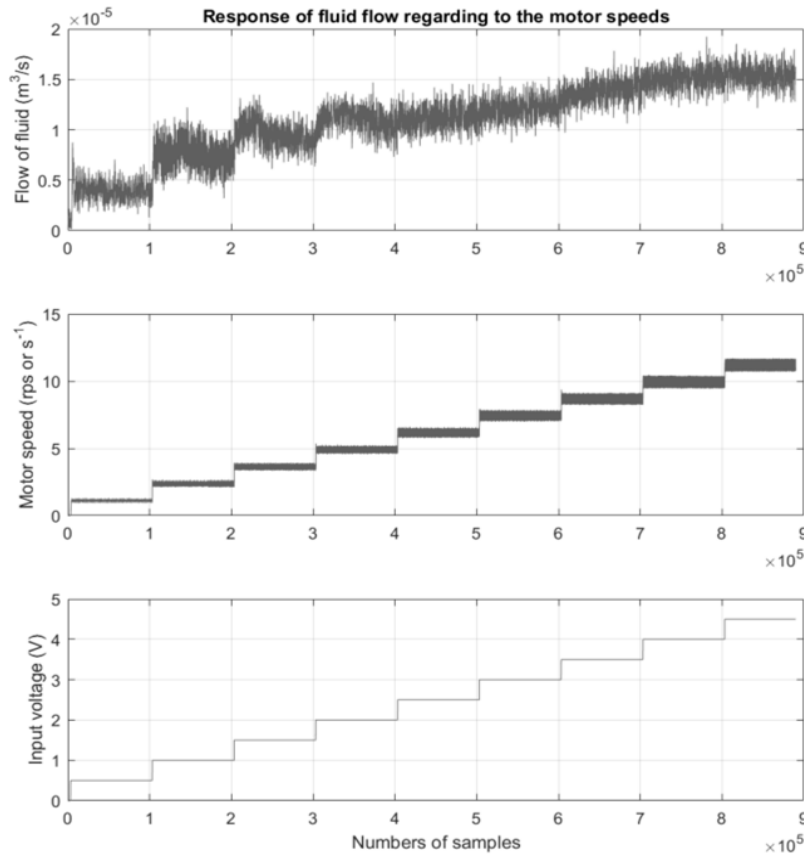


*Fig. 2.12 The flow in the tube (close to the operation area) regarding to the motor speed*

In dynamic reaction, due to the hydraulic capacity of the tube as well as the reaction of the current pressure inside the closed operation area, in the *tube1* of inflow, it contains a small difference of  $\Delta Q_1$  between the flow created at the *pump1* ( $Q_{p1}$ ) and the inflow of fluid ( $Q_{in}$ ) into the operation area. In other words, a part of the flow  $Q_{p1}$  does not get completely out of the tube and this causes to the remainder of  $\Delta Q_1$ . Similarly, in the inverse direction of the outflow in the *tube2*, the difference of flow  $\Delta Q_2$  is created by the outflow of  $Q_{out}$  and the flow at the *pump2* ( $Q_{p2}$ ). Moreover, during the operation, the dynamic components of dropped pressure and flow might occur from the turbulent flow which is depicted more details in Section 2.3.5.

Generally, the the block diagram for modelling of the tubes reaction is described in Fig. 2.13.

From the relationship between the pressure and the flow at the *pump1*, the pressure change ( $\dot{p}_1$ ) is defined in (2.6a); the same situation to the *pump2*, the change of  $\dot{p}_2$  is defined in (2.7a). It is noted that  $C_{tube}$  is represented to the hydraulic capacity of the tubes. Furthermore, blocks of ‘static gain’ in Fig. 2.13 represent to the static resistances (called  $R_1$  and  $R_2$ ) of the two tubes. These resistances cause some loss of pressure from the pump to the operation area. These drops of pressure from the two tubes are presented in (2.6b) and (2.7b).

$$\dot{p}_1 = \frac{Q_{p1} - Q_{in}}{C_{tube}} = \frac{\Delta Q_1}{C_{tube}} \quad (2.6a)$$

$$R_1 \cdot Q_{in} = p_1 - p_{knee}; \quad \text{or:} \quad p_1 = p_{knee} + R_1 \cdot Q_{in} \quad (2.6b)$$

$$\dot{p}_2 = \frac{Q_{p2} - Q_{out}}{C_{tube}} = \frac{\Delta Q_2}{C_{tube}} \quad (2.7a)$$

$$R_2 \cdot Q_{out} = p_2 - p_{knee}; \quad \text{or:} \quad p_2 = p_{knee} + R_2 \cdot Q_{out} \quad (2.7b)$$

whereas:

$$\Delta Q_1 = Q_{p1} - Q_{in} \quad (2.8)$$

$$\Delta Q_2 = Q_{p2} - Q_{out} \quad (2.9)$$

$$Q_{sum} = Q_{in} - Q_{out} \quad (2.10)$$

In ideal case, the pressure in the surgical region would be stable when the inflow  $Q_{in}$  is equal to the outflow  $Q_{out}$ . However in real device simulator or in the real MIS to the patient, it is impossible to get in ideal case that the  $Q_{in}$  exactly equals to  $Q_{out}$ . This means that there always exists some error or loss of flow between the inflow and the outflow in real-time experiments.

Due to the response of the tube in experiments, the hydraulic capacity  $C_{tube}$  is approximated by  $9.75e-11$  (m<sup>3</sup>/Pa) in simulation.

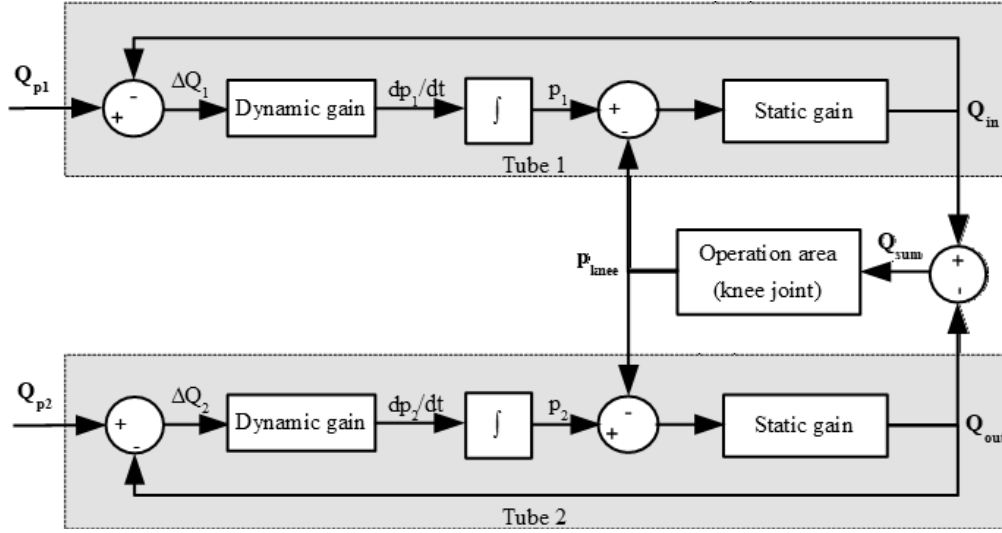


Fig. 2.13 Block diagram for modelling of the tubes in MIS

### 2.3.4 Modelling of the operation area

The process of the knee arthroscopy as an example of the MIS was proposed for the investigation. During the stage of verification in experiments, the operation area was modelled by a plastic ball simulator called the knee model (Fig. 2.14).

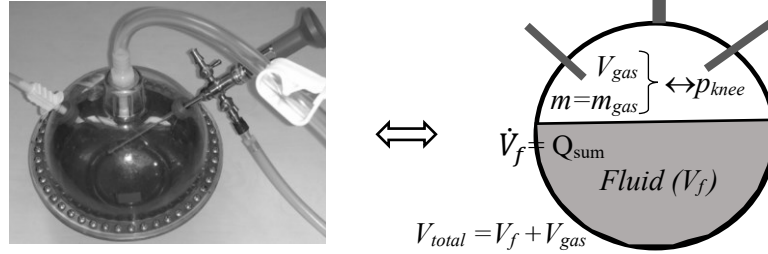


Fig. 2.14 The reservoir is used for the simulation of the operation area with some trocars

The pressure in the knee model is called  $p_{knee}$ . This pressure is considered to the value of SASP which should be lower than SBP of the patient as mentioned in section 2.2 above. Any change of pressure  $\dot{p}_{knee}$  depends on the two parameters: the total flow of incompressible fluid into the area, and the capacity of the knee. This change is described in (2.11), where  $C_{knee}$  is capacity of the knee model which describes the ability of the volume change via the pressure change of the knee.  $Q_{sum}$  is the total flow coming actually in the knee during MIS as indicated in (2.10).

$$\dot{p}_{knee} = \frac{Q_{sum}}{C_{knee}} \quad (2.11)$$

It should be noted that the troubles of haemorrhage and fluid depletion into the tissue might happen during MIS. Assuming that  $Q_{hae}$  is represented to the flow of the haemorrhage when  $p_{knee}$  is lower

than SASP. Likewise,  $Q_{dep}$  is defined as the flow of the fluid depletion which happens when  $p_{knee}$  is higher than SASP. Therefore, the pressure in the surgical area  $p_{knee}$  should be close to the desired value of SASP. This subjects to the minimization values of  $Q_{hae}$  and  $Q_{dep}$  in the troubles of MIS. From this situation, the actual flow  $Q_{sum}$  in (2.10) can be rewritten in (2.12).

$$Q_{sum} = Q_{in} - Q_{out} + Q_{hae} - Q_{dep} \quad (2.12)$$

By defining the loss of flow during MIS  $Q_{loss}$ :

$$Q_{loss} = (Q_{dep} - Q_{hae}) \quad (2.13)$$

Additionally with the assumed value of  $Q_{ext}$  equally to some other types of flows lost during MIS, the total error of flow  $Q_{err}$  is assigned in (2.14). This error of flow includes the values of  $\Delta Q_1$  and  $\Delta Q_2$ ; and from (2.8), (2.9), the equation (2.12) can be rewritten as (2.15).

$$Q_{err} = Q_{ext} + Q_{loss} \quad (2.14)$$

$$Q_{sum} = Q_{in} - Q_{out} - Q_{err} \quad (2.15)$$

This total error of flow  $Q_{err}$  is nonzero in this nonlinear process of MIS.

In addition, by following the principle of ideal gas equation in (2.16), the product of the pressure  $p_{knee}$  and the volume of available gas  $V_{gas}$  in the knee is proportional to the mass  $m$  of gas:

$$p_{knee} \cdot V_{gas} = m \cdot R_c \cdot T_c \quad (2.16)$$

$$p_{knee} = \frac{m \cdot R_c \cdot T_c}{V_{gas}} \quad (2.17)$$

where  $R_c$  is the gas constant, and  $T_c$  is the temperature of gas.

Taking derivation the equation (2.16) on two sides and ignoring the change of temperature:

$$\dot{p}_{knee} \cdot V_{gas} + p_{knee} \cdot \dot{V}_{gas} = \dot{m} \cdot R_c \cdot T_c \quad (2.18)$$

In the closed surgical area of MIS containing some fluid and gas, it is considered to have no change of gas amount during MIS. This means that the mass ' $m$ ' of gas is a constant. The equation (2.18) can be thus rearranged into (2.19). This is clear that the change of pressure in the operation area is mutually depended on the change of gas volume  $V_{gas}$ , or the gas compression in the knee model.

$$\dot{p}_{knee} = -\frac{p_{knee}}{V_{gas}} \cdot \dot{V}_{gas} \quad (2.19)$$

The gas volume ( $V_{gas}$ ) is inversely proportional to the fluid volume ( $V_f$ ) as in (2.20).

$$V_{gas} = V_{total} - V_f = V_{total} - (V_0 + \int_0^t Q_{sum} dt) \quad (2.20)$$

where  $V_{total}$  represents the total volume; and  $V_0$  is the initial fluid volume in the knee model.

$V_{total}$  and  $V_0$  are considered to the constants. Hence, the derivation of gas volume is (2.21).

$$\dot{V}_{gas} = -Q_{sum} \quad (2.21)$$

Substituting (2.21) to (2.19), the change of pressure in the knee model can be shown in (2.22).

$$\dot{p}_{knee} = \frac{p_{knee}}{V_{gas}} \cdot Q_{sum} \quad (2.22)$$

Comparing (2.22) to (2.11), it is obvious that the capacity of the knee model  $C_{knee}$  is equal to the ratio between the gas volume and the current pressure in the operation area, presented in (2.23).

$$C_{knee} = \frac{V_{gas}}{p_{knee}} \quad (2.23)$$

### 2.3.5 Influence of turbulent flow to the pressure change in the tubes

Normally, pressure loss in a pipe depends not only on the velocity of the flow but also on the inner diameter ' $D_i$ ' of the pipe. There are two different types: Laminar flow and turbulent flow which can be determined by calculating the Reynolds number given in (2.24) [24], [25], [26]. These types of flows have different calculations of friction factor called  $\lambda_f$  in (2.25) and (2.26).

$$Re = \frac{\text{Fluid velocity} \times \text{internal pipe diameter}}{\text{Kinematic viscosity}} = \frac{V_i \cdot D_i}{\gamma} = \frac{\rho \cdot V_i \cdot D_i}{\mu} = \frac{\rho \cdot Q_i \cdot D_i}{\mu \cdot \text{Area}} = \frac{4 \cdot \rho \cdot Q_i}{\mu \cdot \pi \cdot D_i} \quad (2.24)$$

where  $\gamma$ : Kinematic viscosity;  $\mu$ : dynamic viscosity; fluid velocity  $V_i = \frac{Q_i}{\text{Area}} = \frac{4 \cdot Q_i}{\pi \cdot D_i^2}$ ; ( $Q_i$ : flow)

If the Reynolds number  $Re$  is less than 2000, then the process is in laminar flow. When  $Re$  is greater than 4000, then it is called turbulent flow. In case of  $2000 < Re < 4000$ , it is in transition flow (see the Figures 2.15 and 2.16 for the description) [24].

For example, in normal condition of air temperature around 20°C, the fluid inside the pipe is water with parameters: diameter  $D_i = 0.006m$ , density  $\rho = 998.2(\frac{kg}{m^3}) \approx 1e3(\frac{kg}{m^3})$ ,  $\mu = 0.001(\frac{kg}{s})$ , and the inflow of fluid at the *pump1* is  $Q_{in} = Q_i = 0.00001(\frac{m^3}{s})$ . Then the Reynolds number is:

$$Re = \frac{4 \cdot (1e3) \cdot (1e-5)}{\pi \cdot (1e-3) \cdot (6e-3)} = 2122$$

When the inflow  $Q_{in}$  is set to  $0.000015(\frac{m^3}{s})$ , then the Reynolds number is:

$$Re = \frac{4 \cdot (1e3) \cdot (15e-6)}{\pi \cdot (1e-3) \cdot (6e-3)} = 3183$$

These two cases of Reynolds numbers are in the range of transition flow.



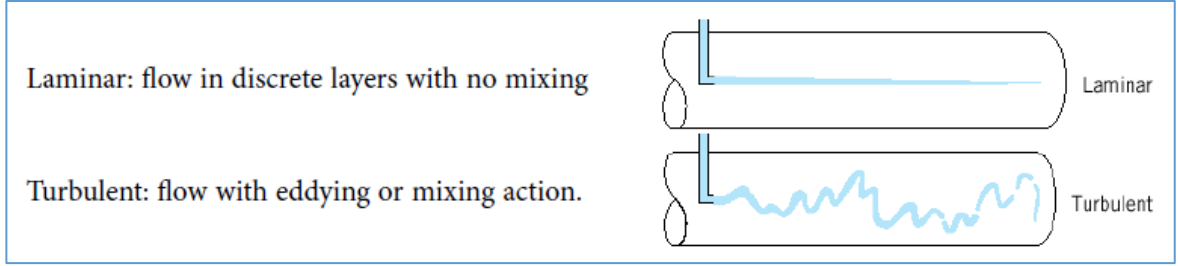


Fig. 2.15 Simple description of laminar and turbulent flows [24]

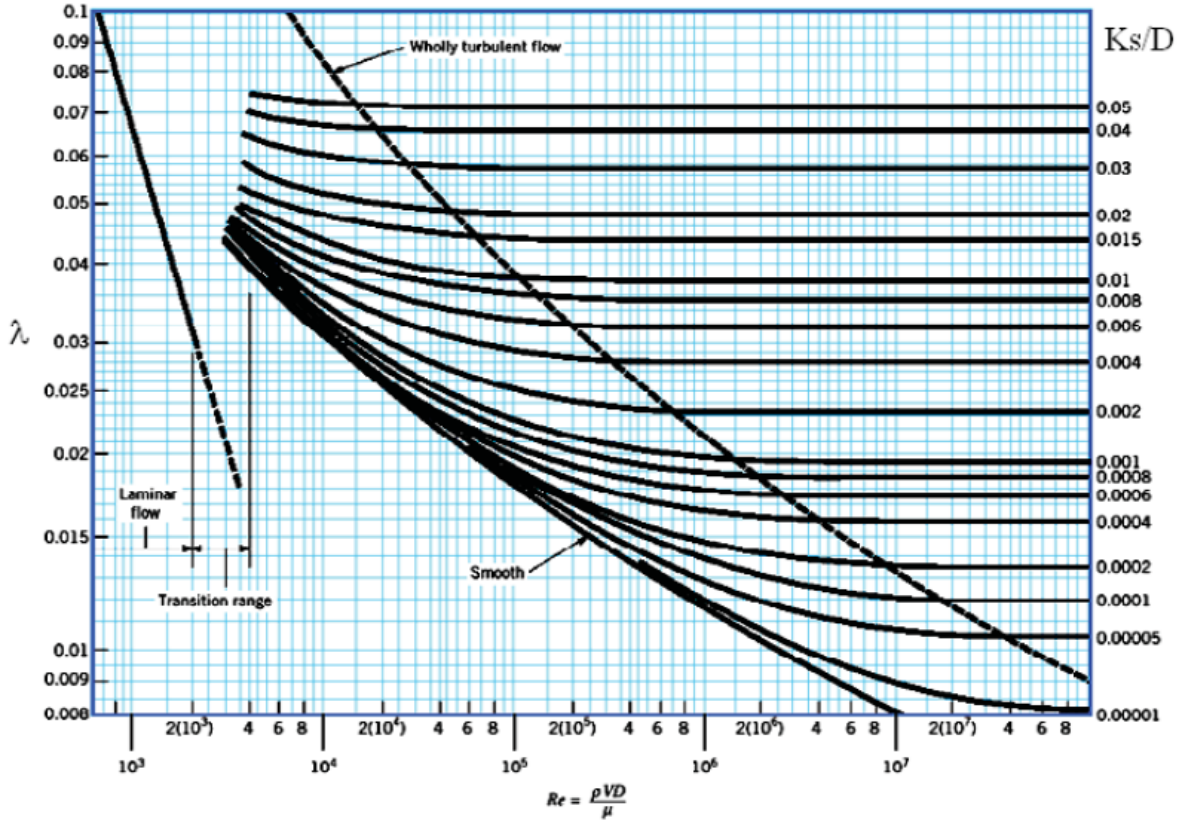


Fig. 2.16 Friction factor and Moody diagram (Note in figure:  $D = D_i$ ,  $\lambda = \lambda_f$ ) [24]

Combining to the conditions of flushing fluid during MIS, The process is in laminar flow when the inflow of rinsing fluid  $< 0.00001(\frac{m^3}{s})$  is equivalent to the case of voltage input  $u_I$  to the motor  $MI < 1.3V$ . And the friction factor  $\lambda_f$  is then computed by (2.25). Otherwise, when the flow of the process goes over the value of  $0.000015(\frac{m^3}{s})$  (this approximates to voltage input  $u_I$  of the motor  $MI$  around 1.7V), then the flow is turbulent. In this case, the friction factor  $\lambda_f$  is computed by Colebrook-White formula of (2.26).

$$\lambda_f = \frac{64}{Re}; \quad (\text{for laminar flow: } Re < 2300) \quad (2.25)$$

$$\frac{1}{\sqrt{\lambda_f}} = -2 \log \left( \frac{k_s}{3.7 D_i} + \frac{2.51}{\text{Re} \sqrt{\lambda_f}} \right); \text{ (for turbulent flow: } \text{Re} > 4000 \text{)} \quad (2.26)$$

Where  $k_s$  is called the roughness factor. For a plastic pipe,  $k_s = 0.03\text{mm}$ .

On another side, from the difference between the larger diameter pipe and the smaller diameter trocar, this appears a turbulent flow. In general therefore during MIS, there always exists a turbulent flow from the pipe to the model of knee via trocars. From the equation (2.26), it is clear that the friction factor  $\lambda_f$  can be written as a function corresponding to the inflow  $Q_{in}$  in (2.27).

$$\lambda_f = f(Q_{in}) = \beta \cdot Q_{in}^2 \quad (2.27)$$

The parameter  $\beta$  is considered to be a kind of flow resistance from the turbulent flow. This parameter represents to an additionally dynamic element of pressure from the roller pump to the knee model during MIS.

By adding this factor of friction as a loss pressure from the *pump1* to the knee model during arthroscopic process, the equation (2.6b) is completely rewritten as in (2.28) with the turbulent flow appearance.

$$p_1 = p_{knee} + R_1 \cdot Q_{in} + \beta \cdot Q_{in}^2 \quad (2.28)$$

### 2.3.6 Modelling of disturbances from the knee angle changes

As introduced in Chapter 1, there are some possibilities of the knee angle flexions that cause the change of pressure in the knee significantly during MIS. These changes of pressure disturbances depend on the injected volume of fluid in the knee during MIS, as shown in Fig. 1.3. These cases of angle changes are considered to the disturbances of the process that effect to the stability of the whole controlled system during MIS. These cases should be identified for realization in simulations and in real-time experiments.

#### 2.3.6.1 The flexion angles between 0 and 30°

From the surveys in [16], the changes of knee angle between 0 and 30° gave nearly the same response of pressure change. So it can be indicated by the curve approximately in Fig. 2.17. The transfer function in this case of disturbance in MIS is identified as in type of  $I-T_I$  form described in (2.29) at the working point of 40ml injected volume in Fig. 2.17.

$$G_D(s) = \frac{K_D}{T_I s(1+T_1 s)} \quad (2.29)$$

whereas:  $K_D = \frac{20}{26} (mmHg/ml) = \left(\frac{20}{26}\right) * 133.32(Pa/ml) = 102.55(Pa/ml)$ ;  $T_I = 26 (ml)$ ;  $T_1 = 14 (ml)$ .

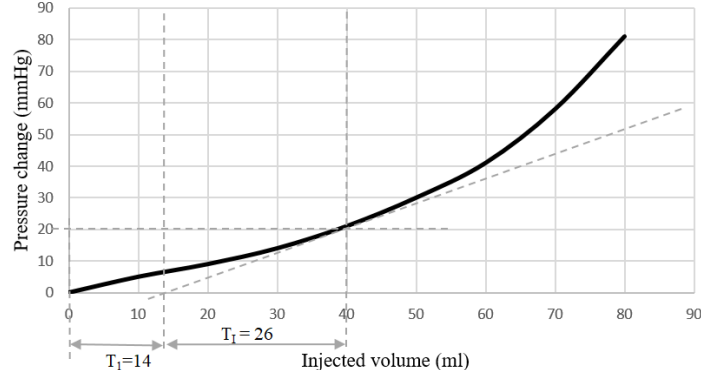


Fig. 2.17 Pressure - injected volume relationship in cases of flexions 0-30°

### 2.3.6.2 The flexion angle of 60°

At the angle knee changed about 60°, the given data is in Fig. 2.18 based on the data of [16]. The transfer function is identified similarly to (2.29) with the different parameters set of  $K_{D\_60}$ ,  $T_{I\_60}$  and  $T_{I\_60}$  as below.

$$K_{D\_60} = \frac{35}{38} \text{ (mmHg/ml)} = 122.79 \text{ (Pa/ml)}; T_{I\_60} = 38 \text{ (ml)}; T_{I\_60} = 2 \text{ (ml)}.$$

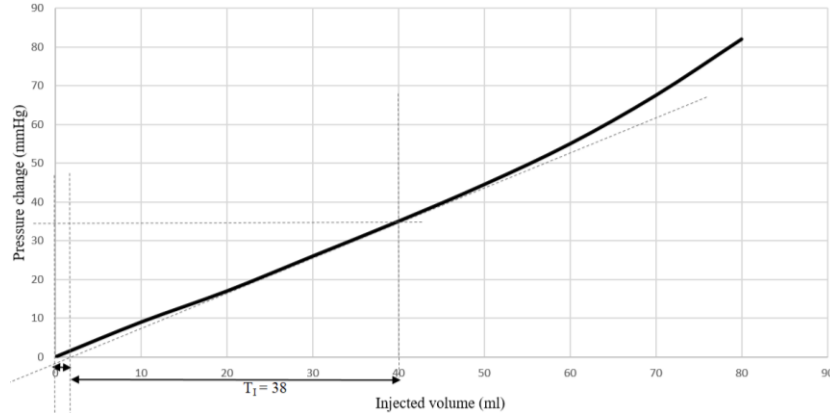


Fig. 2.18 Pressure - injected volume relationship in case of flexion around 60°

### 2.3.6.3 The flexion angle of 80°

Basing on the data from [16] redrawn in Fig. 2.19 for the angle knee flexion 80°, it is interest to note that the response of pressure is nearly the same to a linear change with the proportional gain of  $K_{D\_80} = 55/40 \text{ (mmHg/ml)} = 183.32 \text{ (Pa/ml)}$ ,  $T_{I\_80} = 0$ , and  $T_{I\_80} = 40 \text{ (ml)}$ . The transfer function of the disturbance in this case is (2.30).

In experiments, those cases of the angle flexions are calculated and performed by the support of the HIL-Simulator which is going to be briefly introduced in section 2.4.

$$G_D(s) = \frac{K_D}{T_I \cdot s} \quad (2.30)$$

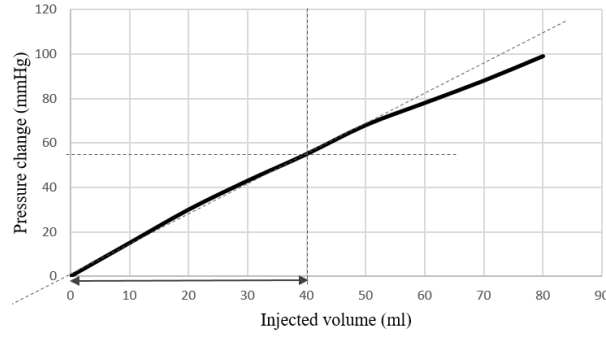


*Fig. 2.19 Pressure-injected volume relationship in case of flexion around 80°*

### 2.3.7 State space presentation of the knee model

State space presentation of the knee model plays an important role for modelling of the plant which is useful not only in identification but also in estimation of the controlled process. In general, a state space formation of a linear process includes a state space equation and an output equation described in (2.31) and (2.32) correspondingly.

$$\dot{x} = A \cdot x + B \cdot u ; \text{ or: } \dot{x} = f(x, u) \quad (2.31)$$

$$y = C \cdot x + D \cdot u ; \text{ or: } y = g(x, u) \quad (2.32)$$

Vector  $\dot{x}$  represents to the first order differential equations of the state variables. Input vector is  $u$ , and vector of output is  $y$ . In linear time-invariant systems,  $A$ ,  $B$ ,  $C$ ,  $D$  are determined as constant matrices. In cases of nonlinear, time-variant systems, then the functions of  $f(x, u)$  and  $g(x, u)$  represent to the state space and output presentation generally.

During MIS, the pressure in the closed OA of the knee model is influenced almost by the actual flow change into the area. This change of pressure is indicated in (2.22). This equation can be rewritten as (2.33).

$$\dot{p}_{knee} = \frac{1}{C_{knee}} \cdot (Q_{in} - Q_{out} - Q_{err}) \quad (2.33)$$

As indicated in Fig. 2.11, the change of pressure  $\Delta p$  in the knee is a nonlinear component corresponding to the actual flow of  $Q_{sum} = (Q_{in} - Q_{out} - Q_{err})$ . In addition,  $C_{knee}$  from (2.23) is also a variant parameter which is depended on both the volume of gas  $V_{gas}$  and the pressure of the knee  $p_{knee}$  currently. Based on previous mathematical equations for process modelling, there are four selective cases of state space presentation of the nonlinear process suggested as follows.

#### **Case 1: One state presentation**

By assuming that the state of the operation area is  $x = p_{knee}$ , the input is  $u = [u_a; u_b]$  ( $u_a = Q_{in}$ ,  $u_b = Q_{out} + Q_{err}$ ), then the state space equation (2.33) can be rearranged in (2.34). On the other hand,

since the equation (2.28) has been determined and considered to an output measurement, it can be rewritten in (2.35). In real device simulator experiment, the measurement is performed by the usage of available pressor sensor at the roller *pump*l.

$$\dot{x}_{(1state)} = \dot{p}_{knee} = \begin{bmatrix} \frac{1}{c_{knee}} & -\frac{1}{c_{knee}} \end{bmatrix} \begin{bmatrix} u_a \\ u_b \end{bmatrix} = f_1(x, u) \quad (2.34)$$

$$y_1 = p_1 = [1][p_{knee}] + R_1 \cdot u_a + \beta \cdot u_a^2 = g_1(x, u) \quad (2.35)$$

### **Case 2: Two states presentation**

In this case, the equations (2.6a) and (2.33) can be combined and rewritten in (2.36) as a state space presentation with two state variables ( $p_{knee}$  and  $p_l$ ).

$$\dot{x}_{(2states)} = \begin{bmatrix} \dot{p}_{knee} \\ \dot{p}_1 \end{bmatrix} = \begin{bmatrix} \frac{1}{c_{knee}} \cdot (Q_{in} - Q_{out} - Q_{err}) \\ \frac{1}{c_{tube}} \cdot \Delta Q_1 \end{bmatrix} = f_2(x, u) \quad (2.36)$$

where:  $x = \begin{bmatrix} p_{knee} \\ p_1 \end{bmatrix}$  is a vector of two state variables; input  $u = [u_a; u_b; u_c]$ ; ( $u_a = Q_{in}$ ,  $u_b = Q_{out} + Q_{err}$ ,  $u_c = \Delta Q_l$ ).

And the output equation of measurement (2.28) can be rewritten for the case of two states in (2.37) whereas  $p_l$  is determined by (2.28).

$$y_2 = p_1 = \dot{x} = [0 \quad 1] \cdot \begin{bmatrix} p_{knee} \\ p_1 \end{bmatrix} = g_2(x, u) \quad (2.37)$$

### **Case 3: Three states presentation**

This is an alternative presentation from the case 2 above. When the parameter of flow lost during MIS ( $Q_{err}$ ) is considered as a variable in state space presentation, then the equations (2.36) and (2.37) can be rewritten in (2.38) and (2.39) respectively.

$$\dot{x}_{(3states)} = \begin{bmatrix} \dot{p}_{knee} \\ \dot{p}_1 \\ \dot{Q}_{err} \end{bmatrix} = \begin{bmatrix} \frac{1}{c_{knee}} \cdot (Q_{in} - Q_{out} - Q_{err}) \\ \frac{1}{c_{hyd}} \cdot \Delta Q_1 \\ 0 \end{bmatrix} = f_3(x, u) \quad (2.38)$$

where:  $x = \begin{bmatrix} p_{knee} \\ p_1 \\ Q_{err} \end{bmatrix}$  is a vector of three state variables; input  $u = [u_a; u_b; u_c]$ ; ( $u_a = Q_{in}$ ,  $u_b = Q_{out}$ ,  $u_c = \Delta Q_l$ ).

$$y_3 = p_1 = [0 \quad 1 \quad 0] \cdot \begin{bmatrix} p_{knee} \\ p_1 \\ Q_{err} \end{bmatrix} = g_3(x, u) \quad (2.39)$$

#### **Case 4: Four states presentation**

With the structure of four wheels at each roller pump and the peristaltic movement of fluid inside the tube, it creates pulsation in pressure at the pump [27]. This might result in the turbulent flow as well as harmonic oscillators from wave frequency of fluid. These results influence on the actual flow and the pressure in the operation area. Therefore, the noise from wave induced motion of fluid should be filtered and reduced. Consulting from the citation [28], a noise-driven filter is appropriate used as a second order form as (2.40).

$$G_{filter}(s) = \frac{\omega_0^2 s}{s^2 + 2\zeta\omega_0 s + \omega_0^2} \quad (2.40)$$

where  $\zeta$  is damping coefficient; and  $\omega_0$  is undamped natural frequency.

By considering  $\dot{\eta} = \psi$  as the first order presentation of wave-induced motion, then the following equations can be presented in differential expressions:

$$\dot{\eta} = \psi \quad (2.41)$$

$$\dot{\psi} = -\omega_0^2 \eta - 2\zeta\omega_0 \psi + \epsilon_1 \quad (2.42)$$

where  $\epsilon_1$  is represented to the Gaussian white noise.

Combining the states of  $p_{knee}$  from (2.33) and  $Q_{err}$  together with the expressions of (2.41) and (2.42), a vector of four state variables is  $x = [\eta \ \psi \ p_{knee} \ Q_{err}]^T$ ; and a state space presentation in nonlinear process is completely presented in (2.43).

$$\dot{x}_{(4states)} = \begin{bmatrix} \dot{\eta} \\ \dot{\psi} \\ \dot{p}_{knee} \\ \dot{Q}_{err} \end{bmatrix} = \begin{bmatrix} \psi \\ -\omega_0^2 \eta - 2\zeta\omega_0 \psi + \epsilon_1 \\ \frac{1}{C_{knee}} \cdot (Q_{in} - Q_{out} - Q_{err}) + \epsilon_2 \\ 0 + \epsilon_3 \end{bmatrix} = f_4(x, u, \epsilon) \quad (2.43)$$

where: input  $u = [u_a; u_b]$ ; ( $u_a = Q_{in}$ ,  $u_b = Q_{out}$ );  $\epsilon$  represents to the process noise.

Variable  $\psi$  is defined as an additionally dynamic element of pressure from the roller *pump1* via the tube into the knee model. Hence, (2.28) is entirely rewritten in (2.44) with the variable  $\psi$  added.

$$p_1 = p_{knee} + R_1 \cdot Q_{in} + \beta \cdot Q_{in}^2 + \psi \quad (2.44)$$

The output equation is presented in (3.45) whereas  $v$  stands for the measurement noise.

$$y_4 = p_1 = [0 \quad 1 \quad 1 \quad 0] \cdot \begin{bmatrix} \eta \\ \psi \\ p_{knee} \\ Q_{err} \end{bmatrix} = g_4(x, u) + v \quad (2.45)$$

## 2.4 Hardware interfaces in MIS

It is worth mentioning that the author's research could not be completed without the presence of hardware interfaces support, especially the hardwares of In/Out interface and the HIL-Simulator which are going to be introduced as following. Firstly, the Input/Output hardware interface is used to communicate and convert signals between the programs or softwares, simulink package from the computer to the actuators of the hardware simulator in real-time execution. Secondly, the HIL-Simulator is utilized for the applications of providing some parameters like physical behaviors from a part of a human body in simulation loops.

### 2.4.1 Input/Output hardware interface as a target computer

The operation of the Input/Output (I/O) hardware interface can be generally described in Fig. 2.20 with the block of '*Target computer*' in the middle. This is a product of MicroLabBox implemented in this thesis. This '*Target computer*' is a compact designed platform of development I/O interface system for the laboratory use [29].

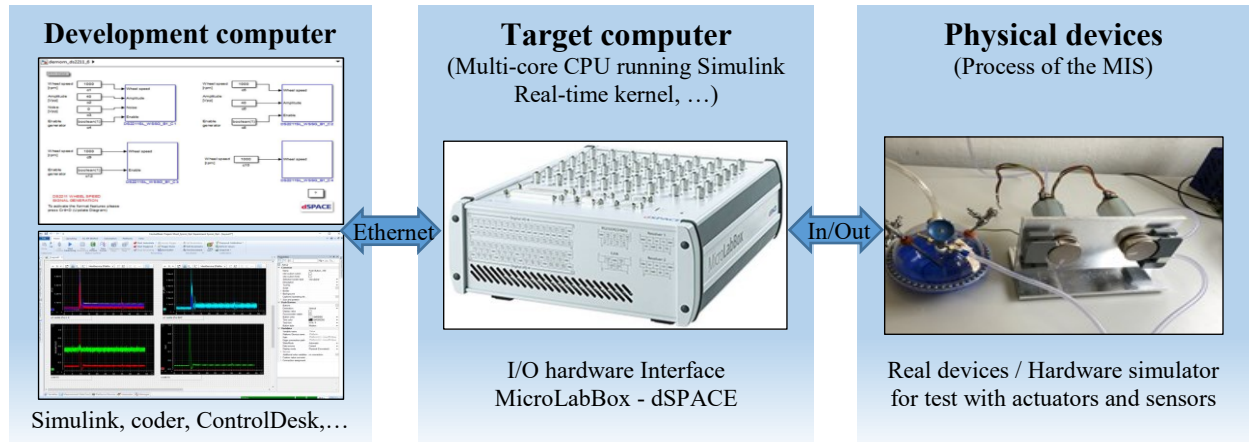


*Fig. 2.20 I/O interface connection between the development computer and physical devices*

MicroLabBox is used to implement data acquisition applications efficiently for both industry and academia. The programs or Simulink blocks, coders, controllers from the '*Development computer*' shall be compiled and downloaded to the target computer for the execution via Ethernet protocol. The I/O signals compiled from the programs can be converted by the DAC from the target computer transporting to the '*physical devices*'. *Physical devices* include the actuators like DC motors, roller pumps, air pump, and so on. While running the program, some feedback signals from *physical devices* can be converted from analog to digital signals by the ADC of the I/O hardware interface. These converted data shall be sent back to the development computer for analyzing, processing, or displaying data. The programs installed in the development computer such as MATLAB, dSPACE ControlDesk are typical softwares using for the interaction between user programs and physical devices. In this thesis, the author has utilized softwares of MATLAB

2017a and dSPACE ControlDesk 6.1 which are supported for working with MicroLabBox-dSPACE products.

The hardware interface of MicroLabBox has been chosen for the communication in this research for some beneficial features: high computing power and fast I/O, easy wiring, autonomous use, comprehensive and user-friendly software [29].

### ***High Computing Power and Fast I/O***

This hardware interface offers a 2 GHz dual-core real-time processor with fast closed-loop cycle times of less than 15  $\mu$ s. The integrated Field-programmable gate array (FPGA) can be utilized in high-speed computation for some cases of extremely fast control applications. The FPGA technology allows for parallel, exact and fast I/O processing. MicroLabBox provides over 100 I/O interfaces of not only conventional types (analog I/O and digital I/O) but also features specialized interfaces like Ethernet, Controller area network (CAN), and position encoders. In addition, the integrated sensor supply from MicroLabBox provides power for sensors without any additional laboratory devices.

### ***Easy Wiring***

MicroLabBox is available with two types of panel variants for flexible choices: The top-panel variant which is being used in this thesis provides BNC connectors (Bayonet Neill-Concelman), making wiring easy in a laboratory desk. Another type is the front-panel variant which offers D-sub connectors. This type is preferred for integrating MicroLabBox in a stack of laboratory devices. The connector information is printed on each MicroLabBox including the I/O blockset for the implementation software.

### ***Autonomous Use***

This device can be used with or without a host PC. In autonomous mode, without the host PC like in the case the author uses, the real-time application is loaded from the on-board flash memory when MicroLabBox is started. A set of programmable LEDs give status information of the real-time application to the user.

### ***Comprehensive and User-Friendly Software***

MicroLabBox is supported by a dSPACE software package including Real-Time Interface (RTI) for model-based I/O integration into MATLAB Simulink and dSPACE ControlDesk. Many graphical instruments in the ControlDesk software are available for the real-time application variables and parameters during run time. In integrating with MATLAB Simulink, the related blocksets can be used for the simulations and connections with the device of MicroLabBox.



## 2.4.2 Hardware-in-the-Loop simulator

Hardware-in-the-Loop simulator is a combination between the structure of a physical interface and a software model with some related actuators working together to simulate circularly some states of a process. In this stage of research for designing, the HIL-Simulator has been constructed to replace the real parts of a human being. From the authors' idea in the citations of [1] and [7] that focused on the improvement for the MIS equipments, the HIL-Simulator in MIS was established to mimic some physiological behaviors of the patient for the test and validation in laboratory. This is really helpful since the real patient is not allowed in clinical trials for the reasons of safety.

The structure of the HIL-Simulator in MIS for the replacement of the behaviors from the parts of body was simplified in Fig. 2.21. It consists of a software model, actuators, a physical interface interacting to the therapy device, and some sensors for feedback data [7].

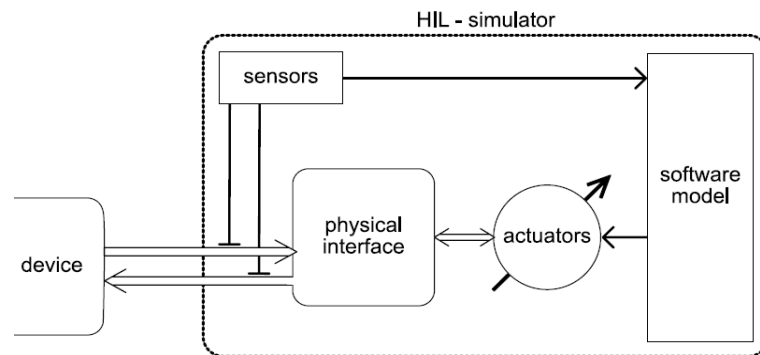


*Fig. 2.21 Simplified description of the HIL-Simulator in MIS [7]*

The operation of the loop is performed iteratively with the simulated state from the software model. This state is interacted with the therapy device tested via the realization of the physical interface and the manipulation of the actuators. The information from the sensors is helpful for a feedback data to the software model. The software model performs some calculations and reproduce some physiological state in the loop. In this thesis, the physical interface is simulated as the knee joint.

### ***Software model***

The function of the software model is to produce physiological state like the behavior of the real part of the patient's body. This software model plays a central role as a flexible module of the HIL-Simulator for controlling the actuators. By changing algorithms and suitable formulas in calculations, the software model can be programed to simulate various physiological states in different parts of the body being investigated in the MIS.

In this research of the knee arthroscopy, the software model was programed to reproduce some dynamic behaviors like the knee of the patient during MIS. In this case, the software model behaves

like the state of current pressure in the knee joint during arthroscopy. And some related equations referring to the knee model from (2.11) to (2.23) were used similarly for the calculations in the programmed software model. Additionally, for the simulation of the knee angle flexions with the pressure changes, the software model of the knee also needs to calculate and reproduce some parameters related to the behavior of the knee flexions. These parameters (indicated by the pressure signals  $p^*$  and  $p^{**}$  in Fig. 2.22) make activation to the actuators interconnecting to the physical interface during arthroscopy. More details for the simulation and parameters are based on features presented in the previous section of 2.3.6 with the correlated equations of (2.29) and (2.30).

### **Physical interface**

Physical interface of the HIL-Simulator is a kind of hardware model that realizes the behaviors and states from the software model. In the knee arthroscopy, this physical interface was constructed for realization parameters like the real patient's knee. And a plastic ball which is shown in Fig. 2.14 as an air/liquid reservoir was used for modelling the physical interface of the knee. The description in Fig. 2.21 is realized with some more details in Fig. 2.22. The therapy device which interacts with the physical interface of the HIL-Simulator is the double roller pump.

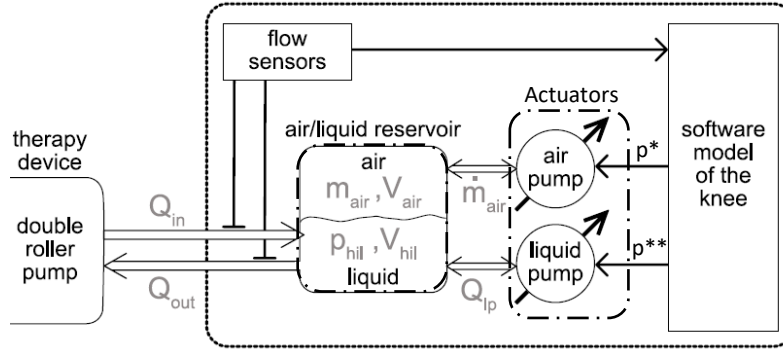


*Fig. 2.22 Signal and states in the HIL-Simulator [7]*

In Figure 2.22,  $Q_{in}$  stands for the inflow of liquid into the reservoir; and  $Q_{out}$  denotes to outflow of liquid from the reservoir. With the assumption of the ideal gas equation like in (2.16) for the reservoir filled with a combined volume of air and liquid, the relationship between the pressure in the HIL-Simulator  $p_{hil}$  and the volume of air  $V_{air}$  can be rewritten in (2.46).

$$p_{hil} \cdot V_{air} = m_{air} \cdot R_{air} \cdot T_{air} \quad (2.46)$$

By assuming an isothermal process inside the reservoir, the equation (2.46) leads to the derivative form of the pressure  $p_{hil}$  in (2.47).

$$\dot{p}_{hil} = \frac{(\dot{m}_{air} \cdot R_{air} \cdot T_{air}) - (p_{hil} \cdot \dot{V}_{air})}{V_{air}} \quad (2.47)$$

where the change of air volume  $\dot{V}_{air}$  inside the reservoir is provided by (2.48).

$$\dot{V}_{air} = Q_{out} - Q_{in} - Q_{lp} \quad (2.48)$$

The parameter of  $Q_{lp}$  is a kind of liquid flow from the actuator (called liquid pump) of the HIL-simulator.

The equations (2.47) and (2.48) show that the pressure  $p_{hil}$  in the reservoir or in the knee model can be controlled by the actuators (via  $\dot{m}_{air}$  of the air pump or via  $Q_{lp}$  of the liquid pump) independently with the interaction of the therapy device DRP.

### Actuators

As described in Fig. 2.22, there are two types of actuators that can be used to activate the change of air ( $\dot{m}_{air}$ ) or activate the liquid flow ( $Q_{lp}$ ). Those actuators are the air pump and the liquid pump. The output signal from the *software model of the knee* provides to the air pump or the liquid pump for a suitable value of  $\dot{m}_{air}$  or  $Q_{lp}$  respectively. This makes an influence to the pressure in the reservoir definitely. Any change of pressure from the reservoir is updated instantly by the software model via the information from the sensors block.

In this research, the air pump was selected for the actuator of the air change influencing to the behavior of the knee model. An overview of the air pump configuration is presented in Fig. 2.23 with a combination of a pneumatic piston drive and a proportional directional control valve connected to the air compressor [7]. From this configuration, both the piston drive and the bidirectional valve with the air compressor are connected to the same physical interface of the HIL-Simulator for controlling the pressure  $p_{hil}$ . Therefore, the usage of piston drive and the usage of controllable electric valve are selective options for pressure control. In experiments, the author chose the air compressor for the air pump actuator with the usage of controllable electric valve.

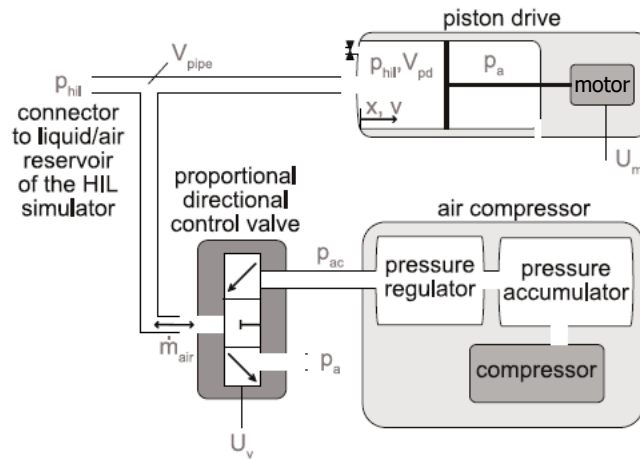


Fig. 2.23 Configuration of the air pump actuator of the HIL-Simulator [7]

In the first option of using piston drive, the pressure of the HIL-Simulator is controlled by the movement of the piston. By controlling the piston drive via a given value of voltage  $U_m$  to the motor, the change of pressure is generated into the reservoir. The operation principle of the piston drive is based on the pneumatic volume variation. It is supposed that there exists two parameters of pressure  $p_{hil}$  and  $p_a$  in the chamber of the piston drive as indicated in Fig. 2.22 ( $p_a$  is the ambient pressure). The variables of  $x$  and  $v$  are represented to the position and the velocity of the piston respectively. These variables can be controlled by providing the signal  $U_m$  to the electric drive of the motor.

Referring from the principle of the Newton's Second Law, the motion equation of the piston is formulated in (2.49).

$$m_r \cdot \ddot{x} = F_m - F_f(v) - F_p \quad (2.49)$$

The driving force  $F_m$  is proportional to the controlled motor voltage  $U_m$ . The function of  $F_f(v)$  is nonlinear and dependent on the speed of motor combined with the engine friction, the coupling and the sealing of the piston drive chamber. Parameter  $F_p$  is the acting force on the piston surface  $A_p$  when the pressure  $p_{hil}$  is different from the ambient pressure  $p_a$ . The value  $m_r$  denotes to the total mass of the system. The position 'x' is defined by (2.50) whereas  $\alpha$  is the rotation factor of the motor, and  $k_{pitch}$  is the spindle pitch of the piston.

$$x = \alpha \cdot \frac{k_{pitch}}{2\pi} \quad (2.50)$$

$$F_m = a_1 \cdot U_m ; (a_1 \text{ is a proportional factor}) \quad (2.51)$$

$$F_p = A_p \cdot (p_{hil} - p_a) \quad (2.52)$$

It should be noted that the resistance between the piston drive chamber and the reservoir was minimized by mechanical design. This leads to the change of pressure  $p_{hil}$  instantly when the volume of the piston drive  $V_{pd}$  is changed. The pneumatic part of the piston drive is now considered as a part of pneumatic reservoir with an additive volume of  $V_{pd}$ . Referring to the equation (2.47) with this additive volume (and the mass of air  $m_{air}$  is a constant), then the variable of  $\dot{p}_{hil}$  is now formed by (2.53).

$$\dot{p}_{hil} = \frac{-p_{hil}(\dot{V}_{air} + \dot{V}_{pd})}{V_{air} + V_{pipe} + V_{pd}} \quad (2.53)$$

The parameter  $V_{pipe}$  is the volume of the pipe connected between the the piston drive chamber and the reservoir. This pipe was designed to ensure the pneumatic resistance minimized. The value of  $V_{pd}$  is defined by piston position  $x$  and the piston surface  $A_p$ .

$$V_{pd} = A_p \cdot x \quad (2.54)$$

The change of piston drive volume is determined by the surface  $A_p$  and the piston velocity  $v$ .

$$\dot{V}_{pd} = A_p \cdot \dot{x} = A_p \cdot v \quad (2.55)$$

In summary, the combination of the piston drive and the air/liquid reservoir for pressure control can be formulated in nonlinear state space presentation of (2.56).

$$\begin{bmatrix} \dot{v} \\ \dot{x} \\ \dot{p}_{hil} \\ \dot{V}_{air} \end{bmatrix} = \begin{bmatrix} \frac{-F_f(v) - A_p \cdot (p_{hil} - p_a)}{m_r} \\ v \\ \frac{-p_{hil} \cdot (\dot{V}_{air} + A_p \cdot v)}{V_{air} + V_{pipe} + A_p \cdot x} \\ Q_{out} - Q_{in} - Q_{lp} \end{bmatrix} + \begin{bmatrix} \frac{a_1}{m_r} \\ 0 \\ 0 \\ 0 \end{bmatrix} \cdot U_m \quad (2.56)$$

In the second option of using proportional bidirectional electric valve with the air compressor, the air mass flow is used to interact and control the pressure  $p_{hil}$  of the HIL-simulator. As described in the lower part of Fig. 2.23, a bidirectional controllable electric valve is combined with the air compressor pump to generate an air mass flow to the air/liquid reservoir. By controlling the air mass flow direction via the voltage value  $U_v$  given to the valve, the pressure in the reservoir is also controlled correspondingly. With the setting of  $U_v$ , the valve can be controlled in one of the three possibilities: closed valve, opened airway from the pressure accumulator to the air/liquid reservoir, or opened airway from the air/liquid reservoir to the ambient air.

The air compressor was used to generate a high level of pressure in the pressure accumulator. Because this high pressure level might vary between the lower and the upper limit in the accumulator, therefore it is necessary to install the pressure regulator for producing the constant pressure  $p_{ac}$  at the defined level.

As described from the citation [7], the air mass flow is determined by (2.57) depending on the parameters: flow cross-section  $A_a$ , pneumatic conductance of the valve  $c_a$ , and the valve specific critical pressure ratio  $b_a$ .

$$\dot{m}_{air} = A_a \cdot c_a \cdot p_{v1} \cdot \begin{cases} 1 & ; if \frac{p_{v2}}{p_{v1}} < b_a \\ \sqrt{1 - \left( \frac{\frac{p_{v2}}{p_{v1}} - b_a}{1 - b_a} \right)^2} & ; if b_a \leq \frac{p_{v2}}{p_{v1}} \leq 1 \end{cases} \quad (2.57)$$

with

$$p_{v1} = \begin{cases} p_{hil} & ; if U_v > 0 \\ p_a & ; if U_v \leq 0 \end{cases} \quad (2.58)$$

$$p_{v2} = \begin{cases} p_{ac} & ; if U_v > 0 \\ p_{hil} & ; if U_v \leq 0 \end{cases} \quad (2.59)$$

$$A = \begin{cases} U_v \cdot A_{max} & ; \text{if } U_v > 0 \\ -U_v \cdot A_{max} & ; \text{if } U_v < 0 \\ 0 & ; \text{if } U_v = 0 \end{cases} \quad (2.60)$$

The parameters of pressure  $p_{v1}$  and  $p_{v2}$  represent to the pressure before and behind the valve respectively. The flow cross-section  $A_a$  will be equal to the nominal value  $A_{max}$  when the valve is completely opened.

In experiments of the research, the valve model was also validated from the measurements. As indicated in Fig. 2.23, the air mass flow  $\dot{m}_{air}$  was integrated to the physical interface of the HIL-Simulator within the part of pneumatic piston drive. Hence, the parameter of  $\dot{m}_{air}$  indicated in (2.57) needs be updated from both equations of (2.47) and (2.53).

$$\dot{p}_{hil} = \frac{(\dot{m}_{air} \cdot R_{air} \cdot T_{air}) - p_{hil} \cdot (\dot{V}_{air} + A_p \cdot v)}{V_{air} + V_{pipe} + A_p \cdot x} \quad (2.61)$$

Noting that the the value pressure  $p_{hil}$  is similar to the value of pressure in the knee model  $p_{knee}$ .

### **Sensors**

The block sensors of the HIL-Simulator (Fig. 2.21 as well as Fig. 2.22) indicates the feedback data providing to the software model of the knee for the update of the reproduced states. In this case, the flow sensors were used to measure the flows  $Q_{in}$  and  $Q_{out}$  which were interacted between the air/liquid reservoir and the therapy device. Those measurements provide helpful information for the calculation and reproduction of the appropriate states at each loop of operation.

In experiments, the flow sensors type *Sonoflow CO.55* were used for the measurements of flows. The advantages from using this type of flow sensor are non invasive contact and high accuracy (under 2% of measurement error).

Figure 2.24 is an overview of the air pump actuator (structured with electric valve and air compressor module) integrated in the HIL-Simulator which was implemented in real-time experiments of the research.

On the other side, as mentioned in section 2.3.6, the behavior of the knee angle flexion from the patient influences to the pressure change during arthroscopy. Hence, this behavior was also integrated in the software model to produce some cases of bending knee as some kinds of disturbance source for supervisory and control strategy. Therefore the controllable electric valve of the HIL-Simulator was also utilized for controlling and eliminating the disturbance source.

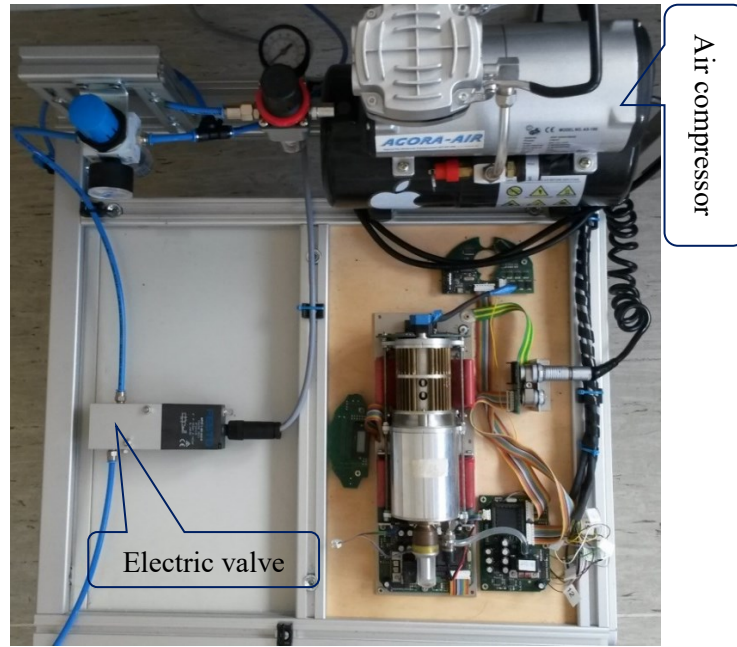


*Fig. 2.24 Actuators with electric valve and air compressor of the HIL-Simulator*

## 2.5 Summary

By this chapter, the author has introduced a general information as well as some basic procedures regarding to modelling of the process in the MIS. Especially, the module of the HIL-Simulator was constructed for the replacement of the real part of the human body in the MIS. For preparation of controller design and supervisor strategy, the modelling of the process in MIS was figured out and constructed for a physical device in real-time simulator. The mathematical equations and dynamic characteristics of the parts used in the MIS are meaningful for the construction of the process simulation in both MATLAB/Simulink and in real-time device simulator. Some various state space presentations of the knee arthroscopy were also presented for implementation and comparison of the results. These are useful for the pressure state estimation since the pressure in the operation area is unmeasurable with the real patient. In Chapter 3, strategy of controller design and supervisory algorithm are going to be presented next before coming to the Chapter 4 of pressure estimation in MIS.





### 3 CONTROLLER DESIGN AND SUPERVISOR STRATEGY

This chapter presents the concepts of controller design and supervisor strategy for the development of the medical device applications in the MIS process. Based on the modelling of the process in Chapter 2, the controller is designed for the desired pressure in the knee model during arthroscopy. This is to ensure a suitable expansion for a clear vision and to reduce the situations of fluid depletion or haemorrhage. In addition, some cases of disturbances from the outflow changes or from the knee flexions which might occur during MIS are also mentioned for supervising and eliminating in the controlled process. From the identified process, the Proportional Integral (PI) controller based on Symmetric Optimum (SO) method (called PI\_SO controller) was designed and implemented. To control the problem of windup phenomenon in the nonlinear process, some optional anti-windup algorithms were proposed to integrate to the designed controller.

#### 3.1 Introduction

The whole controlled and supervised system is configured in Fig. 3.1. The desired pressure is provided from the signal  $p_{ref}$ . This value is considered as the reference of blood pressure from the patient. The goal of designing the controller and supervisor is to maintain the pressure in the knee joint  $p_{knee}$  close to the reference  $p_{ref}$ . By supervising the disturbance source from the signal  $d$ , the block of *controller and supervisor* performs generating the proper signal  $u_1$  for controlling the inflow of fluid. The signal  $d$  represents to the disturbance source. It might come from the outflow changes, or come from the situations of the knee angle changes. Both these changes take effect to the change of pressure  $p_{knee}$  significantly. The algorithm of the supervisor is to detect the disturbance source for eliminating this effect to the controlled pressure  $p_{knee}$ .

In the process of the knee arthroscopy, an *inner disturbance controller* is designed for the elimination of the pressure change from the disturbance of the knee angle change. When the disturbance is detected coming from the change of the knee angle, then this inner controller works and generates the control signal  $u_{val}$ . This signal controls the gas volume in the knee model in order to reduce the change of pressure  $p_{knee}$  suddenly. The *inner disturbance controller* block (dashed block in Fig 3.1) is in “Off” status if there is no disturbance from the knee flexion.

When the disturbance  $d$  is detected coming from the change of outflow, it is considered as the signal  $u_2$  that activates the motor  $M2$ . The control signal  $u_1$  is connected to the motor  $M1$  of the DRP for controlling the inflow regarding to the outflow automatically.

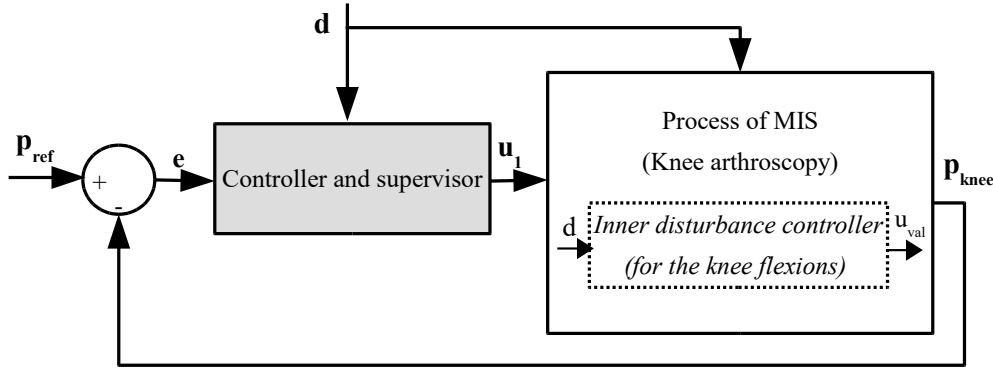


Fig. 3.1 Controller and supervisor strategy for the desired pressure in MIS

The supervisor is assembled to detect any appearance of the knee flexion. When a kind of the knee flexion is detected, then the *inner disturbance controller* will be switched to ‘On’ status. This is to eliminate the sudden change of unwanted pressure in the operation area. During this processing time of the *inner controller*, the principal *controller and supervisor* of the process is temporary switched to ‘*pause*’ status for safety to the patient.

### 3.2 PI controller based on Symmetric Optimum method

As mentioned above, the process of MIS need to be linearized and identified for the controller design. From the step response of the system in MATLAB Simulink, data for modelling can be validated by comparing to the measurement in real-time device simulator experiment. Figure 3.2 shows the response of the pressure in the knee model while providing  $u_2 = 0.25V$  in 5 seconds for the outflow (without any disturbance from the knee flexion); and  $u_1 = 0.25V$  in 10 seconds for providing the inflow into the operation area.

From the upper panel of the Fig. 3.2, in the first 5 seconds, the measured pressure  $p_{knee}$  should remain the same value. However the measurement from real-time device (in blue) from the upper panel of Fig. 3.2 was not probably close to the ideal result from Simulink (in red). This error can be reduced by calibrating the parameter of pressure sensor. In addition, the measured data seemed to be raised gradually by the first 5 seconds. This can be explained from a certain difference between the rotation speeds of the two motors in real-time (see the two measured voltage signals at the lower panel of Fig. 3.2). In the next 5 seconds (remaining only the inflow, no outflow), the pressure was increased rapidly. In the last 5 seconds, both the inflow and outflow were set to zero, then the measured pressure in real-time device had some loss compared to the Simulink result. This is normal in reality because of the nonlinearity of the process. This reduction of pressure might come from the loss of flows, or from the loss of gas in the closed model of the knee during operation.

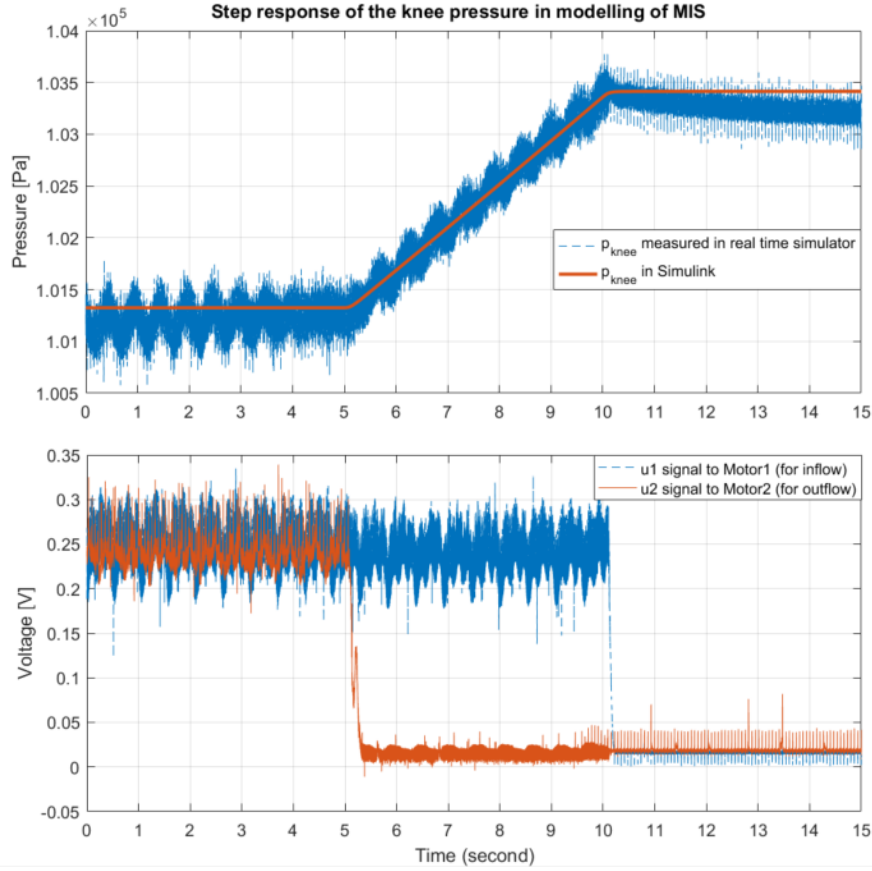


Fig. 3.2 Step response of pressure in the knee model (modelling and real-time)

With the response of the process in Fig. 3.2, the pressure in the knee model is formed as an exponential function. From the measured data in the real device experiment, the process was linearized and identified in (3.1) whereas  $\tau = T_d = 0.006s$  is the dead time. This value can be omitted since it is too small comparing to the time constant of  $T = 0.038s$ . The gain constant  $K = 83.1(Pa/V)$ .

$$G_p(s) = e^{-\tau s} \cdot \frac{K}{s(Ts+1)} \quad (3.1)$$

With this type of response in the process, the PI controller was proposed to design. PI controller is an alternative type from the Proportional Integral Derivative (PID) controller, without derivative element.

Normally, the structure of PID controller is described in Fig. 3.3 [30]. This controller has mathematical formula in (3.2) [31], [32], [33] which was developed over a hundred years ago, and it has been used effectively and widely in various fields of study until now [33].

$$G_{PID}(s) = K_P \left( 1 + \frac{1}{T_I \cdot s} + T_D \cdot s \right) \quad (3.2)$$

where  $K_P$  is proportional gain;  $T_I$  and  $T_D$  are the integral time and derivative time respectively.

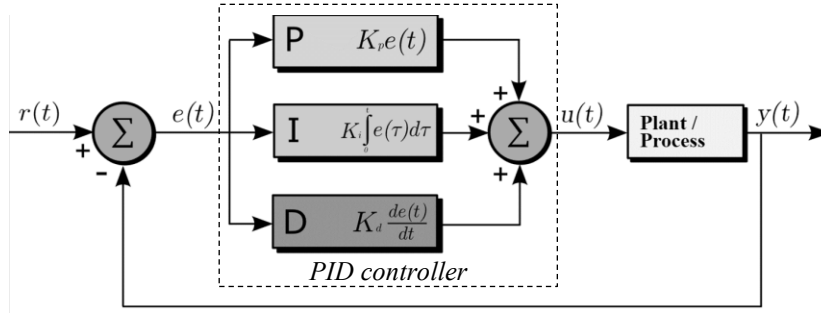


Fig. 3.3 Basic structure of PID controller [30]

The parameters in Fig. 3.3:  $K_I = \frac{K_P}{T_I}$  is the integral gain, and  $K_D = K_P \cdot T_D$  is derivative gain. In the PI controller, the gain  $K_D = 0$ . In this case, the PI controller is formed by (3.3).

$$G_{PI}(s) = K_P \left( 1 + \frac{1}{T_I \cdot s} \right) \quad (3.3)$$

On the other hand, based on the algorithm of Symmetric Optimum from the citations of [32], [33] and [34], the PI\_SO controller is formulated in (3.4). This algorithm is a method for selecting and tuning controller like the methods of analytical designs. This analytical method is performed with plenty options from parameters.

$$G_{PI\_SO}(s) = K_c \frac{(T_N \cdot s + 1)}{T_N \cdot s} \quad (3.4)$$

By comparing to (3.3), the parameters: proportional gain  $K_C = K_P$ ; and the integral time  $T_N = T_I$ .

The main feature of SO algorithm is to obtain the transfer function of the open loop controlled system close to the form of (3.5) according to [33], since the process of (3.1) is considered as the form of (3.6) by ignoring the parameter of dead time  $\tau$ . In addition, the Bode plot of the system is symmetrical around the crossover frequency  $\omega_c = \omega_0$ ; and the maximal phase response is also approached at the crossover frequency  $\omega_c$ .

$$G_{OL\_SO}(s) = \frac{\omega_0^2(2s + \omega_0)}{s^2(s + 2\omega_0)} \quad (3.5)$$

The process (3.1) can be written in (3.6) while the dead time  $\tau \approx 0$ .

$$G_p(s) = \frac{K}{s(Ts + 1)} \quad (3.6)$$

In fact, from the process (3.6), the transfer function of the open loop controlled process is shown in (3.7) which is simplified by the block diagram of Fig. 3.4.

$$G_{OL}(s) = \frac{Y(s)}{R(s)} = G_p(s) \cdot G_{PI\_SO}(s) = \left( \frac{K \cdot K_c}{T_N} \right) \cdot \frac{1}{s^2} \cdot (T_N \cdot s + 1) \cdot \frac{1}{(T \cdot s + 1)} \quad (3.7)$$

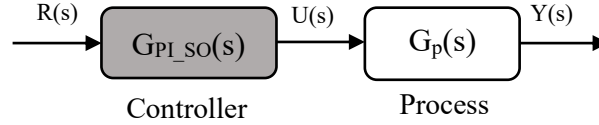


*Fig. 3.4 Simplified structure of the open loop controlled process*

The authors Holger Lutz and Wolfgang Wendt in [34] proved that the parameters of  $K_C$  and  $T_N$  in (3.4) are determined by (3.9) and (3.10) depending on the computed parameter 'a' in (3.8). The symbol  $\omega_c$  in (3.11) designates the crossover frequency of the process  $G_p(j\omega)$  in frequency domain.

The parameter 'a' is determined by the selection of the phase margin ( $PM$ ) called  $\varphi_R$  from the Bode diagram of the open loop controlled process. The value  $\varphi_R$  in this case is calculated by (3.11), according to the existed components of the transfer function in (3.7) [31], [32], [33], [34].

$$a = \frac{1 + \sin(\varphi_R)}{\cos(\varphi_R)} ; \text{ (with } a > 1 \text{)} \quad (3.8)$$

$$T_N = a^2 \cdot T \quad (3.9)$$

$$K_C = \frac{1}{a \cdot K \cdot T} \quad (3.10)$$

$$\varphi_R = \pi + \varphi(\omega_c) = \pi - \pi + \tan^{-1}(T_N \omega_c) - \tan^{-1}(T \omega_c) \quad (3.11)$$

In the frequency domain, (3.6) can be rewritten in (3.12). Likewise, (3.7) is rewritten in (3.13).

$$G_p(j\omega) = K \cdot \frac{1}{(j\omega)} \frac{1}{(T \cdot j\omega + 1)} \quad (3.12)$$

$$G_{OL}(j\omega) = \left(\frac{K \cdot K_C}{T_N}\right) \cdot \frac{1}{(j\omega)^2} \cdot (T_N \cdot j\omega + 1) \cdot \frac{1}{(T \cdot j\omega + 1)} \quad (3.13)$$

Figure 3.5 is an illustration of the linearized process  $G_p(j\omega)$  in frequency domain without controller. It can be seen that at the crossover frequency of  $\omega_c = 42.66$  rad/s, the phase margin  $\varphi_R$  is determined from the phase plot and (3.14). Gain margin ( $GM$ ) in this case is equally to  $+\infty$ dB.

$$\varphi_R = \pi + \varphi(\omega_c) = \pi - \frac{\pi}{2} - \tan^{-1}(T \omega_c) = 180^\circ - 90^\circ - 58.33^\circ = 31.67^\circ \quad (3.14)$$

From the possitive values of the gain margin and the phase margin, it is proved that the process is satisfied with the stability criteria in the closed loop controlled system.

In fact, the conditions of gain margin and phase margin for a stable response are formulated in frequency domain of (3.15 and 3.16).

Gain margin at the crossover frequency  $\omega_c$ :

$$M(G_{OL}(j\omega_c)) = 1 \Leftrightarrow \frac{K \cdot K_C}{T_N} \left( \frac{1}{(\omega_c)^2} \right) \left( \frac{\sqrt{(T_N \cdot \omega_c)^2 + 1}}{\sqrt{(T \cdot \omega_c)^2 + 1}} \right) = 1 \quad (3.15)$$

Phase margin at the crossover frequency  $\omega_c$ :

$$\left. \frac{d(\varphi_R)}{d(\omega)} \right|_{\omega=\omega_c} = \frac{T_N}{1+(T_N \cdot \omega_c)^2} + \frac{-T}{1+(T \cdot \omega_c)^2} = 0 \quad (3.16)$$

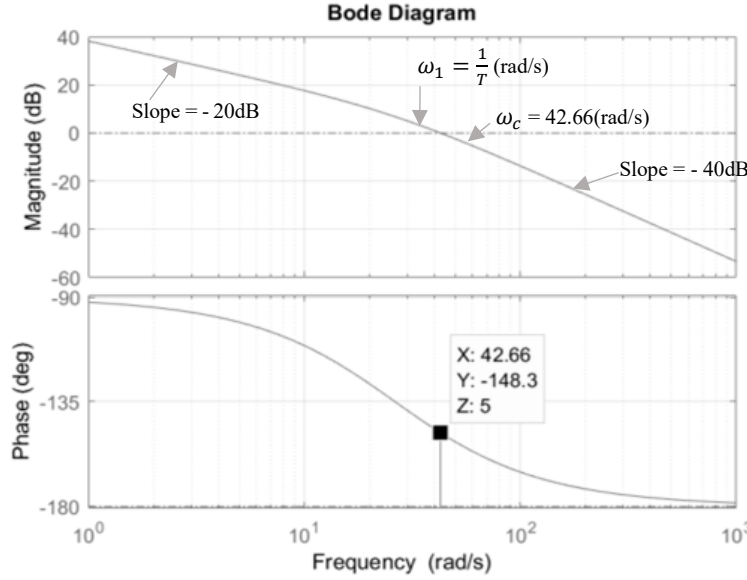


Fig. 3.5 Frequency response of the linearized process of  $G_p(j\omega)$

Definitely, with every value of  $T_N \neq T$ , the crossover frequency in (3.13) is computed by (3.17).

$$\omega_c = \frac{1}{\sqrt{T_N \cdot T}} \quad (3.17)$$

By substituting (3.8) and (3.17) into (3.15), it is proved that the proportional gain  $K_C$  of the controller is determined by (3.10).

In summary, the parameters  $K_C$  and  $T_N$  shall be changed when the phase margin  $\varphi_R$  is changed.

Combining the characteristics between the stability criteria in Bode plot and the equations of (3.8) and (3.9) for  $\varphi_R$  and  $T_N$  parameters, it is noted that the value  $T_N$  must be greater than the time constant  $T$  because of the compensation for a stable controlled process. From this point, therefore the phase margin should be chosen greater than  $31.67^\circ$ , and the upper limit is smaller than  $90^\circ$ .

Now the equation (3.6) can be rearranged generally as a form of second order expression in (3.18).

$$G_p(s) = \frac{1}{s} \cdot \frac{\frac{K}{T}}{\left(s + \frac{1}{T}\right)} = \frac{1}{s} \cdot \frac{\omega_n^2}{(s + 2\zeta\omega_n)} \quad (3.18)$$

where  $\omega_n$  is called the *undamped natural frequency*; and  $\zeta$  is the *damping ratio* of the process.

The three typical cases of choosing phase margin  $37^\circ$ ,  $60^\circ$ , and  $78^\circ$  are presented more details in the following sub-sections (from 3.2.1 to 3.2.3) for analyzing the quality of the controller.

The parameters of  $\omega_n$  and  $\zeta$  denote to the dynamic behavior of the process. With a typical second order form, the value  $\zeta$  is in the range of ( $0 < \zeta < 1$ ) in which the closed loop poles are complex conjugates and lie all in the left-half of 's' plane. And the controlled system has a little bit oscillatory response at the transient period (the system is underdamped). Otherwise, if the damping ratio  $\zeta > 1$ , then the controlled system is overdamped with the longer transient time in the step response [31]. When  $\zeta = 0$ , then system is oscillated periodically. These cases of variuos values of  $\zeta$  affecting to the behavior of a second order process in close loop control are presented in Fig. 3.6.

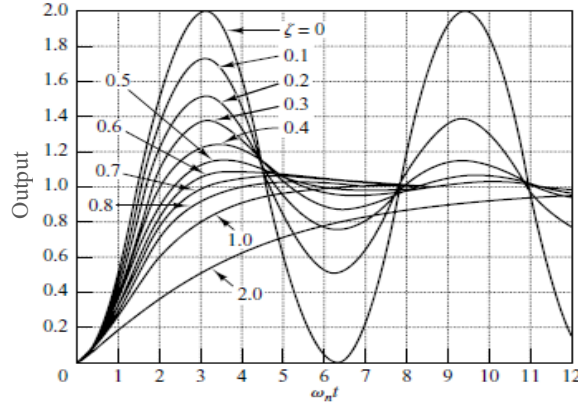


Fig. 3.6 Responses of a close-loop second order system regarding to various values of  $\zeta$  [31]

### 3.2.1 Analytical case of 37° in phase margin

In this case, parameters of PI\_SO controller are determined from the calculated parameter ' $a_{(37)}$ '.

$$a_{(37)} = \frac{1 + \sin(37^\circ)}{\cos(37^\circ)} \approx 2.006 \quad (3.19)$$

$$T_{N(37)} = a_{(37)}^2 \cdot T = (2.005)^2 \cdot 0.038 = 0.1529 \quad (3.20)$$

$$K_{C(37)} = \frac{1}{a_{(37)} \cdot K \cdot T} = \frac{1}{2.005 \times 81.3 \times 0.038} = 0.1614 \quad (3.21)$$

$$\omega_{c(37)} = \frac{1}{\sqrt{T_{N(37)} \cdot T}} = \frac{1}{\sqrt{0.1529 \times 0.038}} = 13.12 \quad (3.22)$$

The Bode plot of the open-loop controlled process with the PI\_SO controller compensated is depicted in Fig. 3.7. It is obvious that when the integral time is greater than the time constant  $T$  of the process, then the value of  $\omega_c$  is adjusted to the left side (smaller) compared to the original process Bode plot in Fig. 3.5. In addition, the phase plot is maximized and symmetrical at the frequency  $\omega_{c(37)}$ . With the presentation of the integral  $\left(\frac{1}{j\omega}\right)$  element and the derivative element  $(T_N \cdot j\omega + 1)$  in (3.13), so the slope on the magnitude plot has been adjusted as in Fig. 3.7 at two corner frequencies:  $\omega_{N(37)} = \frac{1}{T_{N(37)}}$  and  $\omega_1 = \frac{1}{T} = 26.3$  (rad/s).

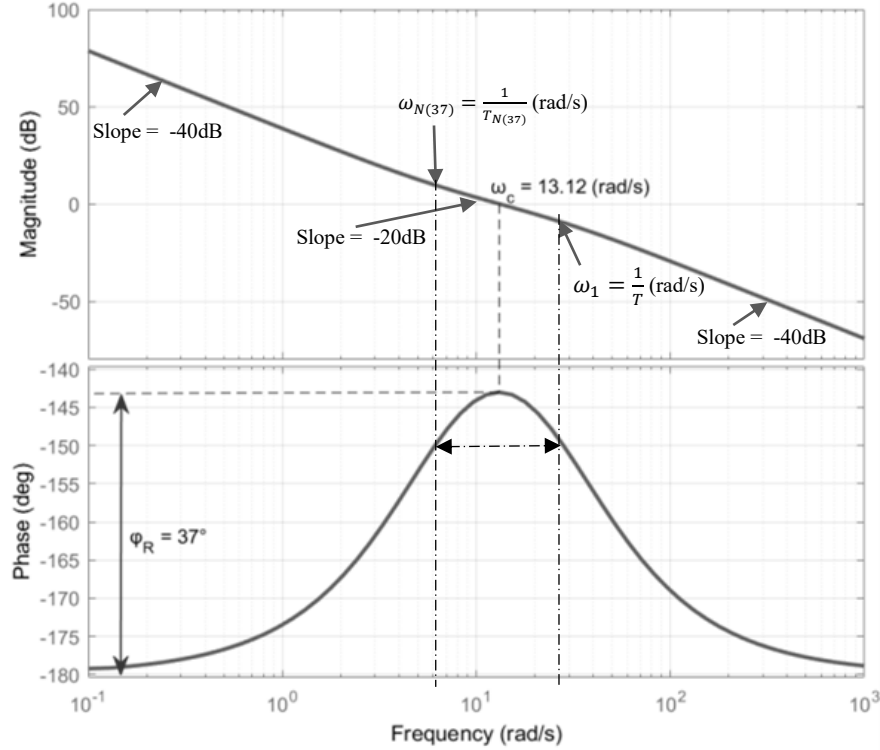


Fig. 3.7 Frequency response of the open loop controlled process  $G_{OL}(j\omega)$  with  $\varphi_R = 37^\circ$

From the upper plot of Fig. 3.7, the slope is started at -40dB, then adjusted to -20dB at  $\omega_{N(37)}$ , and finally adjusted to -40dB at  $\omega_1$ .

### 3.2.2 Analytical case of $60^\circ$ in phase margin

With the selection of phase margin  $\varphi_R = 60^\circ$ , the frequency response of the open-loop controlled process (3.13) has some changes as shown in Fig. 3.8. The parameters of the PI\_SO controller in this case are calculated from (3.23) to (3.26) and summarized in Table 3.1.

$$a_{(60)} = \frac{1 + \sin(60^\circ)}{\cos(60^\circ)} \approx 3.732 \quad (3.23)$$

$$T_{N(60)} = a_{(60)}^2 \cdot T = 0.5293 \text{ (sec.)} \quad (3.24)$$

$$K_{C(60)} = \frac{1}{a_{(60)} \cdot K \cdot T} = 0.0867 \quad (3.25)$$

$$\omega_{c(60)} = \frac{1}{\sqrt{T_{N(60)} \cdot T}} = 7.05 \text{ (rad/s)} \quad (3.26)$$

It should be noted that the value of the corner frequency  $\omega_1 = \frac{1}{T}$  is unchanged for all cases of phase margin selection, because  $T$  is the time constant of the process. On another side, the corner frequency  $\omega_N$  and the crossover frequency  $\omega_c$  are changed depending on the phase margin selected.



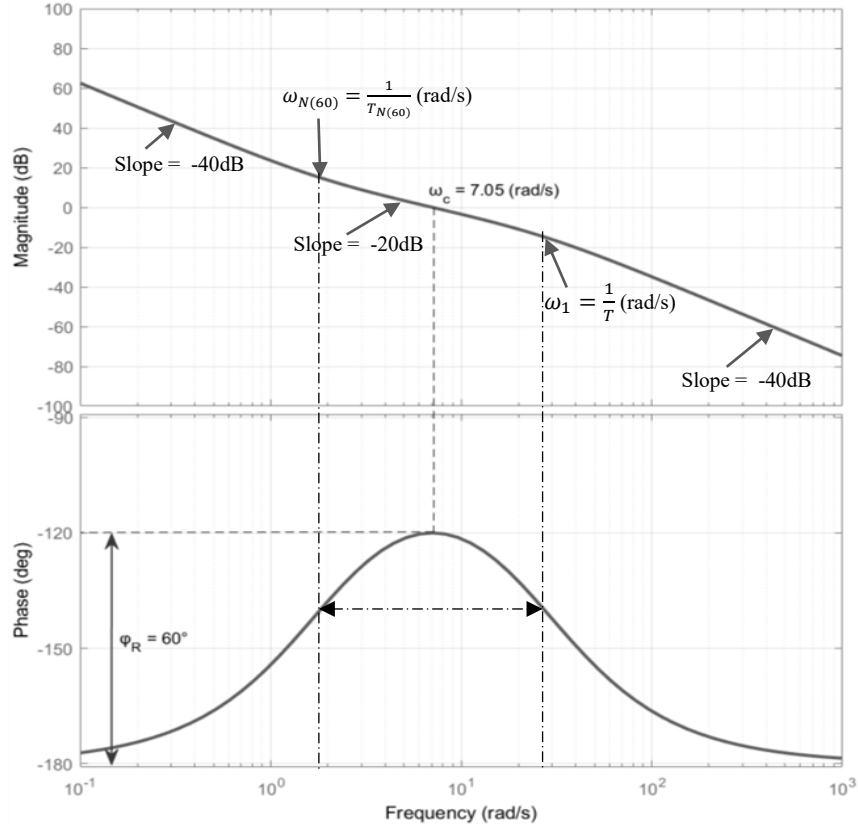


Fig. 3.8 Frequency response of the open loop controlled process  $G_{OL}(j\omega)$  with  $\varphi_R = 60^\circ$

The phase plot is now maximal and symmetrical at another point of the frequency  $\omega_{c(60)}$ .

### 3.2.3 Analytical case of $78^\circ$ in phase margin

With the phase  $\varphi_R = 78^\circ$ , the frequency response of the process (3.13) is shown in Fig. 3.9. The parameters of the PI\_SO controller are computed in (3.27)-(3.30) and summarized in Table 3.1.

$$a_{(78)} = \frac{1 + \sin(78^\circ)}{\cos(78^\circ)} \approx 9.514 \quad (3.27)$$

$$T_{N(78)} = a_{(78)}^2 \cdot T = 3.4399 \text{ (sec.)} \quad (3.28)$$

$$K_{C(78)} = \frac{1}{a_{(78)} \cdot K \cdot T} = 0.034 \quad (3.29)$$

$$\omega_{c(78)} = \frac{1}{\sqrt{T_{N(78)} \cdot T}} = 2.77 \text{ (rad/s)} \quad (3.30)$$

From the three cases of Bode diagrams in Figures 3.7, 3.8, and 3.9, it can be seen that increasing the phase margin makes the corner frequency  $\omega_N$  to be decreased ( $\omega_{N(78)} < \omega_{N(60)} < \omega_{N(37)}).$  Similarly, the crossover frequency is also decreased when the phase margin is increased. These cases can be generally summarized in Fig. 3.10.

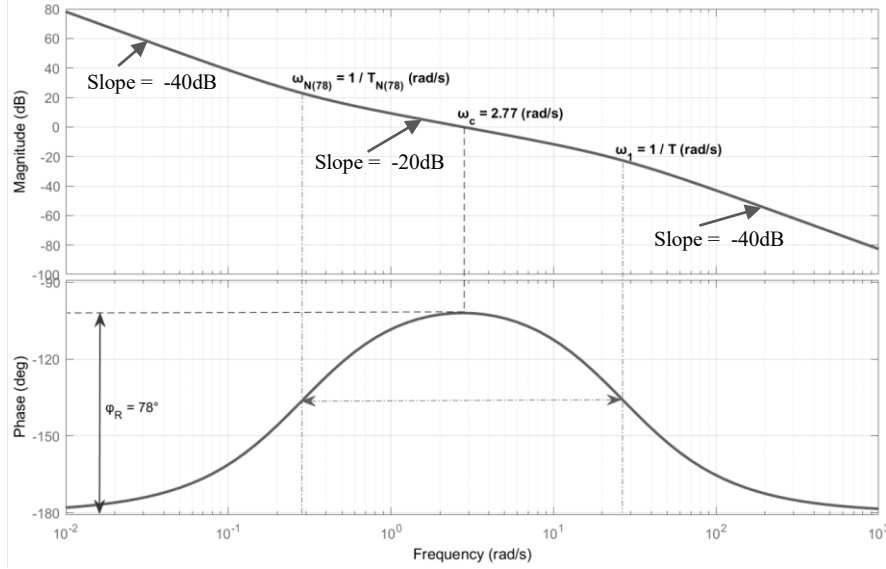


Fig. 3.9 Frequency response of the open loop controlled process  $G_{OL}(j\omega)$  with  $\varphi_R = 78^\circ$

In summary, the linearized process has the form of (3.6) or (3.18) as a special case of the second order form of transfer function. Therefore, the PI\_SO controller was proposed to design in this research [33]. While doing tests with different parameters of phase margin  $\varphi_R$  and damping ratio  $\zeta$  for analyzing quality of the controller in MATLAB Simulink, it is interest to note that the response of the controlled system gave the high overshoots when chosing  $0.5 \leq \zeta \leq 1$  or  $37^\circ \leq \varphi_R < 60^\circ$ . The results of simulation and calculated parameters are summarized in Table 3.1. Noting that the parameters of settling time and overshoot in the last column of Table 3.1 were determined from the results in Simulink with the identified process of (3.6).

Comparing from the three typical cases of phase margin presented in Fig. 3.10, it is worth mentioning that the more the phase margin (or the integral time of the PI controller) is increased, the more the crossover frequency  $\omega_c$  as well as the corner frequency  $\omega_N$  is decreased.

From the parameters and results in Table 3.1, with the value of  $\zeta \leq 1$  (or  $\varphi_R < 60^\circ$ ), the settling time is beneficially reduced less than one second. But the problem is that the overshoot is still so high (more than 20%). These cases of  $\varphi_R < 60^\circ$  are not suitable for pressure control in the real patients of MIS, because the high overshoot of pressure can cause the damage to the patients.

On the other side, with the value of  $\zeta > 1$ , the overshoot is more reduced when the phase margin is more increased in the range of  $(60^\circ \leq \varphi_R \leq 78^\circ)$ . But while increasing the value  $\varphi_R$ , the settling time takes longer. Particularly in the case of  $\varphi_R = 78^\circ$ , the settling time is a little bit slow about 3.4 seconds even though the overshoot is in beneficial point less than 8%. From the Simulink results which will be presented in the following sections, it should be better to choose the suitable parameters of the controller in the phase margin  $\varphi_R \approx 72^\circ$ .

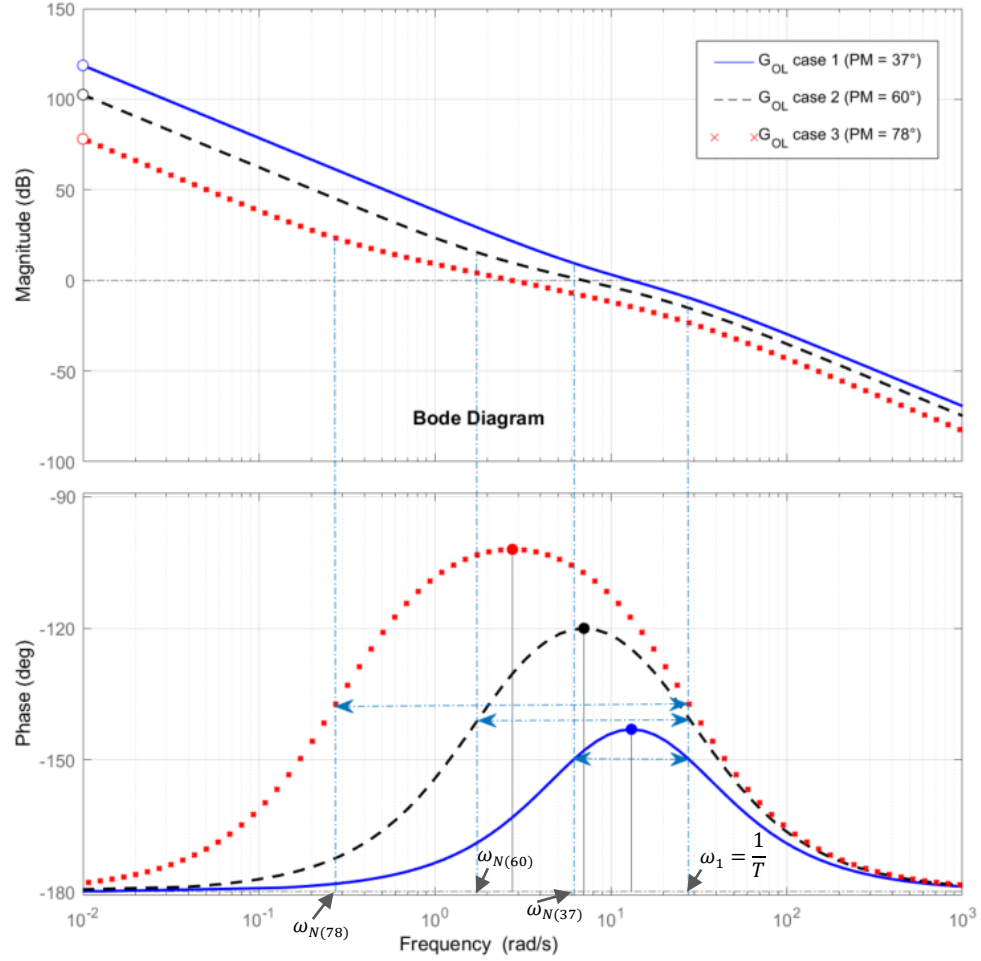


Fig. 3.10 Frequency responses of the open loop controlled process  $G_{OL}(j\omega)$  in 3 cases

Table 3.1 Parameters and results with the PI\_SO controller

Phase margin $\phi_R$ (degree)	damping ratio $\zeta$	Parameter of 'a'	$K_C$ gain	Integral time $T_N$ (sec.)	Crossover Frequency $\omega_c$ (rad/s)	Settling time / Overshoot (sec. / %) (based on identified process)
37°	$\approx 0.5$	2.006	0.1614	0.1529	13.12	0.60 / 49.80
45°	0.707	2.414	0.1341	0.2215	10.09	0.70 / 36.80
50.69°	0.9	2.8	0.1156	0.2979	9.4	0.75 / 29.40
53.13°	1	3	0.1079	0.342	8.77	0.80 / 26.90
<b>60°</b>	<b>&gt; 1</b>	<b>3.732</b>	<b>0.0867</b>	<b>0.5293</b>	<b>7.05</b>	<b>1.00 / 19.95</b>
<b>72°</b>	<b>&gt; 1</b>	<b>6.3138</b>	<b>0.0513</b>	<b>1.5148</b>	<b>4.168</b>	<b>1.50 / 11.08</b>
78°	> 1	9.514	0.034	3.4399	2.77	3.40 / 7.60

From those cases above, the PI\_SO controller of  $\phi_R = 72^\circ$  is optimized with the settling time around 1.5 second and the overshoot approximately around 10%.

It is important to state that the PI\_SO controller presented above was designed for a linearized process. In the real device simulator of the knee arthroscopy, the process is nonlinear. Therefore the windup phenomenon might happen by the integral part of the controller during the operation. An exceeded value from the controller might result in some faults to the actuators like the motors and risk to the patient. To deal with this problem, an algorithm of anti-windup needs to be integrated to the PI\_SO controller.

### **3.3 Anti-windup algorithm in PI controller**

Windup phenomenon is known as an integrating action which usually happens in integral terms like in the PID or PI controller of the system. During the operation, when the feedback data is not reached to the setpoint, then the controller acts to compensate the control signal of the process for reaching the desired output. While acting, the integrator of the controller might windup to an overload value rapidly. This causes some errors or faults to the two motors at the DRP or the controllable electrical valve. As a consequence of this, the error between the setpoint and the output of the system increases, because the control signal is not true to the desired limitation of the actuators. Hence in this research, it is necessary to implement an anti-windup algorithm to the PI\_SO controller of the nonlinear process in order to limit the rate of change in the control signal. There are some optional methods of anti-windup that can be applied in this research such as: conditional integration, anti-windup tracking by integral time, or back-calculation and tracking by the time constant of the process.

#### **3.3.1 Conditional integration**

This algorithm of anti-windup is considered as the case of switching ‘*On-Off*’ to the integrator. It is based on the conditions of two logical actions: the integral component in PI controller is functioned ‘*On*’ normally while the output of the controller is in the range of conditions; otherwise, the integrator is turned to ‘*Off*’ status when the output of the controller is winded up rapidly out of the limited range. This algorithm is illustrated in Fig. 3.11. Regarding to the characteristic of the DC motors to be controlled in the process of MIS, the condition range of control signal is from 0 to 5V. Therefore, the logical comparison blocks [ < ‘0’ ] and [ > ‘5’ ] are used for creating the logical output ‘*CO*’ signal in selecting signal to the integral term.

With the feature of ‘*On-Off*’ switching integrator regarding to the conditions, in literature from the citation [33], the disadvantage from this algorithm is that the control signal may get stuck at a non-zero control error while the integral term holds a big value by the time ‘*Off*’. Additionally, the transition time is occurred instantaneously. However, By implementing this method in modelling simulation as well as in real-time experiment, the author did not undergo this type of stuck.

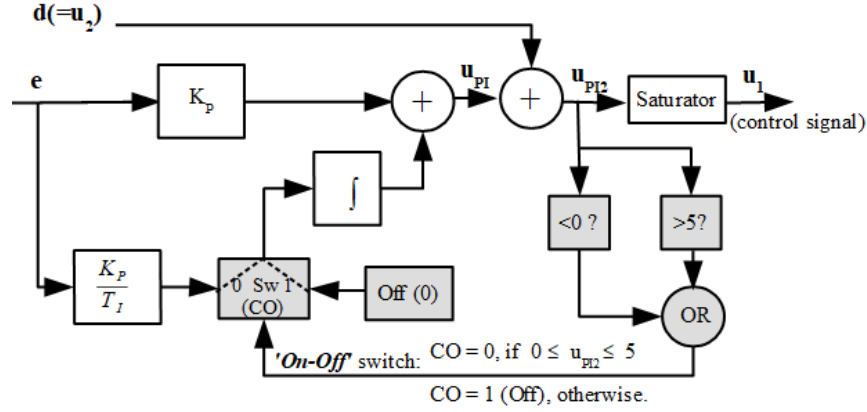


Fig. 3.11 Conditional integration algorithm integrated in PI controller

### 3.3.2 Anti-windup tracking by the integrating time

From the disadvantage of ‘On-Off’ switching instantaneously mentioned above, the method of *anti-windup tracking by the integrating time* can be applied. This algorithm is shown in Fig. 3.12 (a, b). In this case, the integral part is forced to assume other preload values during saturation [33].

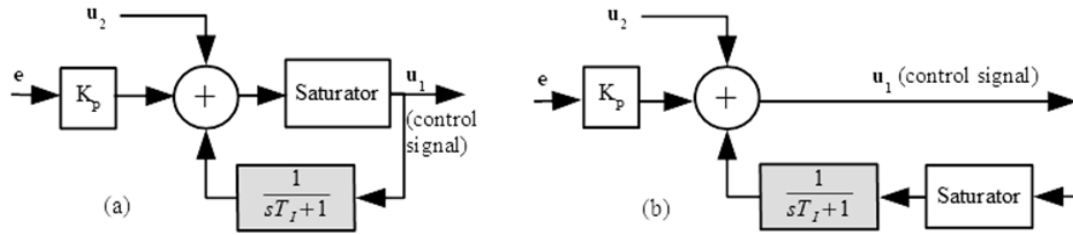


Fig. 3.12 Anti-windup tracking by integrating time in PI controller

The tracking time for anti-windup is the integral time of the PI controller. In addition, the *saturator* is incorporated with the integrating term to avoid windup circumstance. It does not make influence to the proportional part of the controller [32], [33]. The schematic (a) on the left side is different from the schematic on the right side by using the control signal  $u_1$  connecting to the actuators of the process. The saturator in Fig. 3.12 (a) will limit the control signal directly. This algorithm requires a good model of the physical saturation. The structure of Fig. 3.12 (b) is used as a modified version from structure (a) and it offers more flexibility [32], [33].

### 3.3.3 Back-calculation and tracking by the time constant

Referring to the citation of [33], a type of back-calculation algorithm is depicted in Fig. 3.13. In order to limit the control signal from the PI controller, a saturator is used for the guaranteed input of the actuators. The error between the input and the output of the saturator is then added to the integral term of the PI controller. This makes the controller to recompute the integral gain to a new value that can limit the windup phenomenon of the control signal. It is advantageous to use the

element of  $\frac{1}{T}$  in order to reset the integrator not instantaneously but dynamically by the time constant  $T$  of the process.

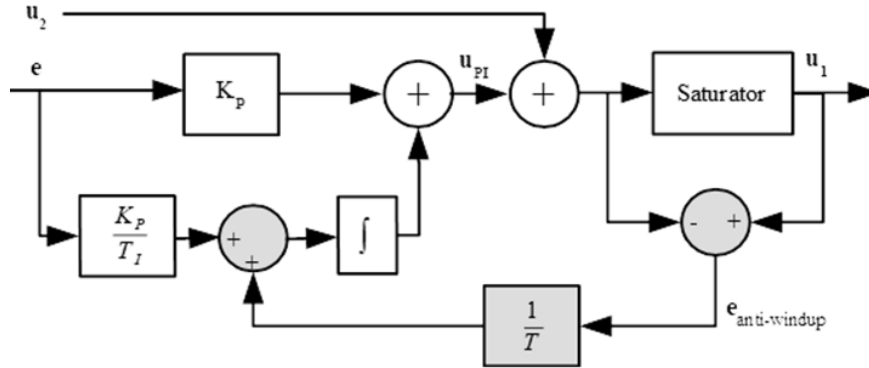


*Fig. 3.13 Type of incremental algorithm of anti-windup integrated to the PI controller*

### 3.4 Inner disturbance controller for the changes of the knee flexion

It should be noted that in the controller design progress, the system might face with various disturbances from the body reaction of the patient individually. Particularly, to handle the reactions of the knee flexions, a supervising algorithm based on the approachment of *Isaka et al* was developed in [35]. It is meaningful for online updating parameters which allow the controller action to reduce the disturbance from body reaction effectively.

As mentioned in Section 2.3.6, during MIS with the knee joint, some situations of unwanted disturbances from the knee flexion might occur. Any type of bending or straightening leg leads to a sudden change of pressure significantly in the knee joint. This reaction could not be responded and controlled smoothly without using inner disturbance controller. Therefore, these cases of pressure changes should be early detected iterately for the elimination of pressure disturbance.

#### 3.4.1 Using separate PI\_SO controller for the inner disturbance elimination

Choosing an algorithm in controller design depends on the structure or characteristics of the plant to be monitored and supervised individually. According to the references of [16], [19] with the relationship between pressure and volume of fluid injected in Fig. 1.3, the curves of pressure responses are formed as an exponent expression when the knee angle is bended up to  $60^\circ$ . It was identified as an  $I-T_I$  type in Section 2.3.6. Hence, the inner controller was designed with another separate PI\_SO controller. The parameters of the PI\_SO controller in this case are calculated in the same formulas of (3.8), (3.9), and (3.10) but in different values. The controller output is used to control the bi-directional electrical valve of the HIL-Simulator for the gas volume into or out of the knee model. This obtains the stability of pressure in the operational area from the disturbance

of the knee flexion. The structure of the inner controller is shown in Fig. 3.14. In this case, the disturbance signal  $d$  is defined as the signal  $u_3$  which is represented to the expression of the knee flexion data, not the data  $u_2$  from the outflow of fluid.

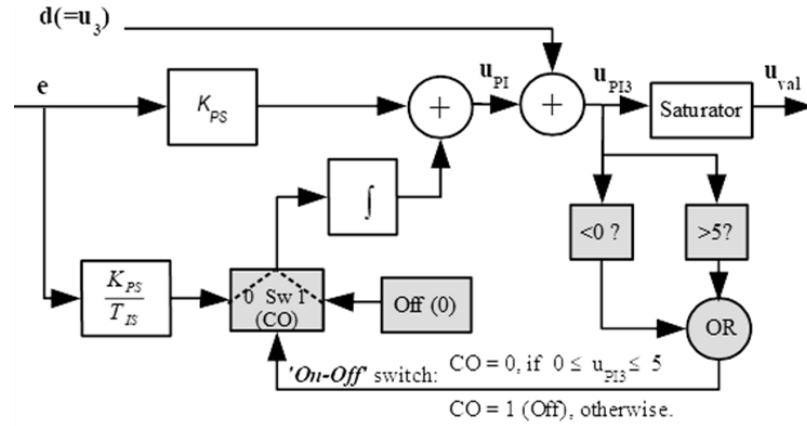


*Fig. 3.14 Structure of the inner disturbance controller for the knee flexion*

### 3.4.2 Using empirical Proportional controller

In another case of disturbance from the knee flexion reaction around  $80^\circ$  depicted in Fig. 2.19 (Section 2.3.6), it should be simplified to implement a Proportional controller for the supervisory algorithm to against the disturbance of pressure. And a suitable parameter of the controller can be found empirically while doing experiments or in Simulink.

Because most of cases in MIS are applied in a small volume of fluid injected to the knee joint, with a suitable value of empirical proportional  $P$  gain from the controller, it can be used for all most cases of supervised control in eliminating the pressure disturbances from the knee flexion.

### 3.5 Simulation results of pressure control

This section presents some results of the modelling process of MIS in MATLAB Simulink version R2016b. The responses of the controlled process were implemented in both cases of without and with supervisory actions. These results take an important role to perform the next stage of experiments in real-time device simulator. Fours typical cases of phase margin selections for controller parameters are shown for analyzing the function of the controller in simulation before doing in real-time experiment. After all, It should be better to choose the best controller parameters in implementation. In addition, for the supervisory tests, some disturbances of pressure like the disturbances of the knee flexions are implemented to the system. This is to evaluate the quality of the controller and supervisor working together for the stability of pressure in the knee model.

### 3.5.1 Simulation results of controller without supervisor

By combining between the equations of the controller (3.4) and the linearized function of the plant in (3.6), the controlled process was also identified. By using Simulink blocks in MATLAB, the process of the knee arthroscopy as well as the controller was constructed. During investigation, the author presented simulations with various cases of phase margin choices for analyzing and validating. It was recognized that the result of controller design with the case of  $72^\circ$  in phase margin was satisfied and optimized for the settling time and overshoot criterions. This result is indicated in Fig. 3.15 with the response of controlled pressure  $p_{knee}$  and the control signal  $u_1$ . Other cases of controller design results with the parameters in phase margin of  $37^\circ$ ,  $60^\circ$ , and  $78^\circ$  can be seen in the Appendix A at the end of this thesis.

In this case, companion with the overshoot down to a half (around 33%) compared to the case of  $PM = 60^\circ$  which is indicated in Appendix A, the rise time is more increased (about 1.47s). The time response of the controller is also better than from the cases of  $PM = 60^\circ$ .

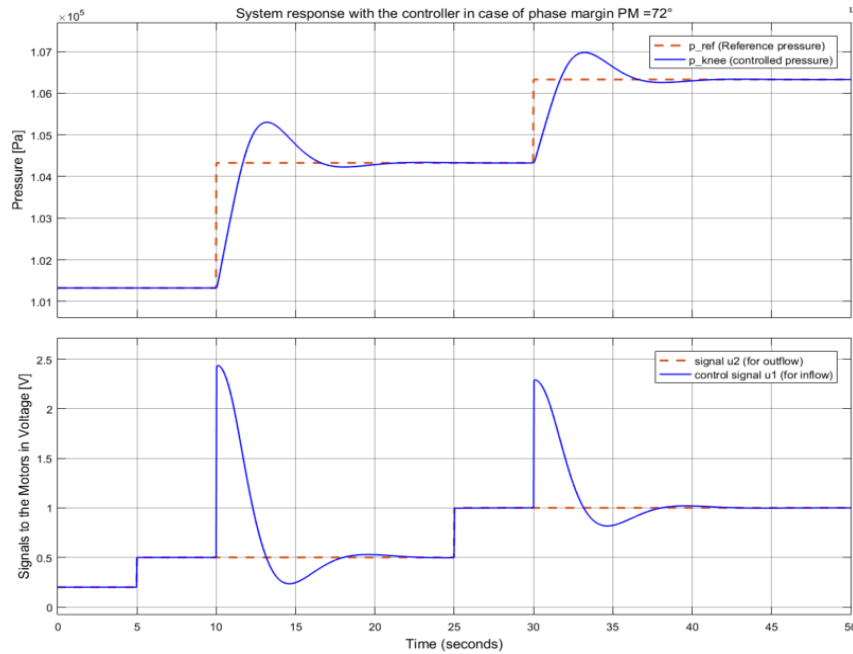


*Fig. 3.15 Response of system with the controller in the case of phase margin  $PM = 72^\circ$*

### 3.5.2 Simulation results of controller with the supervisor of the knee flexion disturbances

For supervisory strategy of pressure disturbances from the knee flexions during arthroscopy, the software model of the knee in the HIL-Simulator needs to be updated in computing and simulating for producing some more appropriate states of the knee flexions. Algorithm for supervision and control was realized in Simulink first. The supervisor was also tested in alternative cases of phase



margin parameters:  $37^\circ$ ,  $60^\circ$ ,  $72^\circ$  and  $78^\circ$ . The following result is shown with the case of controller parameters in the  $72^\circ$  of phase margin (Fig. 3.16). The comparison of supervised controller results in other cases of the phase margin  $37^\circ$ ,  $60^\circ$ , and  $78^\circ$  are presented in Appendix A.

As mentioned in the stage of controller design above, the more the phase margin increased (between the range of  $37^\circ$  and  $78^\circ$ ), the longer the rising time taken and the lower the overshoot occurred. Therefore, it should be an optimized case while choosing this case of phase margin ( $72^\circ$ ) for the supervising and controlling the process in real-time device simulator experiments, because the rise time is reasonable around 1.5 seconds.

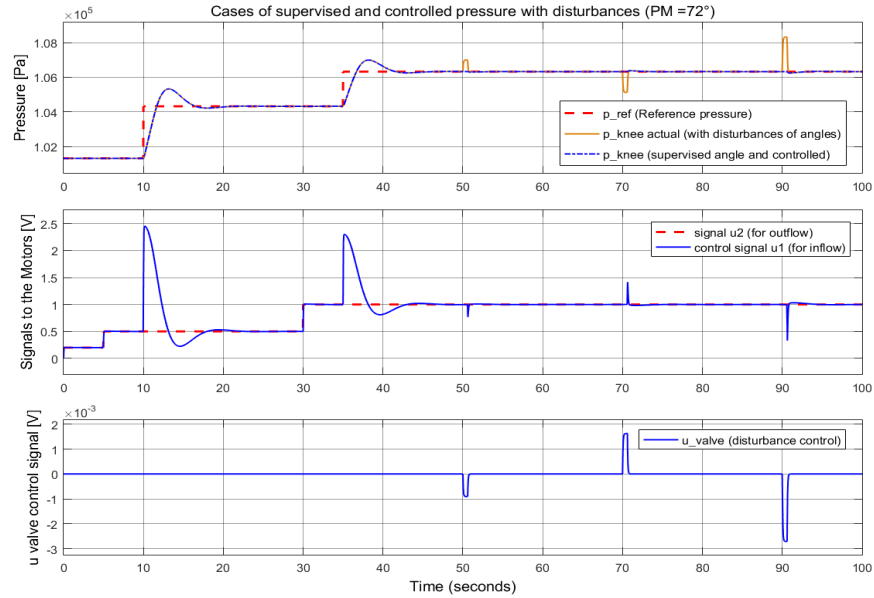


*Fig. 3.16 Case of controller with disturbances supervisory (PM =  $72^\circ$ )*

### 3.6 Real-time device simulator results

Complementing with the results in Simulink presented, it should be meaningful to perform similar cases of tests in real-time device simulator. In this case, the HIL-Simulator was used for the replacement of the real patient with the knee model. Because the research is on the stage of verification and evaluation, therefore the tests on the real patients or animals are not allowed for the safety of living entity. A real device simulator of the knee arthroscopy was concreted as a physical interface with the DRP. And a plastic ball was used to imitate like the operation area of the knee joint. The controllable electrical valve of the HIL-Simulator was utilized in actuating gas/air to the knee model. The following experimental results in real-time are also arranged in two groups: cases of controller without supervision, and cases of controller with supervision.

### 3.6.1 Experimental results of controller without supervisor

As shown in Fig. 3.17, the response of controlled pressure has a smooth response with the lower overshoot compared to the cases of lower phase margin (blue signal in upper panel). The parameters of the controller was set with the case of phase margin  $PM = 72^\circ$ . Other results of the controller with different cases of phase margin can be seen in Appendix A.

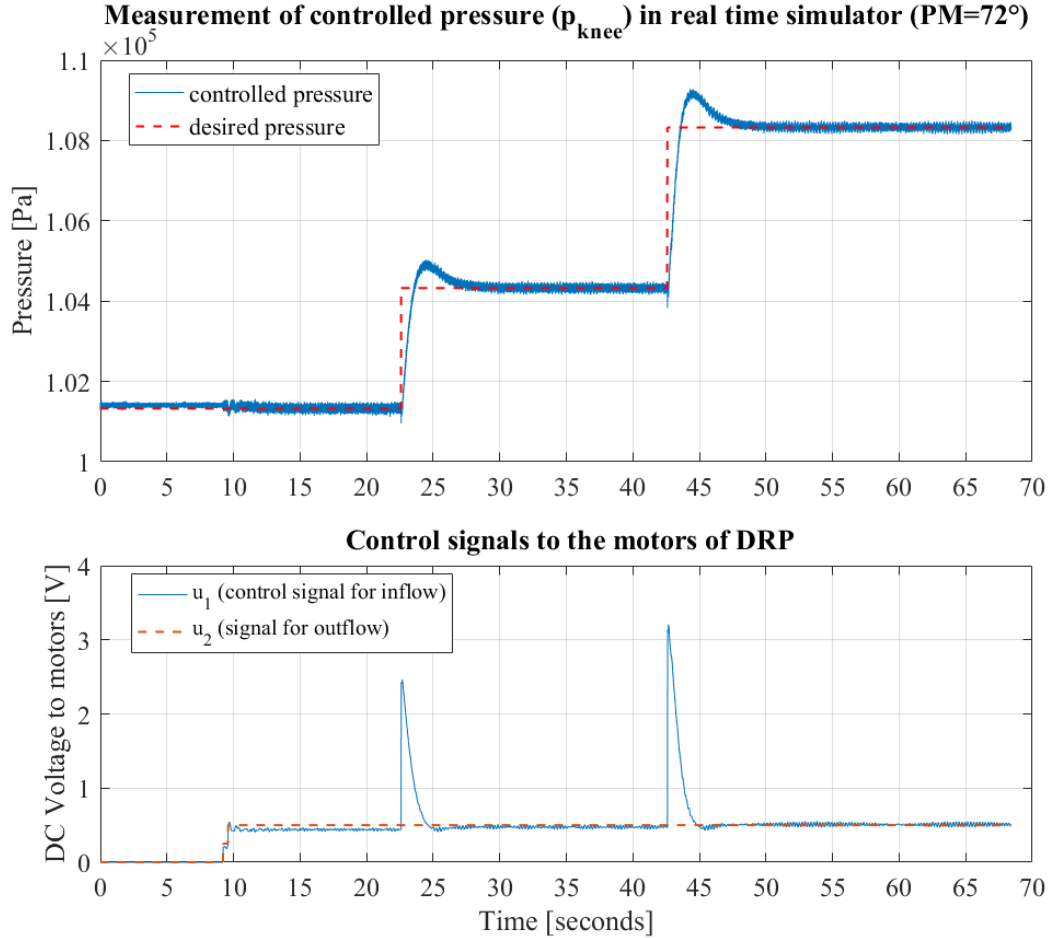


Fig. 3.17 Case of controller without disturbances and supervision ( $PM = 72^\circ$ )

### 3.6.2 Experimental results of controller with supervisor of the knee flexions

In this case, the disturbances of the knee flexions  $30^\circ$ ,  $-60^\circ$  and  $80^\circ$  were performed at the times 44s, 64s and 84s respectively as in Fig. 3.18 (in dark yellow). The pressure in the knee model was controlled and supervised more effectively (with  $PM = 72^\circ$ ). This result is indicated in blue signal with reduced disturbances on the upper plot. On the lower plot of Fig. 3.18, there existed some difference between the control signal for inflow ( $u_1$ ) and the nominal signal for outflow ( $u_2$ ). That was caused by some loss of air or flow of the nonlinear process during arthroscopy. Other results from the cases of phase margin chosen in controller design are shown in Appendix A.

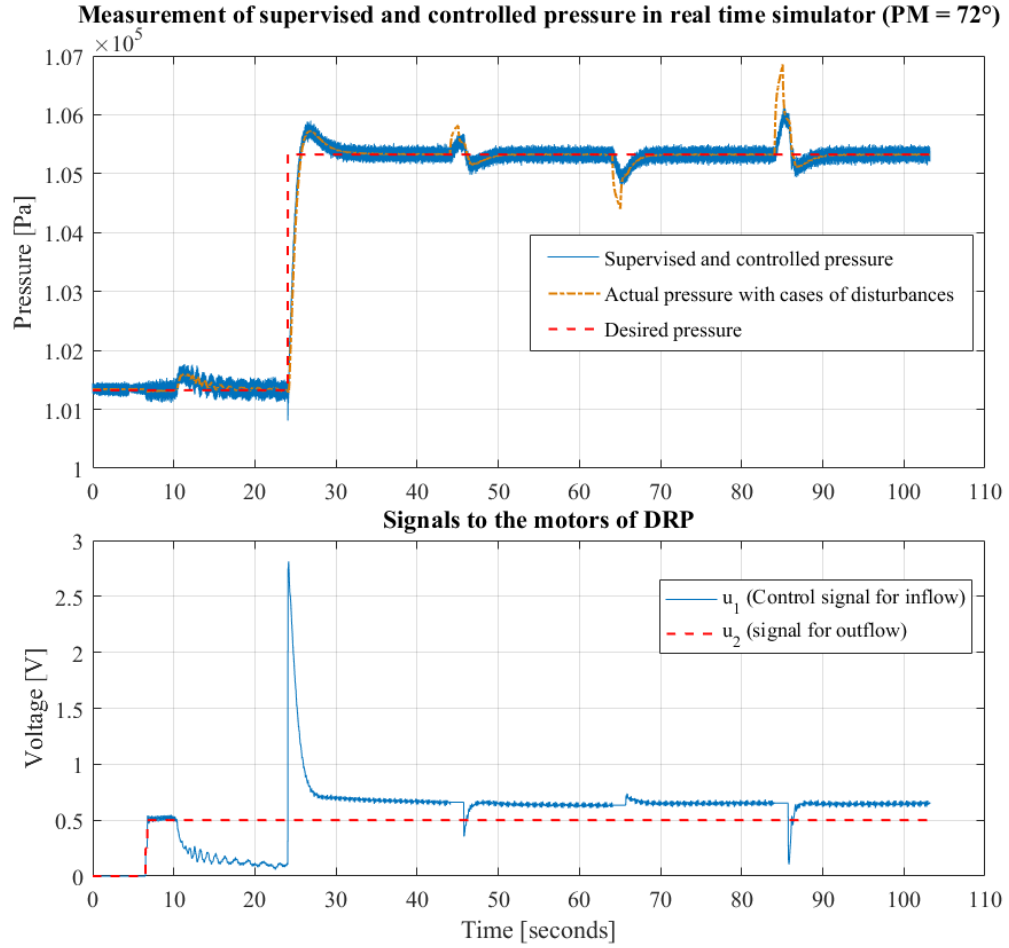


Fig. 3.18 Case of controller with disturbances and supervision (PM = 72°)

### 3.7 Summary

Chapter 3 has been presented with the focused contents of controller design and supervisory algorithm. The proportional and integrated controller based on symmetric optimum was applied not only on modelling system via MATLAB/Simulink but also on real-time device simulator. An anti-wind up algorithm was integrated successfully to the controller and supervisor in order to limit some cases of windup phenomenons which usually occur in nonlinear processes. To analyse and evaluate the quality of the PI\_SO controller, some cases of parameters in phase margin were selected and implemented. On the other hand, a supervisor strategy was given out for solving the types of disturbances like the changes of pressure from the knee flexions during arthroscopy process. And the disturbances were detected and moderated effectively in experiments.

From the results both in Simulink and in real-time simulator presented in Sections 3.5 and 3.6, it is clear that the parameters of the PI\_SO controller from the range of phase margin [72° - 78°] are better for the implementation.

It should be noted that in most of real-time experiment cases, there still subsists some difference between the extra input signal  $u_2$  (to the motor  $M2$  for outflow) and the control signal  $u_1$  (to the motor  $M1$  for inflow). This is normal in reality of real-time device experiments because it always get involved with some loss of flows or loss of pressure in the closed operation area during MIS. This also takes an account to the nonlinearity of the controlled process of the knee arthroscopy.

However, the controller and supervisor were designed and implemented by using the feedback data measured directly from a temporary pressure sensor in the knee model. As mentioned before, this measurement is not allowed in real-life of MIS for some presented reasons. Therefore, an essential problem needs to be solved is that how to apply an estimator for reconstructing the state of pressure in the OA during MIS. This would be a good replacement to the usage of pressure sensor in the knee arthroscopy. And Chapter 4 with the content of pressure estimation in minimally invasive surgery is going to be presented next for this motivation.

## **4 PRESSURE ESTIMATION IN MINIMALLY INVASIVE SURGERY**

This chapter performs methods of pressure estimation for the implementation in modelling and in real device simulator of MIS. Section 4.1 is an introduction of the motivation in pressure estimation of the knee arthroscopy. Section 4.2 presents estimate methods such as Luenberger, basic Kalman filter, and extended Kalman filter for the pressure state estimate in the knee joint. The next sections 4.3 and 4.4 show some results from the research in Simulink and in real-time device simulator experiments respectively. Some discussions and summary of estimation are given out by the end of the Chapter.

### **4.1 Introduction**

State estimator takes an important role in various fields of study while it can extract the information from measured data including noises to a “pure” data. This is to infer the desired information from the related measurement. Some estimation methods have been developed to compute the desired information from the measurements by using the relationships between the measured state and the estimated state in the real process. In addition, the calculation of the desired information is also influenced by the noises like measurement errors, effects of disturbances, lost of information, control actions on the system, and even the prior knowledge of the plant information [36].

In control theory, most concepts in controller design are usually based on measured data from a sensor as a feedback signal. Unfortunately, such a case of measurement in the real knee is invalid because the use of pressure sensor inside the knee joint is not allowed for the safety of the patient. The lack of using sensor might also come from other reasons: high cost sensors and associated accessories, low reliability and responsiveness, or impractical direct measurement [37].

Observer methods have been developed and used as estimators in order to replace feedback sensors in diversity of controlled systems. These observers combine the observable signals with other knowledge of the controlled system to estimate correlated states. The observed signals can be more accurate, lower cost in state estimate, more reliable than sensed signals [37]. The approaches of observer methods have offered to engineers some options to perform the ideas of replacing or reducing the use of sensors for feedback data. Generally, a principle operation of an observer is shown in Figure 4.1. In some cases, the observer can be used to enhance system performance, or can provide observed disturbance signals for the improvement of response in the system [37], [38].

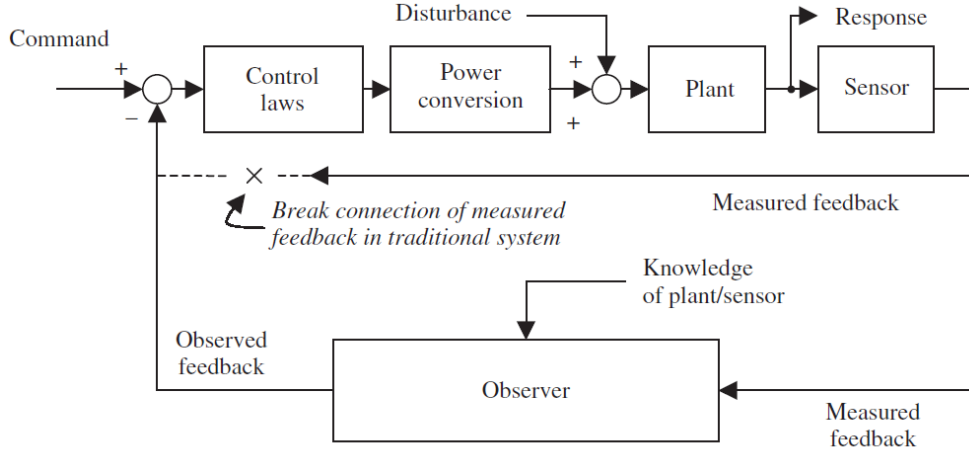


Fig. 4.1 Role of an observer as an estimator in controlled system [38]

As introduced in Chapter 1, the pressure in the operation area needs to be controlled to the desired value. However, the pressure in this area is unmeasurable because of the safety to the patient during MIS. Therefore, it is important to investigate some methods of estimation for the pressure state in the operation area of MIS. The estimated pressure then can be used as a replacement of the measurement for a feedback data to the controller. In this chapter, the author presents some implemented methods of pressure estimation in the following section of 4.2. Then some results from the estimates are shown for comparison and evaluation on the coming next sections.

Based on the relationships of the equations and modelling of process in state space presentation established in Chapter 2, the known inputs data like motors' speed (for flows of fluid) and measurements from available pressure sensors at the DRP are the information providing to the observers in this chapter. A general description of the observer in the MIS is given in Fig. 4.2 [39].

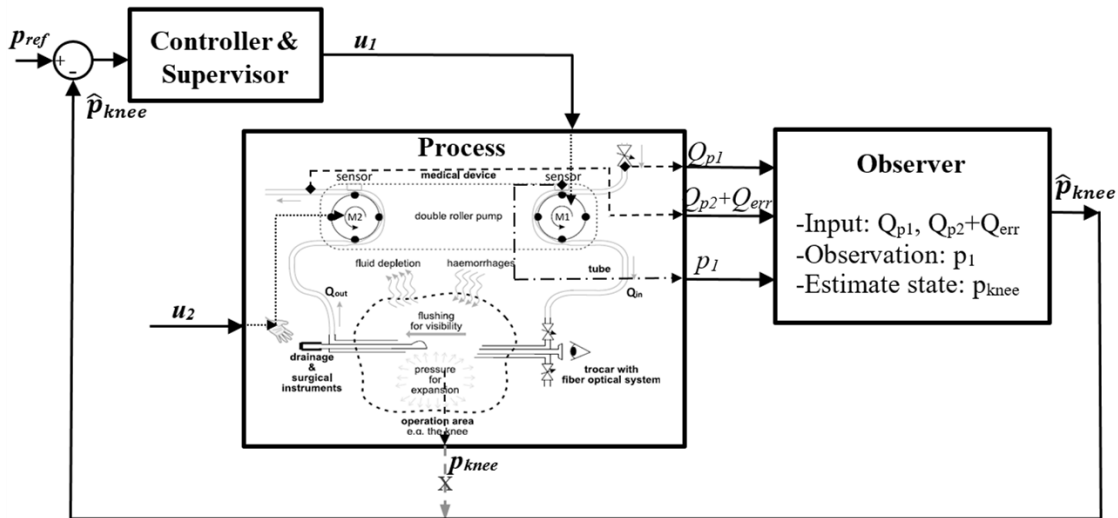


Fig. 4.2 General description of the observer in the controlled process of MIS [39]

## 4.2 Observer methods for pressure estimation in MIS

Generally, an observer is a mathematical structure that interconnects available measurement and plant excitation signals with models of the plant [37]. This is to estimate states of the plant which are unmeasurable by using correlated measured data and some prior known information of the plant. By using observer, it offers estimated state as a feedback signal to the controller. This is really useful because some direct measurements from sensors are not available. In the following sections, three types of observers: Luenberger, basic Kalman filter, and extended Kalman filter are introduced for implementation.

### 4.2.1 Luenberger observer

This is a type of estimator which was developed in the 1970s and implemented in most of linear systems [40]. It was designed to behave estimated states with the reduced noise in the finite-dimensional systems. In general, a linear and finite-dimensional system has a standard form of state space presentation shown in (2.31) and (2.32). The estimator then has a general form of (4.1). Figure 4.3 is a typical description of the observer in state space presentation [31].

$$\dot{\hat{x}} = A \cdot \hat{x} + B \cdot u + K_e \cdot (y - \hat{y}) \quad (4.1)$$

Parameter  $K_e$  represents the gain matrix of the estimator. Matrices  $A$  and  $B$  are determined from the linearized process in state space equation. Symbols  $\hat{x}$  and  $\hat{y}$  are the estimated state and estimated output respectively.

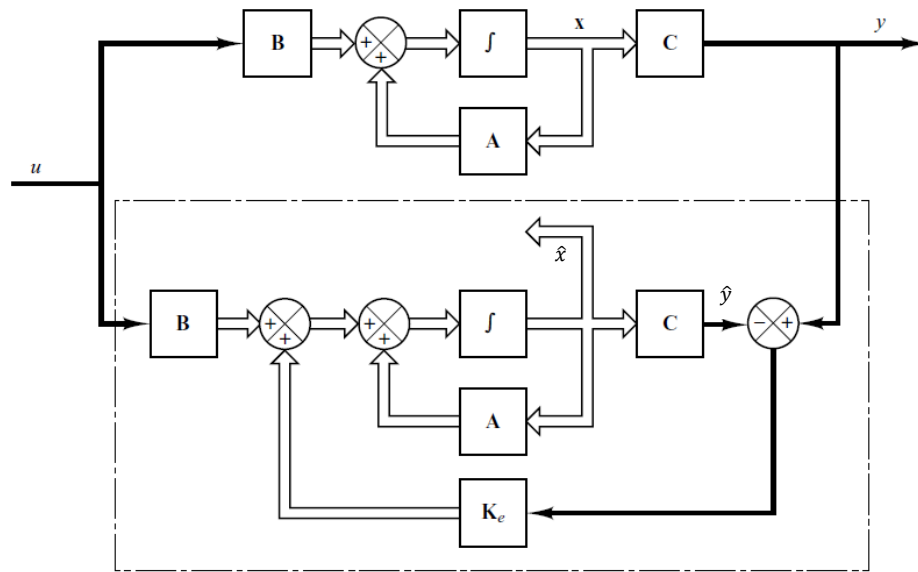


*Fig. 4.3 A typical description of an observer in state space (in dashed block) [31]*

The condition for applying estimator is that the pair of matrices  $A$  and  $C$  is completely observable.

Method of Luenberger observer is similar to the pole placement method. The desired poles should be chosen negatively at every point on the left hand side of the complex plane for the stability.

The characteristic equation in state space presentation of the knee model has the form of (4.2):

$$\det(s \cdot I - A) = 0 \quad (4.2)$$

where  $I$  is a unity matrix.

By solving the equation (4.2), the eigenvalues ( $\lambda_i$ ) are determined. The number of eigenvalues is equal to the number of the states in the model of the knee.

Since the Luenberger observer is usually applied in the linear process, therefore the model of the knee should also be linearized. In this case, the Luenberger observer was implemented with one state variable presentation for a simplification.

In one state presentation, (2.34) and (2.35) can be rewritten in (4.3) and (4.4).

$$\dot{x}_1 = f_1(x, u) = \begin{bmatrix} \frac{1}{c_{knee}} & -\frac{1}{c_{knee}} \end{bmatrix} \begin{bmatrix} u_a \\ u_b \end{bmatrix} \quad (4.3)$$

$$y_1 = g_1(x, u) = p_1 = [1][p_{knee}] + R_1 \cdot u_a + \beta \cdot u_a^2 \quad (4.4)$$

It is assumed that  $A_1$ ,  $B_1$  and  $C_1$  are the Jacobi matrices transformed for the linearization of state space equations of (4.3) and (4.4). These matrices are determined by taking partial derivatives of (4.3) and (4.4).

$$A_1 = \left[ \frac{\partial f_1}{\partial x} \right]_{(\hat{x})} = 0 \quad (4.5)$$

$$B_1 = \left[ \frac{\partial f_1}{\partial u} \right]_{(u)} = \begin{bmatrix} \frac{1}{c_{knee}} & -\frac{1}{c_{knee}} \end{bmatrix} \quad (4.6)$$

$$C_1 = \left[ \frac{\partial g_1}{\partial x} \right]_{(\hat{x})} = [1] \quad (4.7)$$

$$D_1 = \left[ \frac{\partial g_1}{\partial u} \right]_{(u)} = [(R_1 + 2\beta) \quad 0] \quad (4.8)$$

From the pair of matrices  $[A_1, C_1]$  computed above, it is proved that the process of the knee model is completely observable.

By substituting  $A_1$  to (4.2) and solving it, then the only eigenvalue is determined:

$$\lambda = 0 \quad (4.9)$$

The state of Luenberger observer for only 1 state is described in (4.10), with gain matrix  $L = K_e$ .

$$\dot{\hat{x}} = A_1 \cdot \hat{x} + B_1 \cdot u + L \cdot (y - \hat{y}) \quad (4.10)$$



where  $\hat{x} = \dot{p}_{knee}$ ; the observation output  $\hat{y}$  is described in (4.11).

$$\hat{y} = C_1 \cdot \hat{x} + D_1 \cdot u \quad (4.11)$$

Assuming that the error  $e$  is the difference between the state of the process and the estimated state:

$$e = x - \hat{x}; \text{ and then } \dot{e} = \dot{x} - \dot{\hat{x}} \quad (4.12)$$

Combining the equations from (4.3), (4.4), (4.10) and (4.11), then:

$$(\dot{x} - \dot{\hat{x}}) = [A_1 - L \cdot C_1](x - \hat{x}) \Leftrightarrow \dot{e} = [A_1 - L \cdot C_1]e \quad (4.13)$$

The desired characteristic equation including the observer now becomes:

$$\det(s \cdot I - [A_1 - L \cdot C_1]) = 0 \quad (4.14)$$

$$\Leftrightarrow s - [-L] = 0 \quad (4.15)$$

The eigenvalue of (4.15) is:  $\lambda^* = -L$ . In other words, the gain matrix of the observer is:  $L = -\lambda^*$ .

The value  $\lambda^*$  is the desired pole of the desired characteristic equation (4.14). Therefore  $\lambda^*$  can be chosen in any value of negative pole. And the gain of  $L$  is depended on the selection of  $\lambda^*$ .

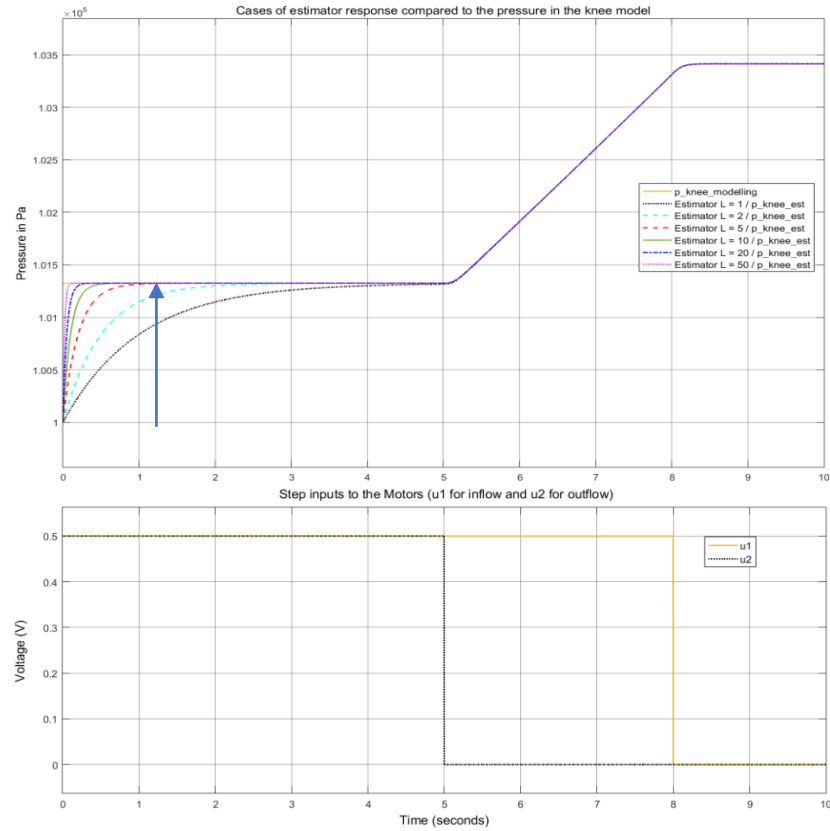


*Fig. 4.4 Response of the Luenberger observer in different values of gain selections*

Figure 4.4 shows some results of the Luenberger method in Simulink with varied values of observer gain  $L$  (from various values of  $\lambda^*$ ) compared to the state of pressure in the knee model (in yellow, upper plot). It is clear that the bigger the gain value of  $L$  is chosen, the faster the response of the estimator is approached. The lower plot of Fig. 4.4 shows the step input  $u_1 = u_a = 0.5V$  for the inflow in 8 seconds while the signal for outflow  $u_2 = u_b = 0.5V$  only in 5 seconds.

From the results with the various gain values of  $L$  implemented in the Luenberger observer, it would be better to choose the eigenvalue  $\lambda^*$  about  $-10$  for a suitable response of the estimator.

#### 4.2.2 Basic Kalman filter

One of the modern estimate methods is Kalman filter which was developed by the years of 1960s based on the minimizing the Mean-square error from the citation of [41]. It deals with the problems of separating signal from an additive combination of signal and noises. While Wiener method was discussed more in theory of minimizing the Mean-square error in time domain, the Kalman technique has still been implemented as a practical solution to several applied filter problems like in the citations of [28], [42], [43], [44], [45], [46], [47], [48]. With the rapid advances in computer technology since the 1960s [49], Kalman filter has been gradually contributed more popular and well done in applications as the means of separating signal from noises. This is considered as a key role of estimator when the noise is mixed in the measurements or in the state of process.

In order to obtain the Kalman filter in discrete data, a recursive computational algorithm of each new estimate step is formed as a mixture of the previous estimated data and the current measurement. The procedure can be described as following steps of estimation [41]:

- **At the first measurement of data  $m_1$ :** the estimate is computed and stored as  $\hat{x}_1$ ;  $m_1$  is discarded.

$$\hat{x}_1 = m_1 \quad (4.16)$$

- **At the second measurement of  $m_2$ :** compute the next estimate depending on the weighted sum of the previous estimate  $\hat{x}_1$  and the current measurement  $m_2$ ; then store the estimate state of  $\hat{x}_2$ ; discard  $m_2$  and  $\hat{x}_1$ .

$$\hat{x}_2 = \frac{1}{2}\hat{x}_1 + \frac{1}{2}m_2 \quad (4.17)$$

- **Similarly at the third measurement of  $m_3$ :** compute the next estimate as a weighted sum of  $\hat{x}_2$  and  $m_3$ ; then store the estimate state of  $\hat{x}_3$ ; discard  $m_3$  and  $\hat{x}_2$ .

$$\hat{x}_3 = \frac{2}{3}\hat{x}_2 + \frac{1}{3}m_3 \quad (4.18)$$

- **Generally, at the  $n^{th}$  measurement of  $m_n$ :** the estimate is computed as a form of (4.19);

$$\hat{x}_n = \left(\frac{n-1}{n}\right)\hat{x}_{n-1} + \left(\frac{1}{n}\right)m_n \quad (4.19)$$

then store the estimate state of  $\hat{x}_n$ ; discard  $m_n$  and  $\hat{x}_{n-1}$ .

Obviously, one of the main features in Kalman filter is the use of the results from the previous estimate to obtain the desired result for the current step. Figure 4.5 is a general description of the Kalman filter operation in MIS.

In general, a continuous-time linear state space modelling of a process was formed as a differential equation of (2.31), and the measurement relationship was presented in (2.32), where:

- $x$ :** Stands for a  $[n \times 1]$  state vector ( $n$  is the number of states of the process)
- $u$ :** Represents for an input vector of the process.
- $y$ :** Output vector of measurement  $[m \times 1]$ , ( $m$  is the number of output signals).
- $A, B, C, D$ :** Computed matrices from the linearized process and measurement.

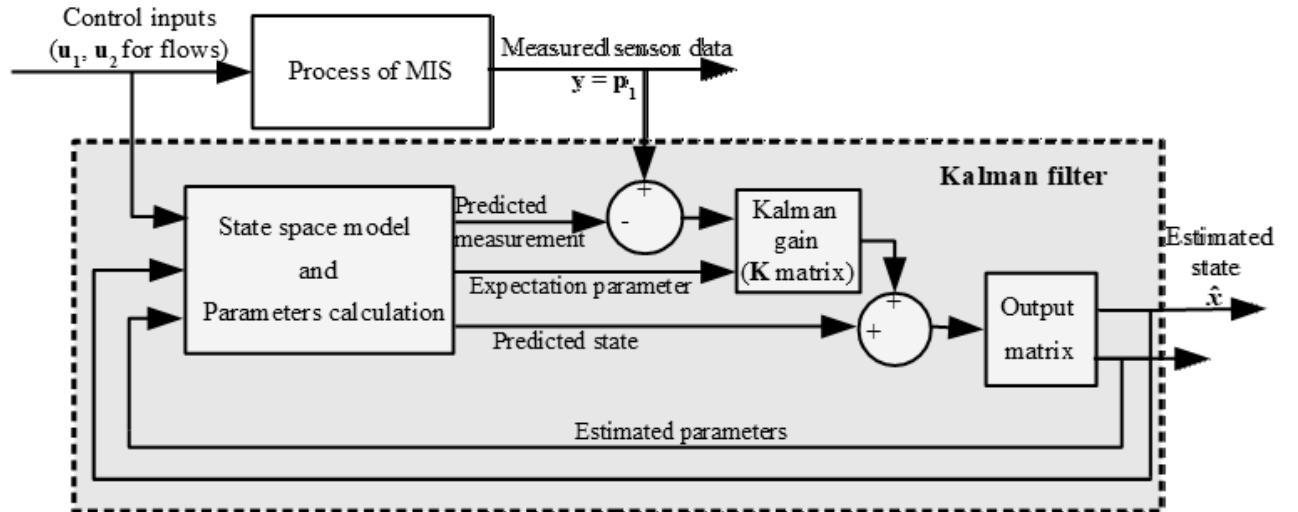


*Fig. 4.5 Functional structure of the Kalman filter in MIS*

And another key element that affects to the result of Kalman filter is the existence of the noises in both process and measurement. Therefore it is necessary to have a representation of these noises modelled in the process and measurement.

By adding terms of noises to the state space model of process and the output equation, and combining the state variable forms presented in (2.34), (2.35), and (2.31), (2.32), the continuous time model description of the Kalman filter including the noise contributions can be rewritten in (4.20) and (4.21) whereas  $\epsilon$  and  $v$  denote to the process noise and measurement noise respectively.

$$\dot{x} = A \cdot x + B \cdot u + \epsilon = f(x, u) + \epsilon \quad (4.20)$$

$$y = C \cdot x + D \cdot u + v = g(x, u) + v \quad (4.21)$$

#### 4.2.2.1 Sampled continuous-time model for filtering

In discrete-time, the continuous expressions of the process (4.20) and measurement (4.21) are sampled by a sampling time called  $T_s$ . Thus, at the discrete-time of  $t_k$ , the output equation (4.21) is equivalent to the form of (4.22).

$$y(t_k) = C \cdot x(t_k) + D \cdot u(t_k) + v(t_k) = g(x_k, u_k, v_k) \quad (4.22)$$

In linear systems, the state space equation (4.20) can be rewritten as the sum of two terms: *initial condition* and *driven response* like in (4.23).

$$x(t_{k+1}) = \Phi(t_{k+1}, t_k) \cdot x(t_k) + \int_{t_k}^{t_{k+1}} \Phi(t_{k+1}, \tau) \cdot B(\tau) \cdot u(\tau) d\tau \quad (4.23)$$

On the right side of (4.23), the first element is called the initial condition which contains the state transition matrix  $\Phi(t_{k+1}, t_k)$ ; and the second element stands for the driven response named  $\epsilon(t_k)$ . It is assumed that the period of sampling time  $(t_{k+1}, t_k)$  is equal to a small constant of  $\Delta t$ . Hence:

$$\Phi(\Delta t) = \Phi(t_{k+1}, t_k) = \mathcal{L}^{-1}[(s \cdot I - A)^{-1}]_{t=\Delta t} \quad (4.24)$$

The equation (4.23) is now rewritten in (4.25).

$$x(t_{k+1}) = \Phi(\Delta t) \cdot x(t_k) + \epsilon(t_k) \quad (4.25)$$

It is now clear that the state transition matrix  $\Phi$  as well as the driven response  $\epsilon(t_k)$  are important parameters for the estimation using Kalman filter. In order to estimate the state of the model at the time  $(t_{k+1})$ , both  $\Phi(\Delta t)$  and  $\epsilon(t_k)$  need to be computed at each time of  $t_k$ . While the matrix  $\Phi(\Delta t)$  is determined by (4.24), the covariance of the term  $\epsilon(t_k)$  must also be calculated by using (4.26) [41], [42]. This covariance is labeled by  $Q(t_k)$ .

$$Q(t_k) = E[\epsilon(t_k) \cdot \epsilon^T(t_k)] \quad (4.26)$$

where

$$\epsilon(t_k) = \int_{t_k}^{t_{k+1}} \Phi(t_{k+1}, \tau) \cdot B(\tau) \cdot u(\tau) d\tau \quad (4.27)$$

#### 4.2.2.2 Numerical evaluation of parameters $\Phi(t_k)$ and $Q(t_k)$

In some case like in a large dimension of a process, it has more difficult for the calculations of the matrices  $\Phi(\Delta t)$  and  $Q(t_k)$  at each time of  $t_k$  because of the complication in (4.24), (4.26) and (4.27). A numerical evaluation method for determining  $\Phi(t_k)$  and  $Q(t_k)$  in a large scale systems has been worked out [50], [51]. This is a helpful solution for the replacement of the above typical mathematical method of sampled continuous-time model. It is especially convenient when using MATLAB. Referring to the continuous-time model presented in Section 4.2.2.1, the numerical evaluation method by the authors in [41], [50], and [51] can be proceeded as following steps:

**Step 1:** Forming a  $[2n \times 2n]$  matrix called  $F$  as in (4.28) ( $n$  is the dimension of  $x$  and  $W$  is the power spectral density of the input  $u$ ). Note that  $W$  is an identity matrix having dimensions compatible with  $B$ ; and the triple product  $BWB^T$  must properly account for the white noise forcing function.

$$F = \begin{bmatrix} -A & \vdots & BWB^T \\ \dots\dots & \vdots & \dots\dots \\ 0 & \vdots & A^T \end{bmatrix} \Delta t \quad (4.28)$$

**Step 2:** Using MATLAB to form the element of  $e^A$ , called  $G$  in (4.29).

For the simplification in equations, the term of ' $t_k$ ' at the sampling time of  $k$  can be written in short with the subscript ' $_k$ ' in discrete-time. So, instead of typing  $Q(t_k)$ , it can be typed  $Q_k$  briefly.

$$G = \exp(F) = \begin{bmatrix} \dots & \vdots & \Phi_k^{-1} Q_k \\ \dots\dots & \vdots & \dots\dots \\ 0 & \vdots & \Phi_k^T \end{bmatrix} \quad (4.29)$$

**Step 3:** Computing matrix  $\Phi_k$  by performing the stranspose matrix  $\Phi_k^T$  on the lower right of  $G$ .

**Step 4:** Obtaining  $Q_k$  by using the upper right of  $G$  in (4.29) and the form of (4.30).

$$Q_k = \Phi_k \Phi_k^{-1} Q_k \quad (4.30)$$

#### **4.2.2.3 Monte Carlo simulation method for a discrete-time process**

Referring to this method from the citation of [41], it is worth to state that the Monte Carlo simulation is really useful, especially in nonlinear filtering problems for applications. Firstly, this is to involve setting up a statistical experiment equivalently to the physical problem of interest. Secondly, the simulation performs and repeats the experiment over and over with typical sequences of random numbers. And finally, it is necessary to analyze the results of experiment statistically. The method is more helpful in understanding the behavior of stochastic systems that could not be able to analyze by usual direct mathematical methods.

Assuming that  $\Phi(\Delta t)$  in (4.25) is known, and  $\epsilon_k$  is a Gaussian white sequence with the known covariance  $Q_k$ . The problem is to generate an ensemble of random trials of  $x_k$ . There are two cases in performing matrix calculations depending on  $\Phi_k$ . In the first case:  $\Phi_k$  is a constant matrix, then the state variables of  $x_k$  can be simply assigned and given numerical values in MATLAB workspace. In other case of a time variable  $\Phi_k$ , the parameters need to be reevaluated in time at each step as the simulation proceed. In this case, generating the term of  $\epsilon_k$  is more difficult because the covariance  $Q_k$  might not be diagonal. Solving this in basic from [41], it should be firstly better to choose the input vector  $u_k$  whose the components are independent from an  $N(0, I)$  population; and then choose a linear transformation of matrix ' $H_k$ ', within the operation of the chosen vector  $u_k$ , in order to yield a  $\epsilon_k$  vector with the desired covariance structure. Note that the desired  $H_k$  is

not unique, therefore covariance  $Q_k$  would also not be unique. But the simple way to form a suitable  $H_k$  is to let it be lower triangular and then solve for the unknown elements.

In mathematical statement,  $\epsilon_k$  can be now rewritten in (4.31).

$$\epsilon_k = H_k u_k \quad (4.31)$$

Therefore:

$$Q_k = E[\epsilon_k \cdot \epsilon_k^T] = E[H_k u_k \cdot (H_k u_k)^T] \quad (4.32)$$

Now, because of choosing the vector input  $u_k$  as independent of  $N(0, I)$  samples, it is obvious that  $E[u_k \cdot u_k^T]$  is determined as a unitary matrix. Hence

$$Q_k = H_k \cdot H_k^T \quad (4.33)$$

#### **4.2.2.4 Recursive loop for the gain calculation of Kalman filter**

In this research, Kalman filter is mainly aimed to estimate the state of pressure in the surgical area based on the measurement data at the DRP during MIS. Criterion for optimization is minimizing the mean-square estimation error of the variable  $x$ . Similarly with the assumed white noise  $\epsilon_k$  of the process,  $v_k$  is assumed to the white noise sequence of the measurement which appears in the observed output equation. As presented,  $Q_k$  is the covariance matrix of the process noise  $\epsilon_k$ . Similarly,  $R_k$  is denoted to the covariance matrix of the measurement noise  $v_k$ . The expectation (signed by  $E[\ ]$ ) between these covariances are generally given in (4.34) – (4.36), according to the citations of [41], [43], [52].

$$E[\epsilon_k \cdot \epsilon_i^T] = \begin{cases} Q_k; & i = k \\ 0 & ; i \neq k \end{cases} \quad (4.34)$$

$$E[v_k \cdot v_k^T] = \begin{cases} R_k; & i = k \\ 0 & ; i \neq k \end{cases} \quad (4.35)$$

$$E[\epsilon_k \cdot v_i^T] = 0; \forall k, i \quad (4.36)$$

To be clear in indication of mathematical equations of estimation as following, the sign of “*hat*” like  $\hat{x}_k$  is defined as an estimate state vector at the time  $t_k$ ; the sign of “*sub\_minus*” stands for a *priori* state, like  $\hat{x}_{k-}$  at the prior time of  $t_k$ ; and the sign of “*sub\_plus*” denotes for a *posteriori* statement like  $P_{k+}$  at the right posterior time of  $t_k$ .

At each sampling time  $t_k$ , the estimated state is formed in (4.37)

$$\hat{x}_k = \hat{x}_{k-} + K_k \cdot (y_k - \hat{y}_k) \quad (4.37)$$

where  $K_k$  is a Kalman gain vector which must be calculated for the correction of  $\hat{x}_k$ .

The Kalman gain  $K_k$  is important for the adjustment of predicted state in estimation. When the difference between the measurement ( $y_k$ ) and the observed state of ( $C_k \cdot \hat{x}_k$ ) is occurred, then the gain  $K_k$  is computed and updated to minimize the difference. This gain is involved to the expectation of the error which is indicated in (4.39) and (4.40) referred to [41], [49].

Reminding the state error from the estimation:

$$e_k = x_k - \hat{x}_k; \quad \text{or:} \quad e_{k-} = x_k - \hat{x}_{k-} \quad (4.38)$$

Relatively, the covariance error would also be defined by  $P_k$  in (4.39). It is tacitly assumed that the estimation error has zero mean.

$$P_k = E[e_k \cdot e_k^T] = E[(x_k - \hat{x}_k) \cdot (x_k - \hat{x}_k)^T] \quad (4.39)$$

Or, the prior covariance error is determined by:

$$P_{k-} = E[e_{k-} \cdot e_{k-}^T] = E[(x_k - \hat{x}_{k-}) \cdot (x_k - \hat{x}_{k-})^T] \quad (4.40)$$

Combining equations (4.22), (4.37) into (4.39), then the covariance error  $P_k$  is rewritten in (4.41).

$$P_k = E\left\{[(x_k - \hat{x}_{k-}) - K_k \cdot (C_k \cdot x_k + \rho_k - C_k \cdot \hat{x}_{k-})] \cdot [(x_k - \hat{x}_{k-}) - K_k \cdot (C_k \cdot x_k + \rho_k - C_k \cdot \hat{x}_{k-})]^T\right\} \quad (4.41)$$

Element of  $(x_k - \hat{x}_{k-})$  is the *a priori* estimation error ( $e_{k-}$ ), and this error is uncorrelated with the current measurement error of the noise  $v_k$ . Therefore, (4.41) can be reformulated into (4.42). This is a perfect expression for the updated error covariance matrix.

$$P_k = [I - K_k \cdot C_k] \cdot P_{k-} \cdot [I - K_k \cdot C_k]^T + K_k \cdot R_k \cdot K_k^T \quad (4.42)$$

Equation (4.42) is also the main information for the calculation of the Kalman gain. By expanding (4.42) for  $P_k$ , it can be rewritten in the form of (4.43).

$$P_k = P_{k-} - K_k \cdot C_k \cdot P_{k-} - P_{k-} \cdot C_k^T \cdot K_k^T + K_k \cdot (C_k \cdot P_{k-} \cdot C_k^T + R_k) \cdot K_k^T \quad (4.43)$$

It is obvious that the second and the third terms on the right side of (4.43) are linear by  $K_k$ ; and the fourth term is quadratic by  $K_k$ . On the other hand, the goal for minimization of  $K_k$  is to minimize the trace of  $P_k$  because it is the sum of mean-square errors in estimation of the state vector. Therefore, by differentiating the trace of  $P_k$  by  $K_k$ , and noting that the trace of  $(P_{k-} \cdot C_k^T \cdot K_k^T)$  is equal to the trace of its transpose ( $K_k \cdot C_k \cdot P_{k-}$ ), the result is:

$$\frac{d(\text{trace } P_k)}{dK_k} = -2(C_k \cdot P_{k-})^T + 2K_k \cdot (C_k \cdot P_{k-} \cdot C_k^T + R_k) \quad (4.44)$$

For the optimal gain in minimizing the mean-square error, (4.44) should be set to zero. Then the Kalman gain  $K_k$  is determined by (4.45).

$$K_k = P_{k-} \cdot C_k^T (C_k \cdot P_{k-} \cdot C_k^T + R_k)^{-1} \quad (4.45)$$

By substituting (4.45) into (4.43), and using some characteristics of straightforward differential calculus approach, then the equation of  $P_k$  calculation is formed in short as (4.46).

$$P_k = (I - K_k \cdot C_k) \cdot P_{k-} \quad (4.46)$$

At the beginning time of the estimation, there is no measurement data nor a priori estimated state. It should be thus proceeded with the provided set of initial parameters of  $(\hat{x}_0, P_0)$  as well as the initial conditions of covariance matrices  $Q_0$  and  $R_0$  which are denoted to the process and measurement noises respectively.

After the prediction of the state  $\hat{x}_k$  with the calculated gain of  $K_k$ , the next step is anticipating the state of  $\hat{x}_{(k+1)-}$  in order to make an optimal use of the measurement  $y_{k+1}$ . This is to adjust the estimated state  $\hat{x}_k$  to correct the error for the next recursive loop of estimation. By using the state transition matrix  $\Phi_k$  at the transitional time and ignoring the contribution of  $\epsilon_k$  (because  $\epsilon_k$  was assumed to have zero mean and not be correlated with any of the previous value), the equation (4.25) results in (4.47).

$$\hat{x}_{(k+1)-} = \Phi_k \cdot \hat{x}_k \quad (4.47)$$

And the *priori* error for the next coming time  $t_{k+1}$  is also formed as (4.48).

$$e_{(k+1)-} = x_{(k+1)} - \hat{x}_{(k+1)-} = (\Phi_k \cdot x_k + \epsilon_k) - \Phi_k \cdot \hat{x}_k = \Phi_k \cdot e_k + \epsilon_k \quad (4.48)$$

It is noted that the elements of  $e_k$  and  $\epsilon_k$  have zero crosscorrelation ( $\epsilon_k$  is the process noise at  $t_k$ ). Hence, the next expression of error covariance matrix  $P_{(k+1)-}$  is computed by (4.49).

$$P_{(k+1)-} = E[e_{(k+1)-} \cdot e_{(k+1)-}^T] = \Phi_k \cdot P_k \cdot \Phi_k^T + Q_k \quad (4.49)$$

Equations of (4.47) and (4.49) are the need for preparation of the next sampling time  $t_{k+1}$  of the estimation, and the measurement of  $y_{(k+1)}$  can now be assimilated as in the previous step.

From the equations (4.37), (4.45), (4.46), (4.47), and (4.49), it can be summarized the steps of each recursive loop in Kalman filter by the chart of Fig. 4.6.

From the figures 4.5 and 4.6, the function of the Kalman filter can be summarized into 2 main steps: predicting state and calculating parameters for the Kalman gain; and updating the predicted state by using the computed Kalman gain and the error between the observation and the measurement.



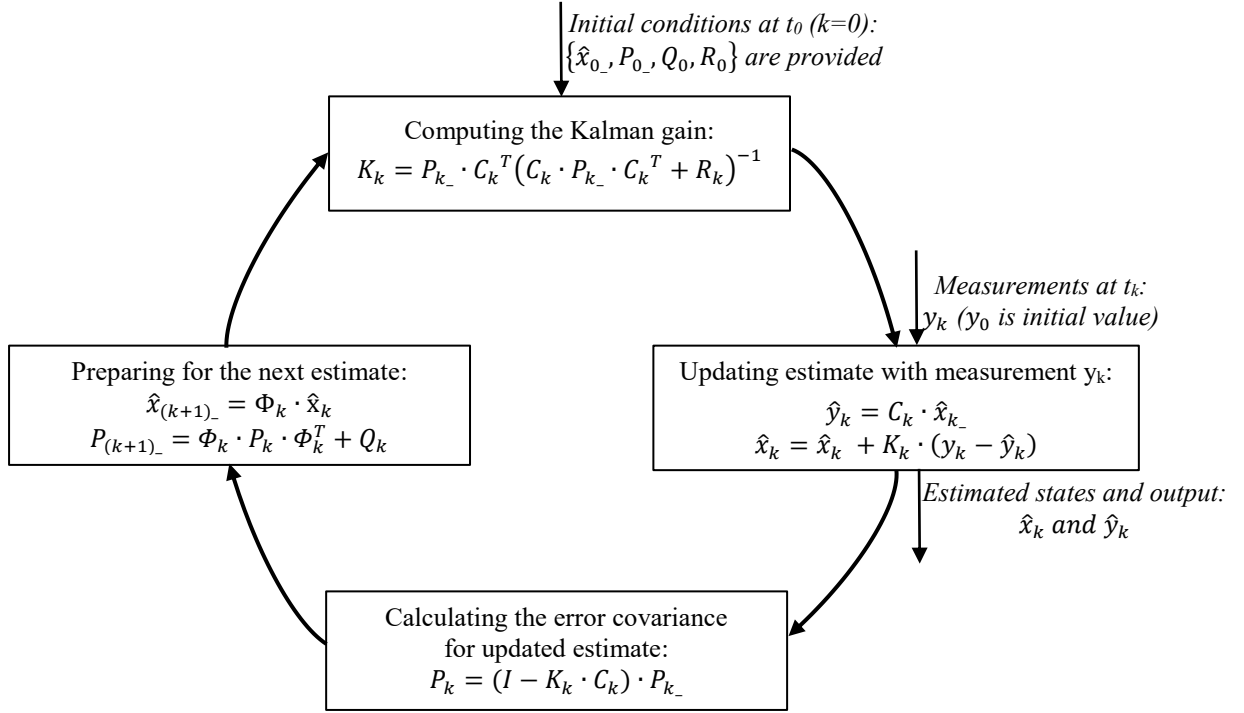


Fig. 4.6 Recursive loop description of a Kalman filter

### 4.2.3 Extended Kalman filter

As presented in Chapter 2, the process of the knee arthroscopy is nonlinear in modelling as well as in implementing with the HIL-Simulator for real-time experiments. Some unwanted noises appear in real-time simulator such as individual characteristics of each actuator, loss of rinsing fluid flows, oscillation of the fluid from the roller pump, appearance of turbulent flow, and the reduction of gas volume during MIS. These terms of unmeasurable noises influence directly on the state of pressure in the knee  $p_{knee}$  during MIS. Therefore the estimate state  $\hat{p}_{knee}$  is influenced by these noises. And the estimate result with the Kalman filter might not be accurate in the nonlinear process. From this point, an algorithm of extended Kalman filter (EKF) was proposed as another method of estimation in this research. This is one of the extension versions based on the basic Kalman filter. The main point of the EKF is local linearization on the trajectory of the process at each sampling time. This can be simply described in Fig. 4.7. [41].

Extended Kalman filter has been implemented widely not only in identifying systems and estimating parameters [53], [54], [55] but also in states estimation as an observer for a sensorless feedback control [28], [44], [56], [57], [58], [59], [60].

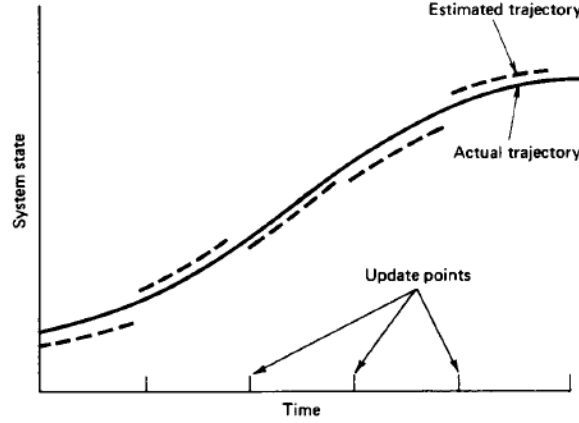


Fig. 4.7 Description of an estimated trajectory with extended Kalman filter [41]

Steps for calculations in recursive loop is similar to the basic Kalman filter with the two main steps: predicting state and calculating parameters for the Kalman gain; and updating the predicted state by using the computed Kalman gain and the error between the observation and the measurement. The different specification in EKF is the performance of formulas in parameters calculation. In addition, the EKF works by using online updated parameters (linearized instantly) from the nonlinear process and the measurement data at each sampling time of  $t_k$ . Figure 4.8 depicts the EKF function with a simplified chart [61]. In the first step, the state variables  $x$  and the state covariance matrix  $P$  are predicted. The Kalman gain is also calculated. In the second step, the estimated states are corrected and covariance matrix is updated by using the computed Kalman gain ( $K_k$ ) and the error of  $(y_k - \hat{y}_k)$ . Vector  $K_k$  is computed based on the current parameters of  $P$ , the linearized observed matrix  $C$ , and the noise covariance of  $R$  from the measurement.

In Fig. 4.8, signal  $vI_k$  is created to correct the estimated states for minimizing error. This signal is computed by using the Kalman gain and the current predicted error. The predicted error is the difference between the measured output and the estimated output.

The operation in recursive loop of the EKF can be expressed briefly as follow [42]:

*Updating the prior data from the estimated states  $\hat{x}_k$  and covariance matrix  $P_{k-}$  at the time  $t_k$ . The loop is initialized at the time  $t_0$  with the provided conditions  $x_0$  and  $P_0$ .*

*Predicting the state vector  $\hat{x}_{(k+1)-}$  and the state covariance matrix  $P_k$ :*

$$\hat{x}_{(k+1)-} = f(\hat{x}_k, u_k) \quad (4.50)$$

$$P_k = A_k \cdot P_{k-} \cdot A_k^T + Q_k \quad (4.51)$$

*Computing the vector of Kalman gain  $K_k$ :*

$$K_k = P_k \cdot C_k^T [C_k \cdot P_k \cdot C_k^T + R_k]^{-1} \quad (4.52)$$

Correcting the predicted state vector  $\hat{x}_{k+1}$  and updating the covariance matrix  $P_{k+1}$ :

$$\hat{x}_{k+1} = \hat{x}_{(k+1)-} + K_k[y_k - C_k \cdot \hat{x}_{(k+1)-}] \quad (4.53)$$

$$P_{k+1} = P_k - K_k \cdot C_k \cdot P_k \quad (4.54)$$

At each point of sampling time, the EKF predicts the states and then corrects the predicted states regarding to the current values of  $K_k$  and  $P_k$  instantly.

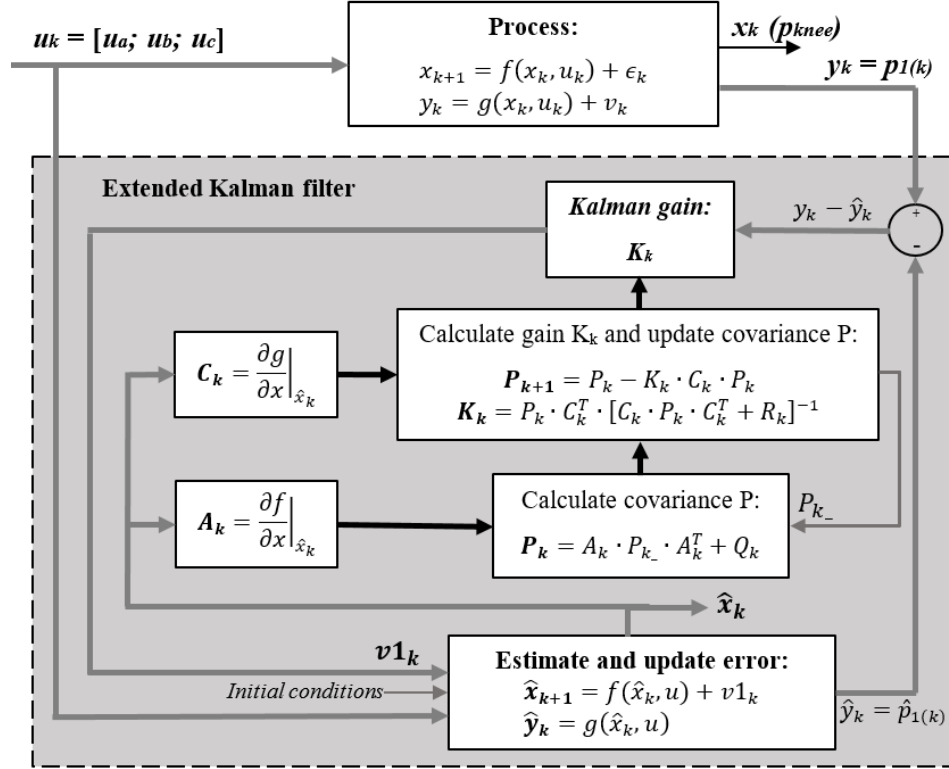


Fig. 4.8 Recursive loop operation of extended Kalman filter [39]

### 4.3 Simulation results

Before doing experiments in real-time device simulator of the knee arthroscopy, some tests on modelling of process in MATLAB Simulink had been done. Furthermore, for the best response from controller design and supervisor on disturbances, the author only chose the parameters of the PI\_SO controller in case of  $72^\circ$  phase margin for observer tests on Simulink as well as on real-time device simulator. Therefore, all the results presented in this chapter are all based on the parameters of the controller in phase margin  $PM = 72^\circ$ .

### 4.3.1 Simulation results with Luenberger observer

Figure 4.9 shows the results of the Luenberger observer for the estimated state of pressure in the knee model with various values of observer gain  $L$ . The observer was implemented with one state variable of  $p_{knee}$  presented in (2.34), and the output for observation is in (2.35). The upper panel of Fig. 4.9 shows the results from four different cases of the using observer gain:  $L = 1; 5; 10; 50$ .

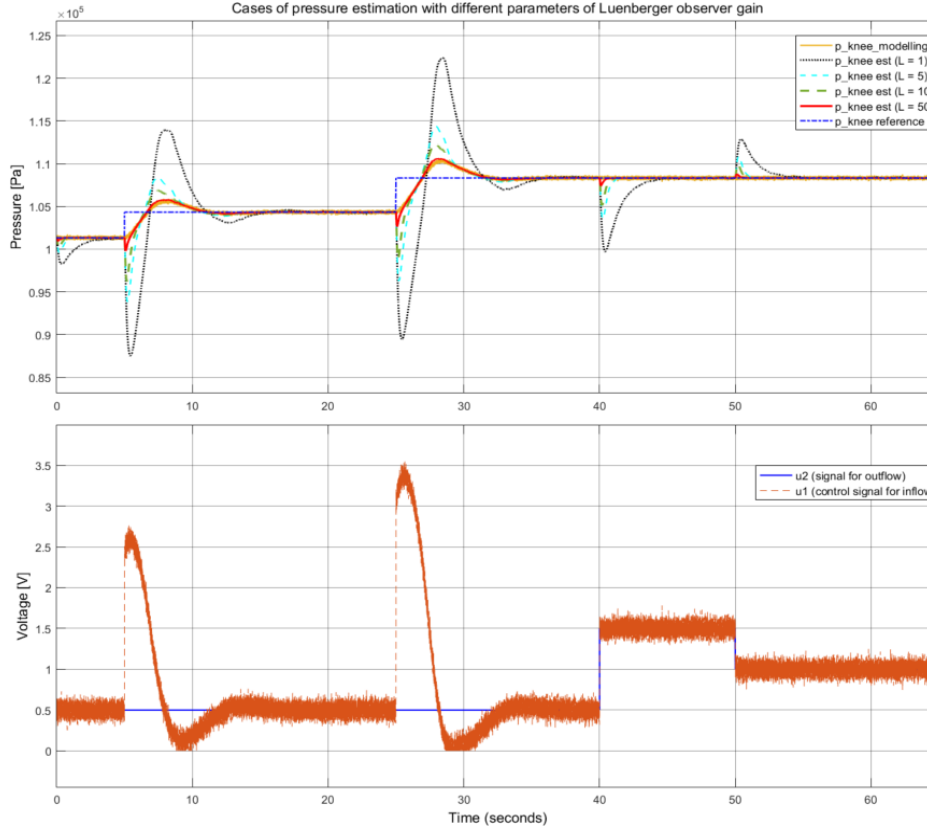
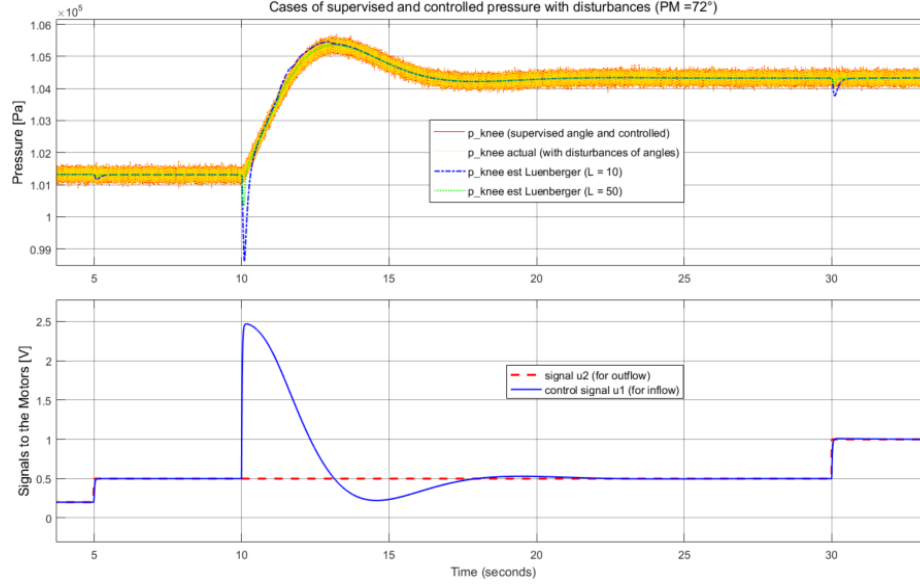


Fig. 4.9 Cases of pressure estimation in different parameters of Luenberger observer gain ( $L$ )

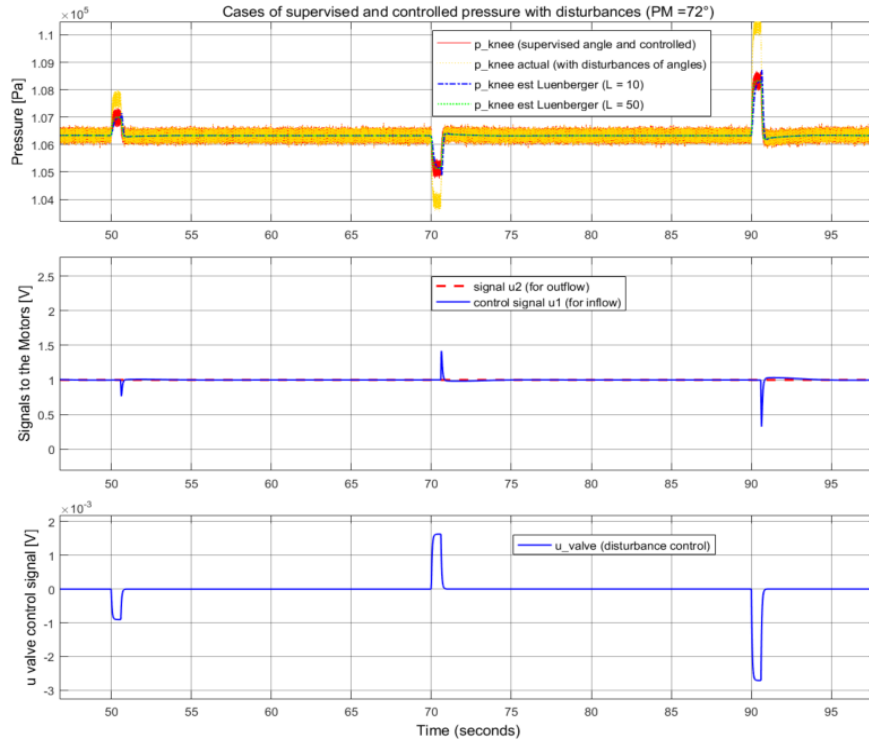
Comparing the cases of estimation to the controlled pressure of the process ( $p_{knee}$  modelling, in dark yellow) on the upper panel of Fig. 4.9, it can be seen that the estimator responses faster when the gain of  $L$  is bigger. The signal in dotted black is the response from the observer with the gain  $L = 1$ . It shows a low response and a high overshoot within the transition time. This equals to the case of pole placement near to the imaginary axis of the complex plane, and gives more fluctuate while having any change from the inflow or outflow, particularly at the time of 40s and 50s with some changes of the outflow (from  $u_2$  signal in the lower plot). The more positive the gain  $L$  is used, the faster and better the response of estimation is. With the case of gain  $L = 50$  (in red signal of the upper panel), the estimated state gets more accuracy and less overshoot.

Figure 4.10 gives more details about two cases of estimation ( $L = 10$  and  $L = 50$ ) on transition time (at 10s) as well as on the time of changing outflow (at 5s and 30s).



*Fig. 4.10 Comparison between two cases of estimation parameters:  $L = 10$  and  $L = 50$*

Figure 4.11 shows the estimate response on three cases of disturbances from the knee angles (bending  $30^\circ$  at the time 50s,  $-60^\circ$  at 70s, and  $80^\circ$  at 90s). Note that during the disturbance time, the inner disturbance controller is switched ‘On’ to control the electrical valve for the balance of pressure in the knee model. This explains the appearance of the signal  $u_{valve}$  (at the lower panel of Fig. 4.11) right before the time of control signal  $u_1$  pulses (in blue, in the middle of Fig. 4.11).



*Fig. 4.11 Luenberger responses while controlling valve for elimination of disturbances*

### 4.3.2 Simulation results with basic Kalman filter

In Kalman filter, the Kalman gain is used to correct the predicted state of  $\hat{p}_{knee}$ , depending on the error between the predicted output  $\hat{p}_1$  and the measurement  $p_1$  of the process. In addition, Providing different initial conditions of noise covariances  $R$  and  $Q$  leads to various results of estimate. The figures from 4.12 to 4.14 show the results with different parameters of  $Q$  applied.

Figure 4.12 is the response of pressure estimation with two cases of Kalman filter. These cases are 1 state and 4 state variables which were formulated in equations (2.34), (2.35) and (2.43), (2.45) of Chapter 2. On the top of Fig. 4.12, the estimated state  $\hat{p}_{knee}$  with 4 states (dash-dot red) is more accurate than the estimated state with 1 state expression (displayed in dark yellow). Moreover, with the change of outflow  $u_2$  at the time 35s, the estimate with 1 state is more sensitive. This can be solved by changing the noise covariance of  $Q$ . Figure 4.13 shows the different results at transition time by changing  $Q$  matrix. For 1 state presentation of Kalman filter in Simulink, referring from the value of  $Q = [1e-14]$ , when this value is more increased, then the estimate error is more reduced. Otherwise, the estimate error is increased when  $Q$  is decreased down to  $[1e-18]$ .

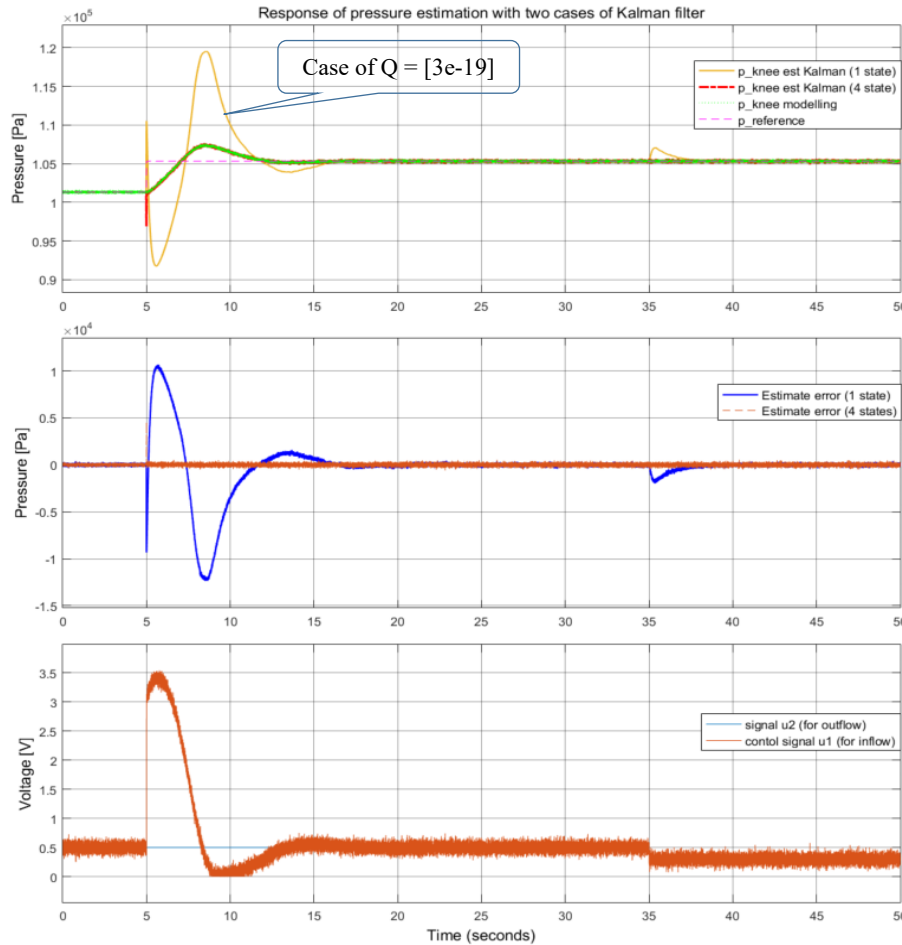


Fig. 4.12 Response of pressure estimation with two cases of Kalman filter.

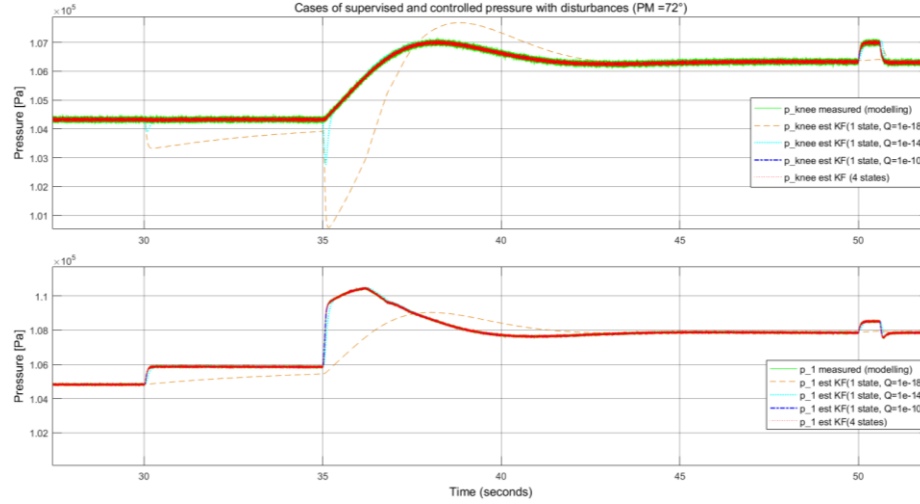


Fig. 4.13 Response of Kalman filter with the state  $\hat{p}_{knee}$  and the observation  $\hat{p}_1$

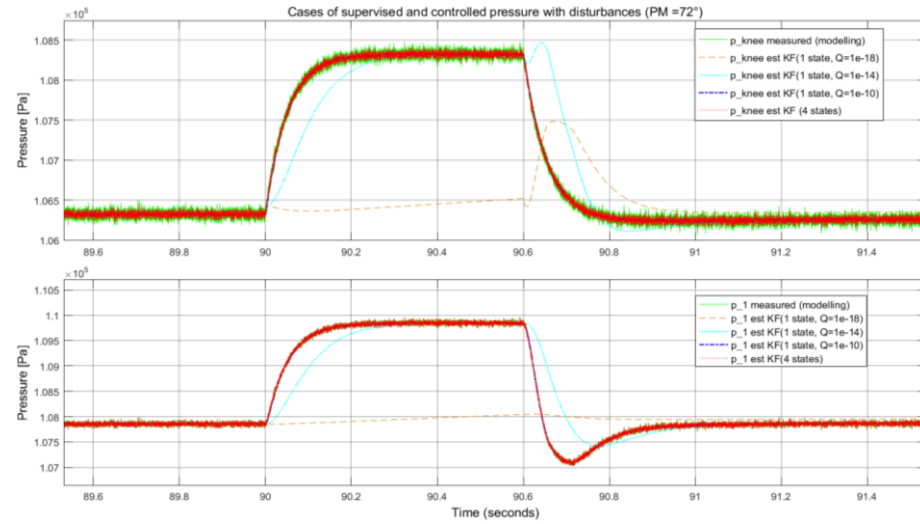


Fig. 4.14 Response of Kalman filter cases during disturbance of the knee flexion.

Figure 4.14 indicates the cases of Kalman filter with the disturbance of the knee flexion (bending  $80^\circ$  at the time 90s). It can be seen from the top panel of Fig. 4.14 that the Kalman filter with 4 states (in red) keep tracking as good as the case of Kalman filter in 1 state with the noise covariance chosen  $Q = [1e-10]$  (in dot-dash blue signal) comparing to the measured pressure  $p_{knee}$  from the process (in green signal).

### 4.3.3 Simulation results with extended Kalman filter

The extended Kalman filter has been developed to implement in nonlinear processes or nonlinear measurements [62], [39]. The EKF works by using linearization online from current trajectory and updating the estimated states from real-time observation instantly [41]. This would give a better result compared to the KF.

Figure 4.15 provides simulation results from the implementation of the EKF with two types: 2 state variables and 4 state variables presentation. Noting that  $Q = [1e-14 \ 0; \ 0 \ 1e-14]$  for 2 states, and  $Q = [1e-8 \ 0 \ 0 \ 0; \ 0 \ 1e-6 \ 0 \ 0; \ 0 \ 0 \ 1e12 \ 0; \ 0 \ 0 \ 0 \ 1e-9]$  for 4 states in this Figure. While the upper plot displays the results of estimated pressure  $\hat{p}_{knee}$ , the middle plot shows the estimate errors of these two types observation. And the errors were minimized comparing to the basic KF method in previous Section 4.3.2. It is clear to state that the fluctuation from the EKF observer was reduced effectively.

In case of 2 states presentation in EKF implementation, by changing the noise covariance matrix  $Q$  from  $[1e-14 \ 0; \ 0 \ 1e-14]$  to various parameters such as  $[1e-10 \ 0; \ 0 \ 1e-10]$  and  $[1e-6 \ 0; \ 0 \ 1e-6]$  relatively, then the estimate results were better with reduced errors and faster response, especially at the transition time and the time of disturbance. These results are indicated in Fig. 4.16 and in Fig. 4.17.

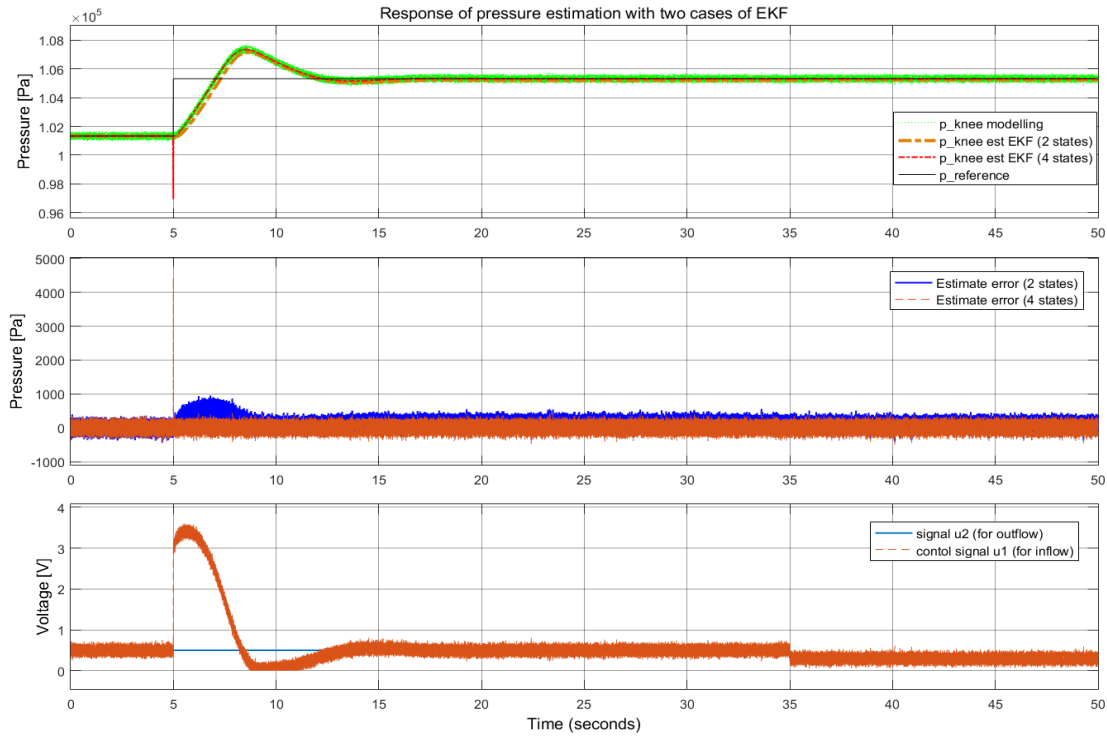


*Fig. 4.15 Response of EKF estimation with two different cases*



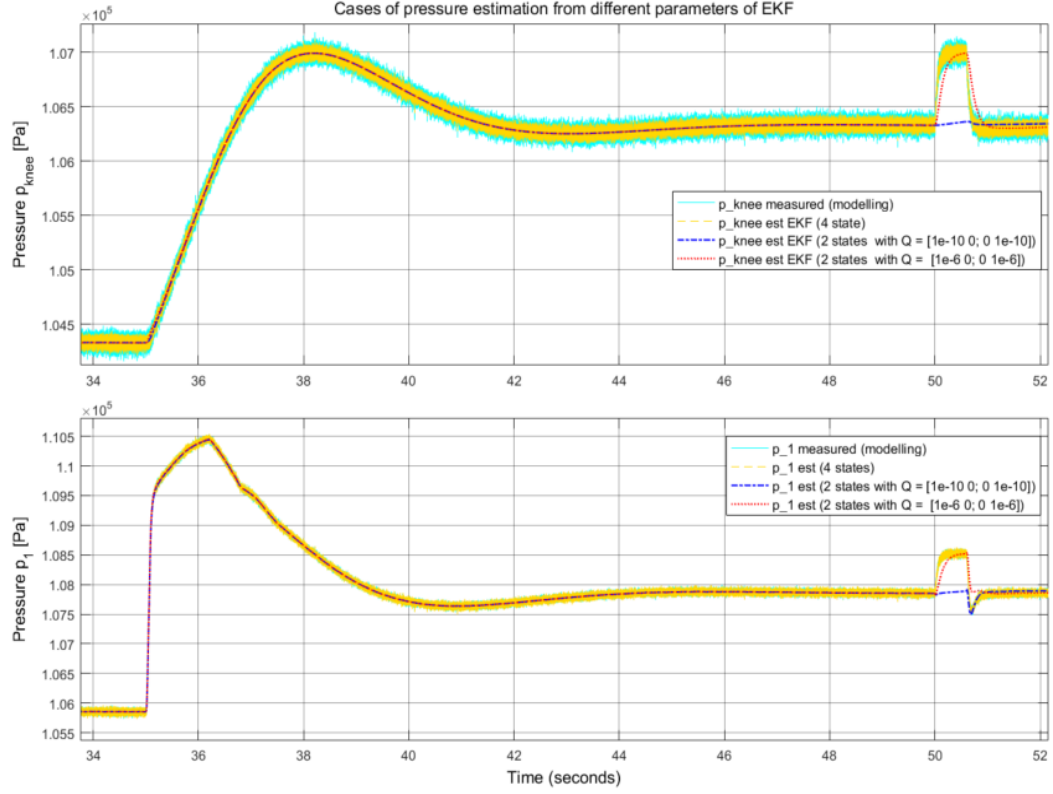


*Fig. 4.16 Response of EKF estimation with disturbance of the knee bending at 50s*

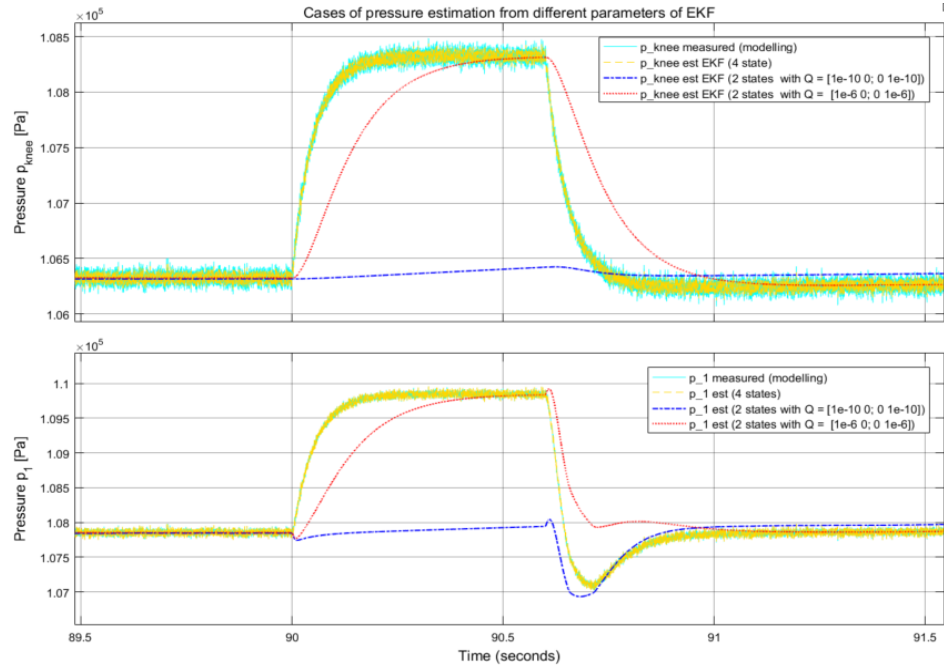


*Fig. 4.17 Cases of pressure estimate in different parameters of EKF during time of disturbance*

On another situation of Simulink with some cases of disturbances from the knee flexions (bending 80° at the time 90s) zoomed in Fig. 4.17, it gives a better result of tracking with the response of

the EKF in 4 states presentation (in yellow signals) compared to the measurement (in light blue). Because the presentation of 4 states variables as in (2.43) included almost all variables of unmeasurable noise information during MIS, while the EKF with 2 states variables in (2.36) provided not enough unmeasurable information. On the other hand, there were some adjustments on the initial condition of the noise covariance of the process  $Q$  in 2 states presentation, and the estimate results from the EKF were improved (in dot red) but it was still not as good as the EKF in case of 4 states. Particularly, From the initial condition of  $Q = [1e-14 \ 0; \ 0 \ 1e-14]$  for 2 states EKF, it can be changed increasing up to  $Q = [1e-6 \ 0; \ 0 \ 1e-6]$  for a better estimate result (see the blue and red signals on the upper plot of Fig. 4.17).

For a good result of estimate with 4 state variables in the EKF, the noise covariance of the process was chosen with value of  $Q = [1e-8 \ 0 \ 0 \ 0; \ 0 \ 1e-6 \ 0 \ 0; \ 0 \ 0 \ 1e12 \ 0; \ 0 \ 0 \ 0 \ 1e-9]$ .

#### 4.3.4 Simulation results with combined state estimator

For the best results after doing with some cases of estimations with various parameters on MATLAB Simulink, the estimated state  $\hat{p}_{knee}$  from the EKF was used as a feedback data to the controller of the process (without using feedback sensor). The response of the controlled pressure is indicated in Fig. 4.18 (red signal on the upper panel).

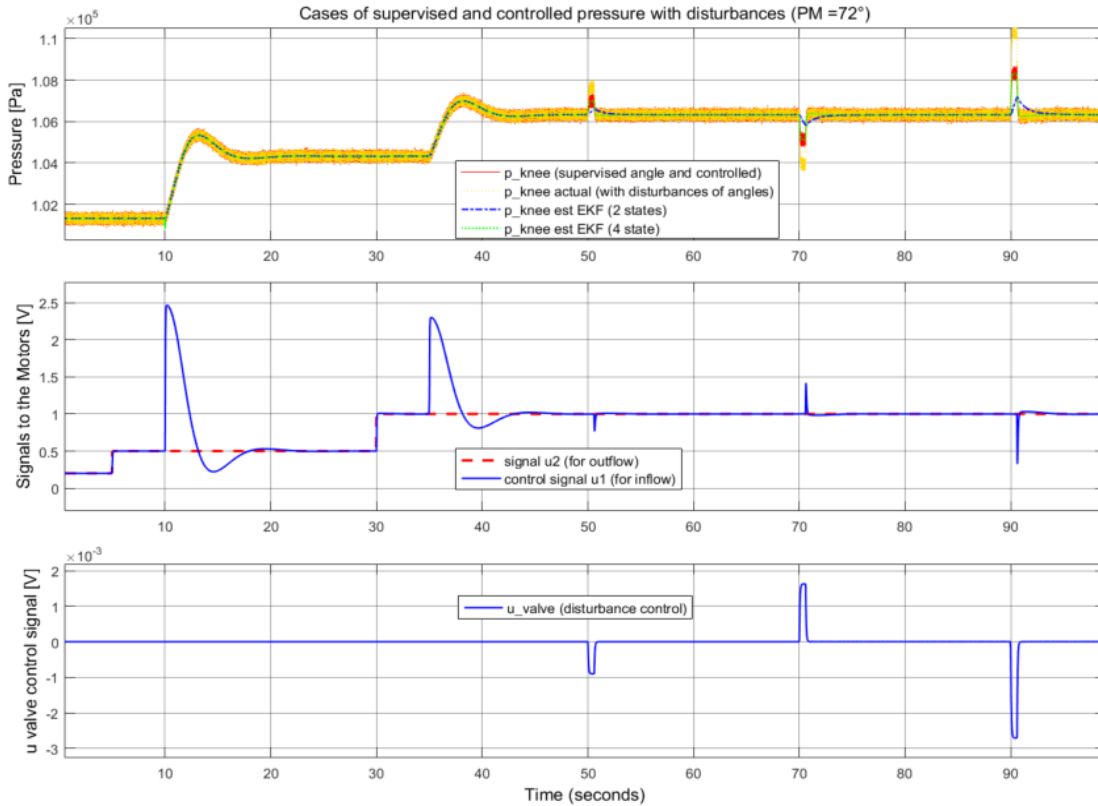


*Fig. 4.18 Simulink results from the combination of 4 states EKF to the controlled system*

## 4.4 Real-time simulator results

This section provides some results of estimate done in real-time experiments with the real device simulator of the knee arthroscopy. While doing with MATLAB Simulink for simulation results (presented in Section 4.3), some noises of process and measurements were assumed. However, these noises are really not exactly the same as the noises occurred in real-time device experiment. Therefore, the results presented in this section are not as ideal as the Simulink results because of the reality and nonlinearity of the the real devices used in the system.

### 4.4.1 Real-time results with Luenberger observer

Figure 4.19 shows the response of estimation in real-time simulator using Luenberger observer.

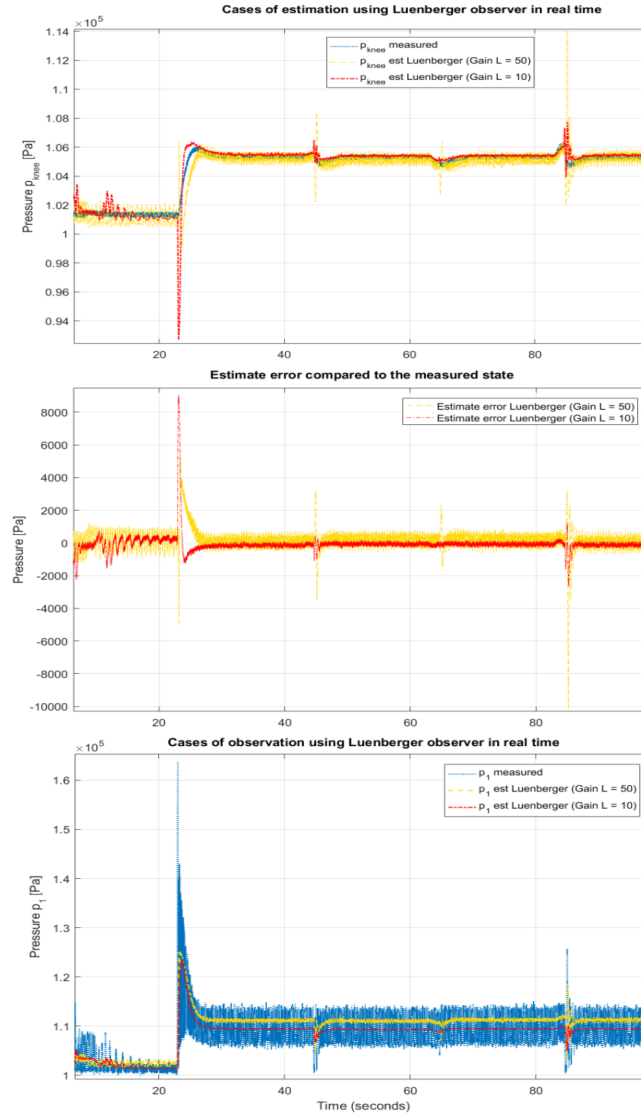


*Fig. 4.19 Experimental results of pressure estimation using Luenberger observer*

It includes some cases of disturbances occurred from the knee flexions. The top panel shows the estimate results of  $\hat{p}_{knee}$ , and the bottom panel gives the results of output  $\hat{p}_1$ . Two different gain  $L$  were implemented :  $L = 50$  and  $L = 10$ . It is seen that with the gain  $L = 50$  (in dashed yellow), the estimator responded faster than the estimate case of  $L = 10$  (in dotted-dashed red). As a result, the fast response estimator might have a higher oscillation in some cases, especially at the transition time or at the time of the knee flexion disturbance. There still existed estimate error. The estimate state of pressure was so sensitive with the disturbances from the knee flexions (the knee bending  $30^\circ$  at the time 44s,  $-60^\circ$  at the time 64s, and  $80^\circ$  at the time 84s).

#### 4.4.2 Real-time results with basic Kalman filter

Figure 4.20 shows some different cases of Kalman filter performance in real-time device simulator.

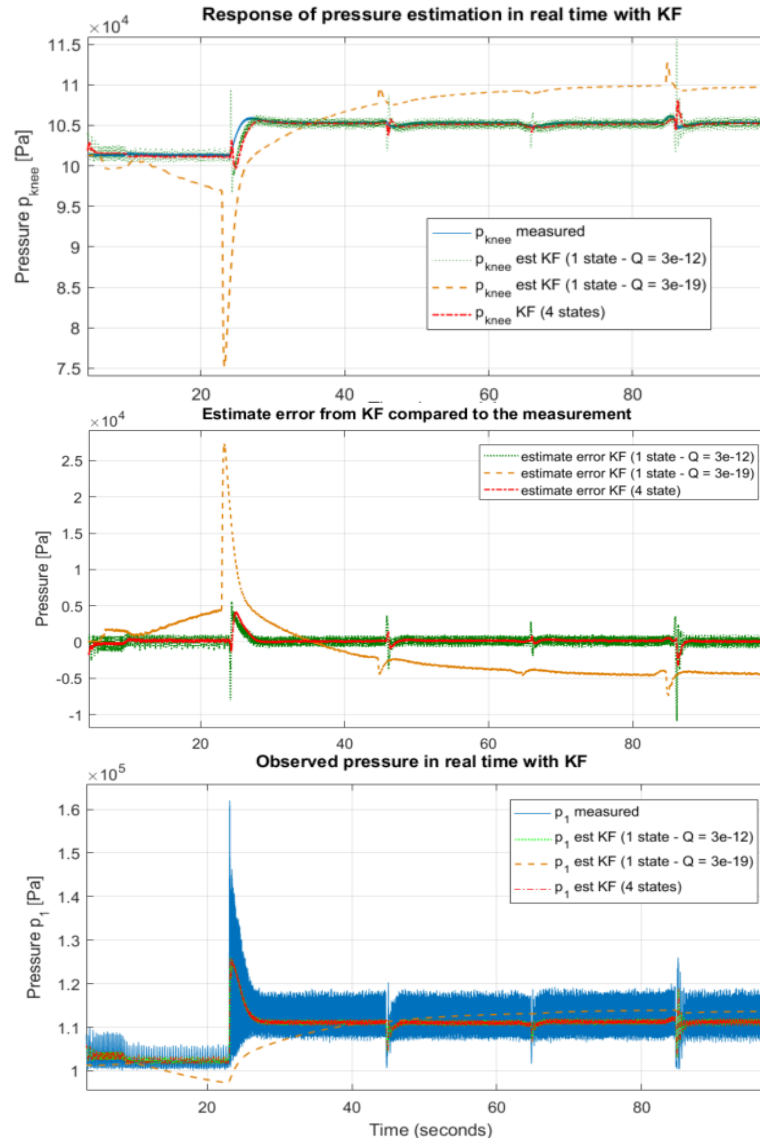
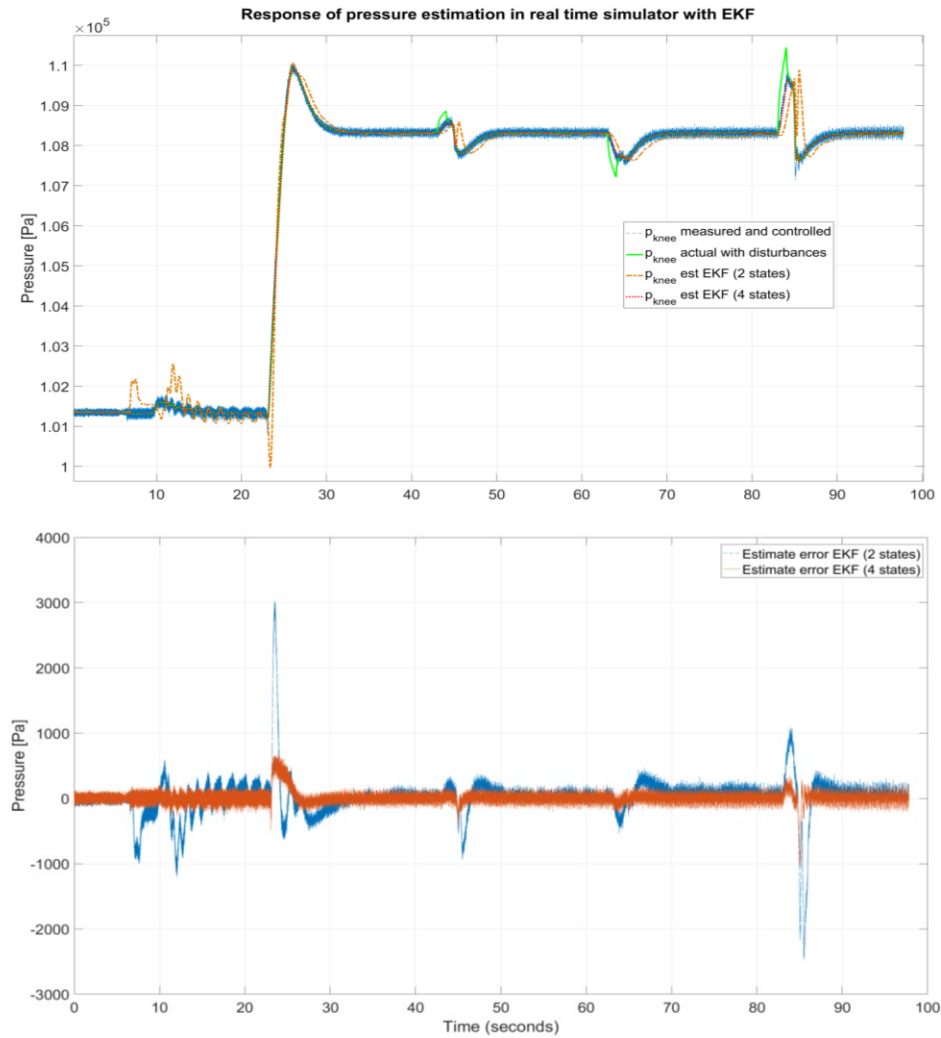


Fig. 4.20 Experimental results of pressure estimation using Kalman filter

The red signals in Fig. 4.20 indicate estimate data from the Kalman filter with 4 state variables. The middle plot shows the estimate errors based on the estimate results on the top panel compared to the measured pressure  $p_{knee}$ . And the bottom graph displays the estimate output pressure comparing to the measurement of  $p_l$  from the DRP. For the case of using 1 state variable in Kalman filter, by changing the noise covariance  $Q$  from  $[3e-19]$  up to  $[3e-12]$  or even  $[1e-10]$ , the estimated state was improved with the reduced error. These changes of estimate results are shown clearly by the dotted green and dashed dark yellow signals in the graphs of the Fig. 4.20.

#### 4.4.3 Real-time results with extended Kalman filter

In extended Kalman filter implementation, the estimate error is minimized comparing to the basic Kalman filter in real-time simulator, even at transition time or at the time of disturbances. Figure 4.21 shows the estimated state (on the upper panel) and the estimate error (on the lower panel).



*Fig. 4.21 Experimental results of pressure estimation using extended Kalman filter*

#### 4.4.4 Real-time result in combination of the estimate state to the controlled process

Based on the results of estimation with observer methods: Luenberger, Kalman filter and extended Kalman filter, the best estimate from the EKF (with 4 states variables) was chosen for the feedback data to the controller of process. Figure 4.22 shows the result from this combination. For evaluating the quality of the estimate state in the controlled process, The actual controlled pressure was measured and indicated with the blue signal. By comparing this measured pressure with the estimate state in yellow signal, it is clear that the estimation from the EKF can be used for the replacement of pressure sensor for a feedback data to the controlled process.

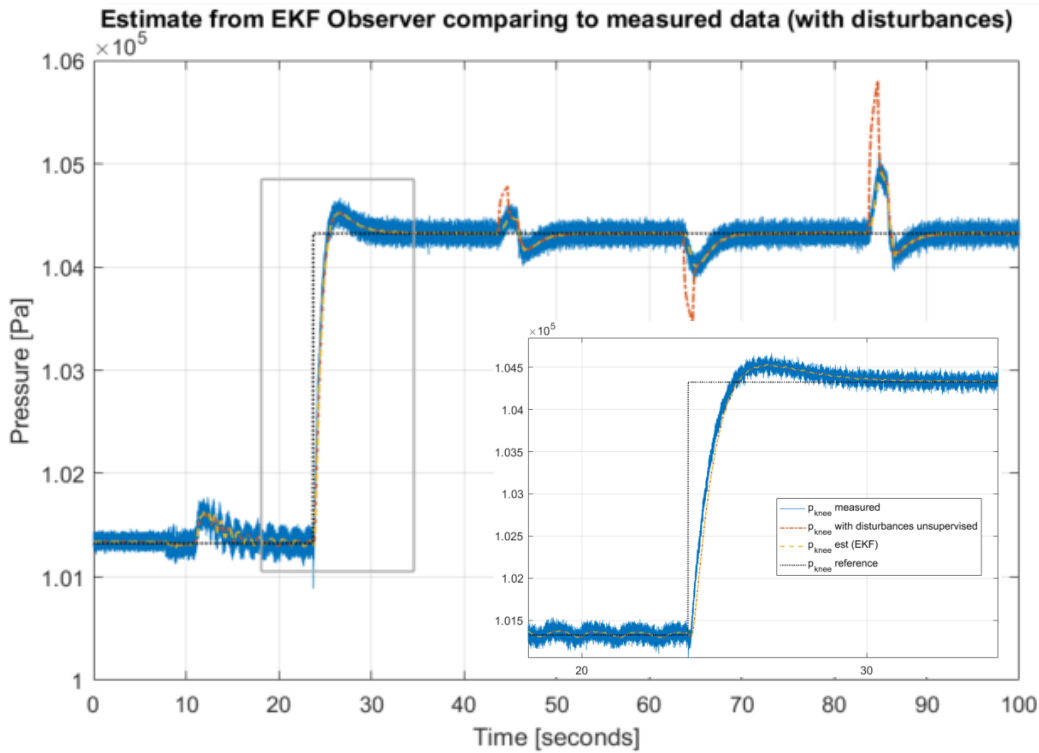


*Fig. 4.22 Result from using estimated state connecting to the controlled process in real-time*

#### 4.5 Discussion of estimate methods

From the three types of observer methods investigated for the pressure estimation in MIS, some ideas are given out for discussion.

- **With the Luenberger method:** it is easy to perform because of the simplification in formulation; there has been many options in choosing observer gain that satisfy the stability and conditions of the observer. The drawback from this method is the sensitivity of observer. This means that the estimate error might go too high during the transition time or time of

disturbance. Another drawback is that it is difficult to solve the eigenvalues for the observer gain calculation in cases of high numbers of state variables.

- ***With the basic Kalman filter:*** This method works with the two main steps of prediction and correction. So the Kalman filter can provide the estimated state more correctly compared to the Luenberger observer. The result from this method depending on the parameters of process noise covariance  $Q$  and measurement noise covariance  $R$ . However, in some cases, it is not easy to find the correct parameters of the noise covariances  $Q$ . In addition, this method is used for linear systems. Thus some estimate error might still exist, especially in the transition time.

- ***With the extended Kalman filter:*** This method was developed and extended from the basic Kalman filter for the applications of nonlinear systems. This advantageous feature gives an optimal algorithm in state estimate compared to those two above observers. In this research, the process of the knee arthroscopy is really nonlinear. And the EKF was applied to estimate the pressure state in the knee model during MIS successfully. In fact, the estimate results from the EKF were more precise than the two observer methods of Luenberger and basic Kalman filter. Finally, the best estimated state of pressure from the EKF was used to interconnect with the closed loop sensorless controlled system effectively. This takes an important role for the real-life applications of the development in medical therapy devices.

## 4.6 Summary

This research is on the verification stage before applying to the real patient, so a temporary pressure sensor was mandatory used in the knee model during MIS for comparing and evaluating the precision of estimated pressure state. The Luenberger method was applied as an optional observer. However, some error has not been solved thoroughly. Additionally, because the Kalman filter was designed to implement basically in linear processes, therefore in this case of pressure estimation, the process of MIS was chosen to obtain with the KF in the working point of the linear area. From this feature, the estimate results from the KF algorithm still exist some error compared to the real state of measured pressure in experiment, especially during the transition time. Finally, the implementation of the EKF has been done more successfully in this nonlinear system of MIS with the minimized error in pressure state estimate results.

While doing experiments with the HIL-Simulator of the knee arthroscopy, there were some unwanted and unmeasurable components of noises. These noises are not avoidable.

The first bothered component is the lost of unmeasurable gas in the operation area. It can be created by the movements of the trocars and surgical instruments which connect to the knee model via the

holes or incisions during MIS. This was the one causing trouble of pressure lost in real-time experiments. This drop of pressure occurred and could not be measured or calculated during MIS.

The second trouble is the loss of fluid during MIS. This might happen internally in the surgical region and cause to the change of pressure. It is similar to the loss of gas when the disturbance is unknown or unmeasured. Therefore it made more difficult to estimate the state precisely because this part influenced directly to the pressure state in the knee model. If the operation is in a short time, then this loss can be omitted. However, when the operation is taken in a long time like an hour, this could be a problem for the estimation, because this amount of loss or raise pressure could not be calculated and estimated accurately. Those are the reasons that take some effects to the precision of estimate in basic Kalman filter or Luenberger observer.

Another trouble is the influence of the fluid flows. This came from the peristaltic motion of the roller pumps and the turbulent flows. From the directly compression of the four flexible roller wheels of the DRP to the soft peristaltic pipe segment, the volume flows inside the pipes at the DRP are not always laminar. It depends on the rotation speeds of the motors. And another turbulent flow came from the junction between the plastic tube and the metal trocar connecting to the model of the knee joint.

In order to overcome those obstacles of nonlinear components that are unmeasurable, the estimator should enclosure all of those states of noises into the prediction. In this research, components of noises were included in the extended Kalman filter with 4 states presentation for estimation. In fact, the estimate error in this case was reduced effectively.



## **5 CONCLUSIONS AND FURTHER WORK**

This final chapter concludes the tasks that have been done in the research as well as some ideas for further work for the development of medical therapy devices in minimally invasive surgery.

### **5.1 Conclusions**

From the author's motivation presented in chapter 1, this thesis has been approached to the objectives for a contribution of pressure control and estimation in minimally invasive surgery. Particularly, the author has worked completely with the following tasks:

- Firstly, this research provided to the author some knowledge basically on procedures of minimally invasive surgery. This is one of the preparations for modelling process of MIS, especially for modelling of the knee arthroscopy.
- Secondly, the research has been carried out with modelling process of the knee arthroscopy of MIS both in simulation and in real-time device simulator. Before doing construction on HIL-Simulator integrated with physical interface of the knee and software model for real-time experiment, modelling process on MATLAB Simulink had been performed. This is really important because of the feasibility in controller design and pressure estimation. In addition, by this performance, some cases of analysis and evaluation were given to avoid some problems or faults that might occur to the real system. To complete the HIL- simulator for the realization of knee arthroscopy in the laboratory of Medical device engineering, Institute of Automation, University of Rostock, we were grateful for the supports on medical devices from the World of Medicine company – W.O.M. Berlin via the project AFluCoMIS. Without their sponsorship, it would be difficult for the author to finish the research in real-time experiments. The construction of the HIL-Simulator module is really important in this research while the experiment on the real patient is not allowed during the stage of investigation and verification. Furthermore, basing on the operation of the concreted system, the process of the knee arthroscopy was identified and linearized. This work is necessary for the preparation of controller design strategy and supervisory algorithms. Some mathematical formulations in state space presentation of the process were also presented in order to implement to the cases of pressure estimation in the knee model during MIS.
- Thirdly, with the identified and linearized process, The PI controller was designed based on Symmetric Optimum method to ensure the stability of pressure in the OA during arthroscopic

performance. Additionally, in nonlinear system, the windup phenomenon usually happens in integrating elements from the process or from the controller, therefore the designed PI\_SO controller was also integrated and well done with the anti windup algorithm. Furthermore, some types of disturbances from the situations of the patient's knee flexion also make some change of pressure in the knee joint. These kinds of unwanted changes were paid attention in order to supervise and eliminate successfully by the supervisory algorithm interacting to the controller of the system.

- Finally, with the goal of providing some methods of pressure estimator for the replacement of pressure sensor in the knee joint of the controlled process of arthroscopy, three types of observers were selected to implement. These types are Luenberger observer, basic Kalman filter, and extended Kalman filter. Pressure estimation is also one of the key roles in this research, because in the controlled system, it is worthful to have a feedback data to the controller while the usage of pressure sensor inside the operation area is not allowed for the patient's safety. By implementing those three types of observers to the modelled process as well as to the real device simulator, the extended Kalman filter gave the best result of estimation compared to the other two observers. And the estimate state of pressure  $\hat{p}_{knee}$  from the EKF was selected to combine to the controller as a feedback data to the controller. The whole controlled system worked effectively with this estimate state.

However, this research has just been reached with the knee arthroscopy but have not been applied in other cases of laparoscopy of MIS. Furthermore, the study has just been in the stage of verification and evaluation. So, the research might be developed with capable of parameters or equipments optimization in order to apply to the real patient services. And finally, the reference values of pressure in this research were tested in various values, but those values were changed manually like the adjustment from the surgeon. So the reference should be improved to adjust optimally and automatically based on the individual physiological state of each patient currently, because the blood pressure on each person can be varied and it depends on many factors such as health status, mentality, weights, ages, and so on.

## **5.2 Further work**

By using the built HIL-Simulator, the research of the knee arthroscopy can be extended to other types arthroscopy like in the wrist or other joints. Additionally, it should be noted to expand the research with the cases of laparoscopy. In cases of laparoscopy, the supported material for visualization is the provision of Carbon dioxide or Helium gas. So, in order to expand the scope of applications from arthroscopy to laparoscopy, instead of controlling the DRP for the flows of rinsing fluid, the system should be controlled with bi-directional electrical valve for the gas volume

into the area like in abdomen. Therefore, it should be noticed to have some calculations on the amount of gas into the area for the desired pressure guarantee.

For applying to the real patient services, the system should be paid attention more to the parameters of blood pressure of each individual body. This would be helpful in choosing a suitable value of pressure reference for the controller. Because the blood pressure parameter is completely different on each patient and it is related to the reference pressure for the controller of the system. And the parameter of blood pressure is depended on many factors such as genders, ages, weights, mentality or current mental health. Thus, in order to have a suitable reference of pressure to the controlled system, it should be expanded with an iterative optimization of settings parameters automatically for the reference values as mentioned in citation [1]. This includes the extended close loop interpretation presented in Fig. 5.1.

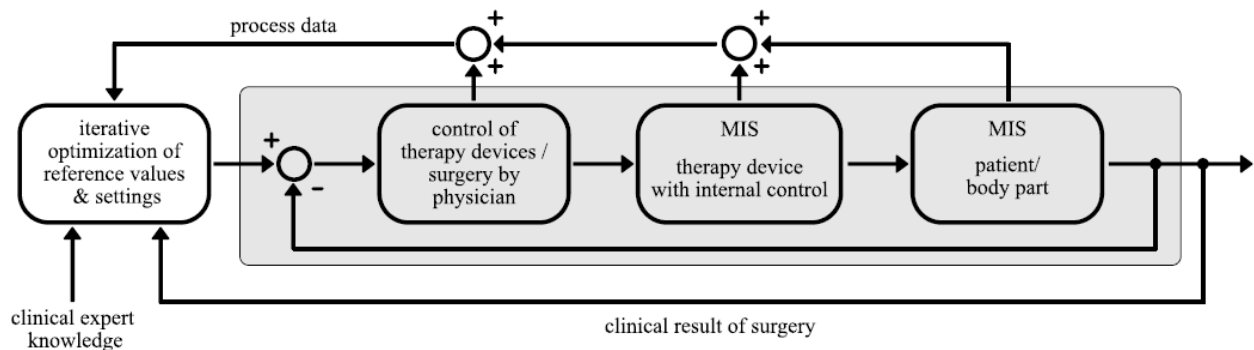


*Fig. 5.1 An interpretation of iterative optimization algorithm in minimally invasive surgery [1]*

This iterative optimization algorithm can be realized by utilizing both feedback data from clinical result of surgery and data bank of blood pressure parameters from clinical expert knowledge or experienced data from the surgeons. The data should be processed, optimized and adapted for the reference values and settings automatically by the intervention of computational statistics and mathematical optimization methods in machine learning.



## APPENDIX A

This appendix presents some alternate results in both simulation and in real-time experiment with the HIL-Simulator for more clear information of analytic explanations in controller design.

### A.1 Results of controller design in simulation

Besides the satisfied results shown in chapter 3 for controller design, it should be clear to present some alternate cases for more proofs of clarification.

#### A.1.1 Simulation of pressure control without disturbances

This section presents three different cases of results by choosing parameters of phase margin in controller design:  $37^\circ$ ,  $60^\circ$  and  $78^\circ$  for analytics.

##### A.1.1.1 Case of phase margin $37^\circ$

The parameters of the PI\_SO controller were presented in Table 3.1. The results of modelling system in Simulink are shown in Fig. A.1, whereas the upper panel is the response of pressure in the knee model ( $p_{knee}$ ), and the control signal is displayed in the lower panel.

It is noted that at the time of 5 second and 25 second in Fig. A.1, the outflow of the rinsing fluid was activated to change (with the dash red signal at the lower panel) while the reference pressure in the knee model remained no change (see the dash red signal at the upper panel), then the signal  $u_1$  for inflow was controlled to change automatically regarding to the signal  $u_2$  of outflow. This is to ensure the desired pressure in the knee model whenever the change of outflow might happen.

With the rising time of 1.218 seconds from the result in Fig. A.1, the response of pressure in the knee model is controlled with the overshoot value around 29.17%. This value of overshoot would be higher than 60% if there was no anti-wind up algorithm for limitation of the voltage to the motors at the double roller pump. This can be seen clearly on the control signal  $u_1$  (for the inflow) at the lower panel of Fig. A.1 with the appearances of saturation periods starting at the times of 10 second and 30 second. This algorithm of voltage limitation therefore also limited the overshoot of the controlled system effectively. Noting that the rising time and overshoot from here are determined from the result of modelled system, not from the identified process. So these parameters are not the same from the parameters shown in the last column of Table 3.1.

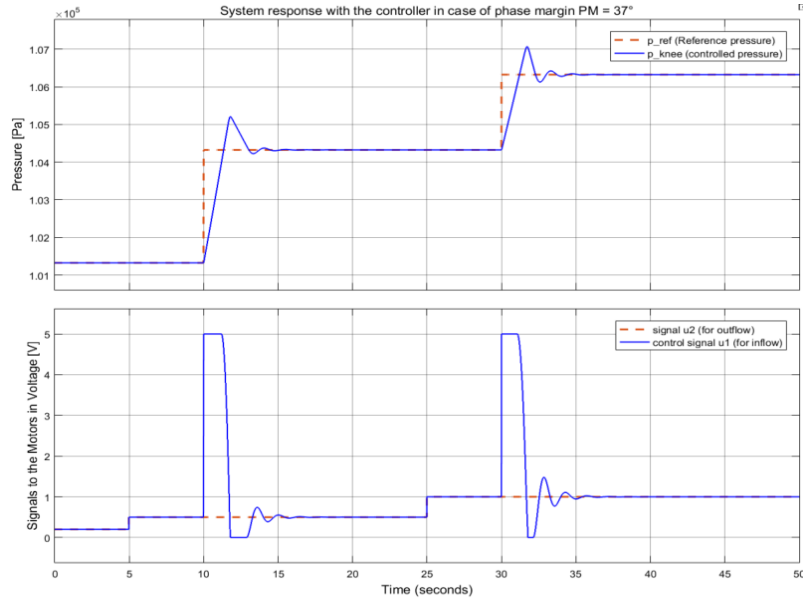


*Fig. A.1 Response of system with the controller in the case of phase margin  $PM = 37^\circ$*

#### ***A.1.1.2 Case of phase margin $60^\circ$***

While doing some changes of various phase margin cases for analyzing, the author realized that the settling time values were nearly not changed much between the cases of  $37^\circ$  and  $60^\circ$ . However, the overshoot values were changed significantly. Particularly, the overshoot from the case of  $60^\circ$  in phase margin was about double times of percentage compared to the case of  $37^\circ$ . The rise time is about 1.22s and the overshoot is around 60%. The result is in Fig. A.2.

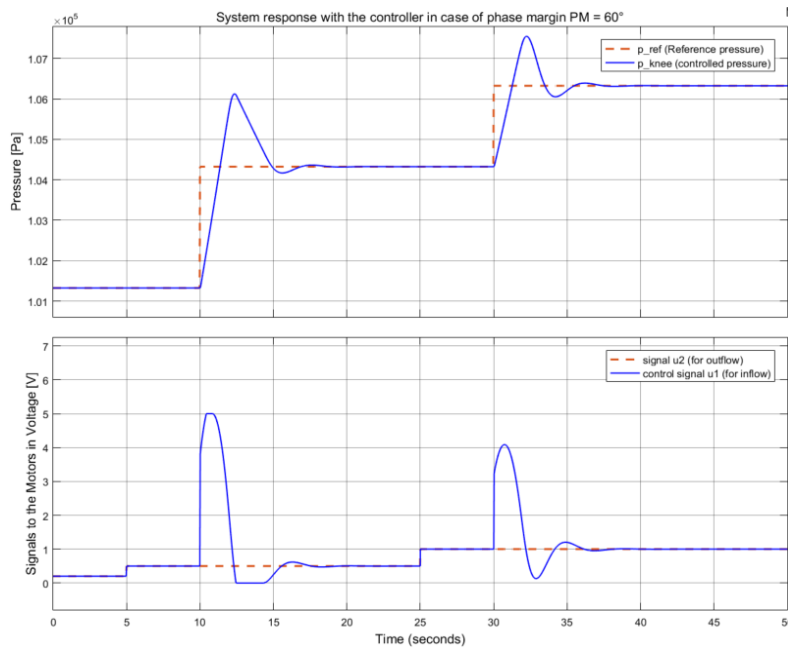


*Fig. A.2 Response of system with the controller in the case of phase margin  $PM = 60^\circ$*

In this case, the windup phenomenon was nearly not happened. In normal, the overshoot would be decreased while increasing the phase margin from  $37^\circ$  to  $78^\circ$ . But within the cases of PM less than  $60^\circ$ , the results proved that controlled system ran into the wind up phenomenon which were successfully againtsted by anti-wind up algorithm. This is to explain the reason why the overshoot in the case of PM =  $37^\circ$  is lower than in this case of  $60^\circ$ . With the increase of phase margin from  $60^\circ$  up to  $78^\circ$ , the response of pressure in the controlled system shall be more sensitive changed in both rising time and overshoot values.

#### ***A.1.1.3 Case of phase margin $78^\circ$***

With the result in Fig. A.3, the good point in this case is that the pressure response was smoother than all the cases above (the overshoot was reduced to 22.5%). On the contrary, the rise time is longer from the other cases (around 2.3 seconds) in Simulink of modelling system. Therefore, with the longer time of response compared to the case of  $72^\circ$  in phase margin (in chapter 3, Fig. 3.14), it might be the only drawback in controller design in this case of  $78^\circ$ .

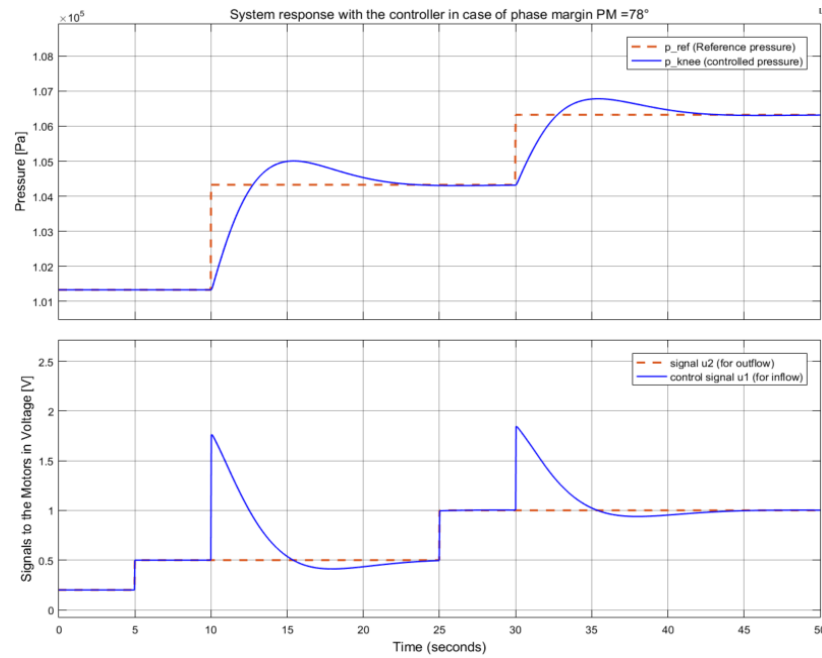


*Fig. A.3 Response of system with the controller in the case of phase margin PM =  $78^\circ$*

### **A.1.2 Simulation with supervisory algorithm of the knee flexion disturbances**

#### ***A.1.2.1 Case of phase margin $37^\circ$***

As shown in Fig. A.4a, There are three typical cases of results in disturbances supervisory: flexions of the knee in  $30^\circ$ ,  $-60^\circ$  and  $80^\circ$  starting at the seconds of 50, 70 and 90 correspondingly (signal  $p_{knee}$  actual in dark yellow, the controlled pressure in blue on the top plot). Figure A.4b shows

more detail of the result in period of time “zoom block” from Fig. A.4a. In the lower panel, a negative value of ‘ $u_{\text{valve}}$ ’ signal (disturbance control) was appeared to eliminate the positive change of actual pressure disturbance in the knee.

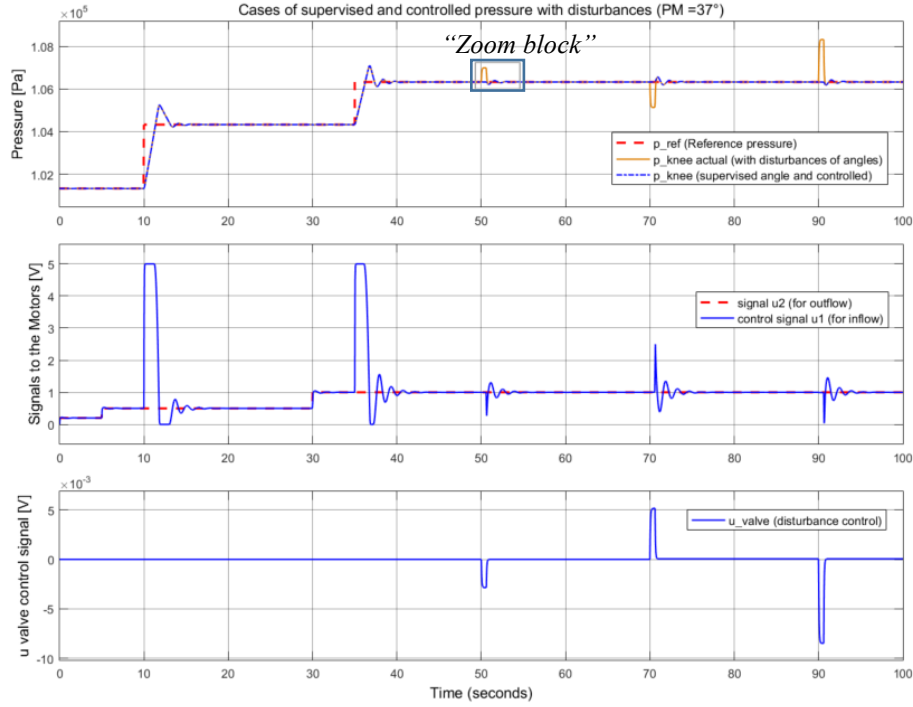


*Fig. A.4a Case of controller with supervised disturbances ( $PM = 37^\circ$ )*

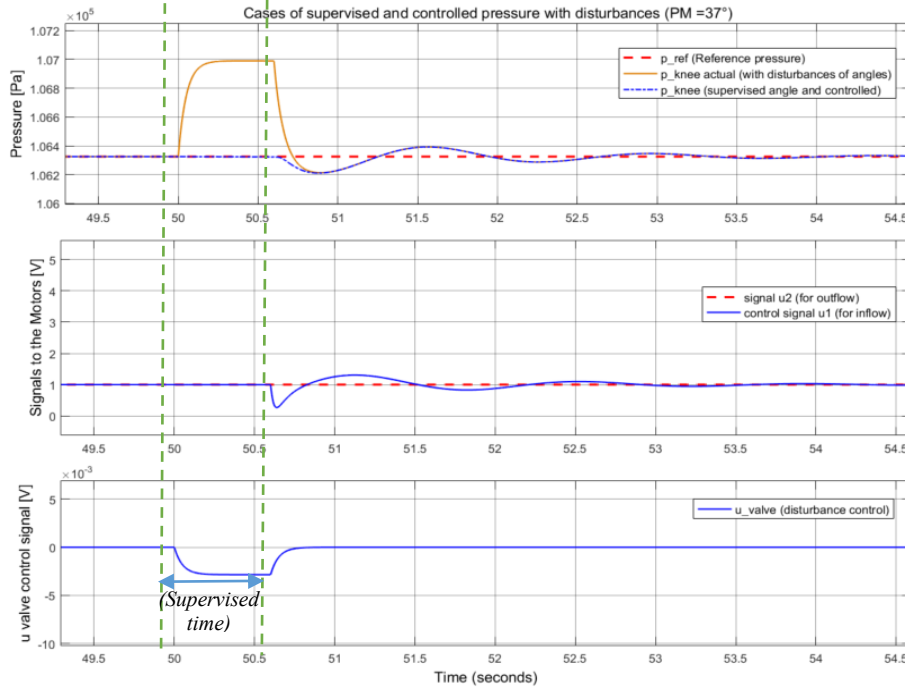


*Fig. A.4b Description of disturbance period “Zoom block” from Fig. A.4a*



### A.1.2.2 Case of phase margin $60^\circ$

Similarly, the same cases of disturbances for supervised and controlled process with  $PM = 60^\circ$  was tested with the flexions of the knee in  $30^\circ$ ,  $-60^\circ$  and  $80^\circ$  starting at the seconds of 50, 70 and 90.

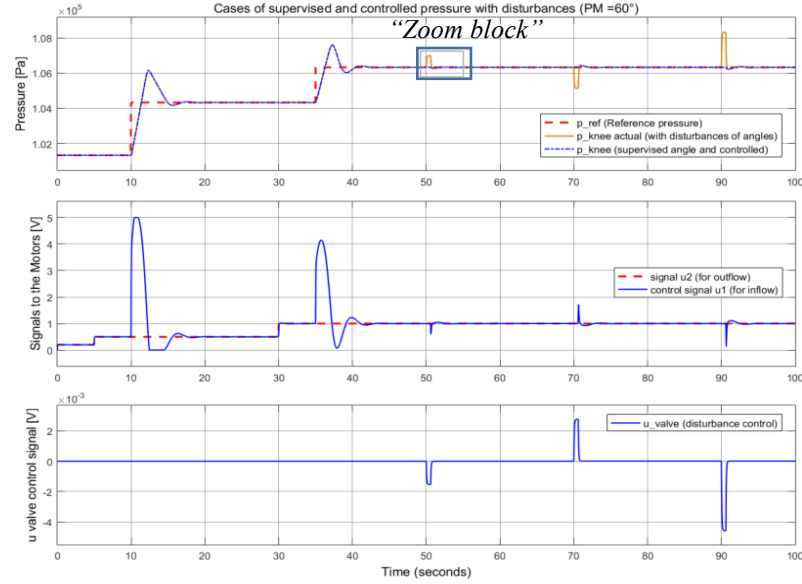


Fig. A.5a Case of controller with supervised disturbances ( $PM = 60^\circ$ )

The results in Fig. A.5a indicate that the response is some how better than in the case of  $PM = 37^\circ$ . Figure A.5b is a detail description of the “Zoom block” marked in Fig. A.5a. It can be seen that the disturbances of pressure from the knee flexions was reduced in this case also.

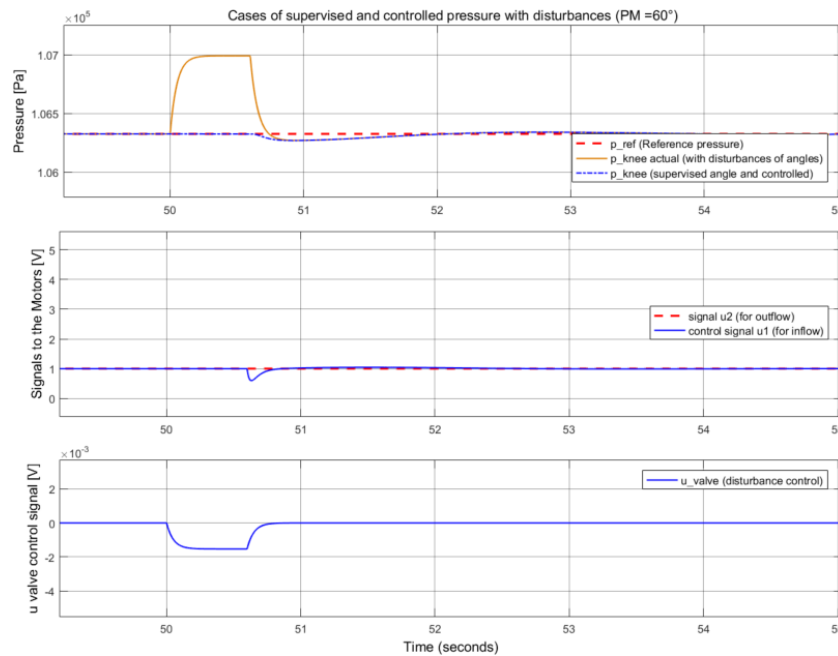


Fig. A.5b Description of disturbance of the “Zoom block” from Fig. A.5a

### A.1.2.3 Case of phase margin $78^\circ$

Although the case of phase margin  $PM = 72^\circ$  is an optimal choice for a reasonable response of rising time, but the case of  $PM = 78^\circ$  is also another option for the choice in real-time experiment because of the lower overshoot compared to the case of  $72^\circ$  phase margin. The result in Simulink with the disturbances of pressure in  $78^\circ$  of phase margin is presented in Fig. A.6.

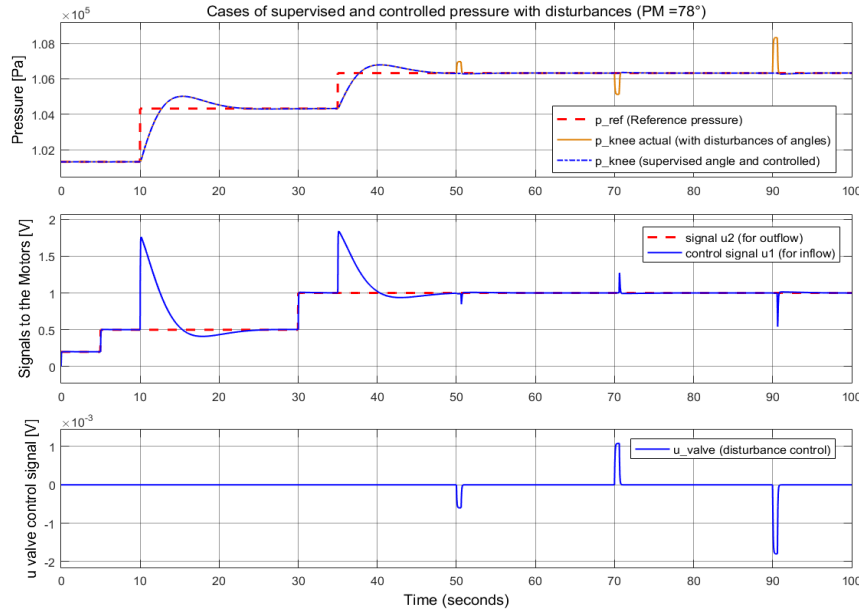


Fig. A.6 Case of controller with disturbances supervisory ( $PM = 78^\circ$ )

## A.2 Experimental results of controller design in real-time device simulator

### A.2.1 Experimental results of controller without supervisor of disturbances

#### A.2.1.1 Case of phase margin $37^\circ$

The upper panel of Fig. A.7 is the response of controlled pressure in the knee model (in blue signal). The reference pressure is in dashed black. The lower panel presents two signals of voltage  $u_1$  and  $u_2$  to the DC motors called the control signals of inflow and outflow respectively.

It can be seen that at the beginning time from 0 to 13 seconds, when the outflow is set to zero (no flow of rinsing fluid out of the knee model), then the inflow is also controlled to zero and there is less oscillation in measured controlled pressure. When the signal of  $u_2$  is changed to nonzero, then the control signal of  $u_1$  is adapted automatically to keep the track relatively close to the signal of  $u_2$ . During this time period (after 13 seconds in Fig. A.7), the measured data from both controlled pressure and control signal of  $u_1$  have bigger ranges of oscillation. These phenomenon can be explained by the reflexion from the actual pressure in the knee model reacting to the pressure at

the DRP. Furthermore, because of the peristaltic feature from the four free wheels, therefore the flows at the DRP are transferred by series of fluid packages. This also causes to some oscillation.

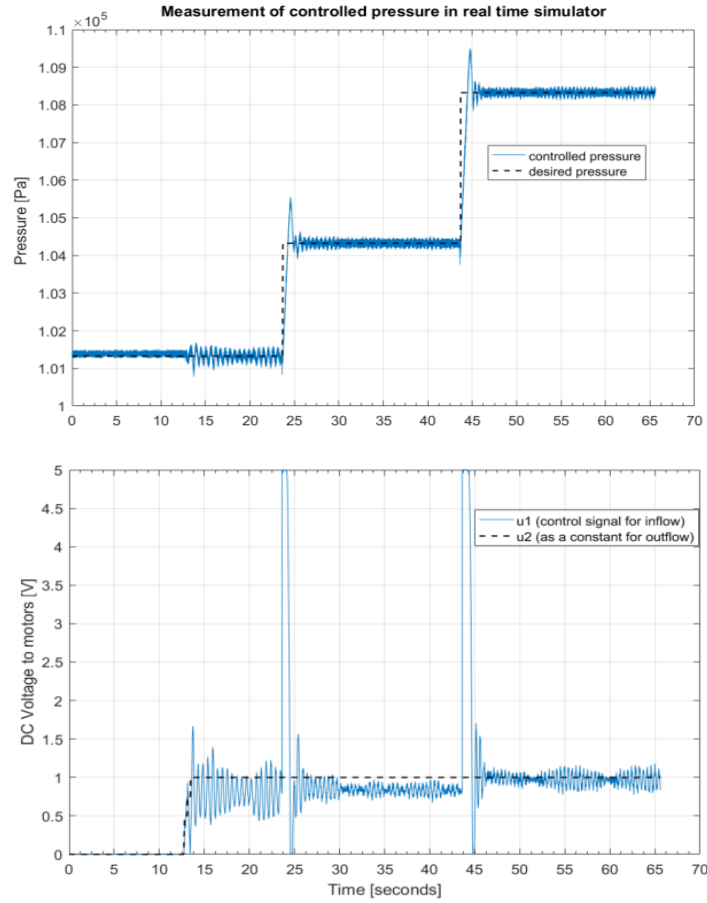


*Fig. A.7 Case of controller without disturbances and supervision ( $PM = 37^\circ$ )*

In this case, the measurement from the control signal  $u_1$  is not close correctly to the signal of  $u_2$ . This is proved that there always exists some noise from the loss of flow or pressure in the knee model; some noise from encoding and decoding of the discrete signal during operation; or some noise from the sensor itself during measurement of real-time devices experiment.

#### ***A.2.1.2 Case of phase margin $60^\circ$***

Comparing with the result in Fig. A.7, the response of pressure in this case (blue signal in Fig. A.8) has bigger overshoot. This was explained with the same case in Simulink presented in section A.1.1.2, because of the anti-wind up strategy during transition time.

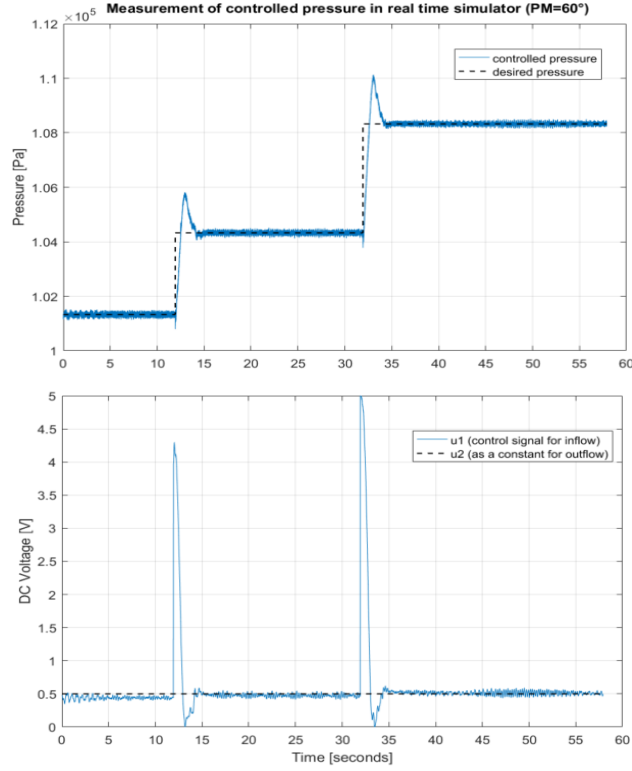


*Fig. A.8 Case of controller without disturbances and supervision ( $PM = 60^\circ$ )*

### ***A.2.1.3 Case of phase margin $78^\circ$***

While doing experiment, the author also tried to give some pressure loss as a type of disturbance at the output. Then the controlled pressure in the knee model was still remained stable at the desired value. And this resulted in some difference between the inflow and the outflow. The difference between them is indicated by signals  $u_1$  and  $u_2$  in the lower panel of Fig. A.9.

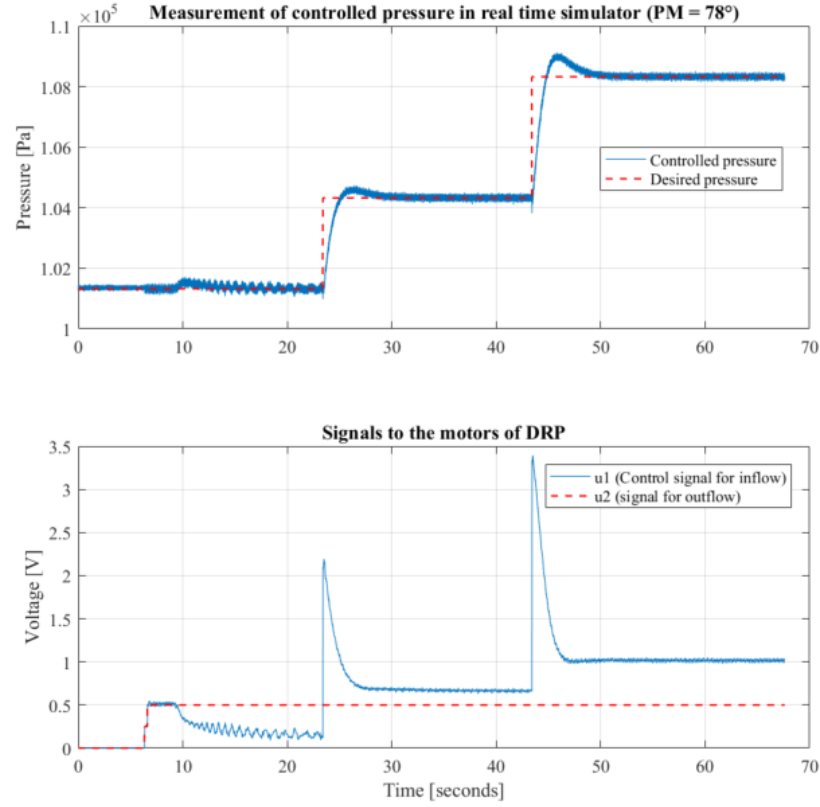


*Fig. A.9 Case of controller without disturbances and supervision (PM = 78°)*

## **A.2.2 Experimental results of supervised controller with the knee flexion disturbances**

### ***A.2.2.1 Case of phase margin 37°***

There are three types of disturbances as the knee angle changes at different times (noises from knee flexion of 30° at 45s, knee flexion of -60° at 65s, and knee flexion of 80° at 85s respectively) in this case of PM = 37°. The result is shown in Fig. A.10 . Because the controller feature in this case works ineffectively, therefore it is easy in getting fluctuation with the disturbances. This is the reason leading to the unexpected result as in Fig. A.10 . The disturbances of pressure to the process were not supervised and controlled efficaciously.

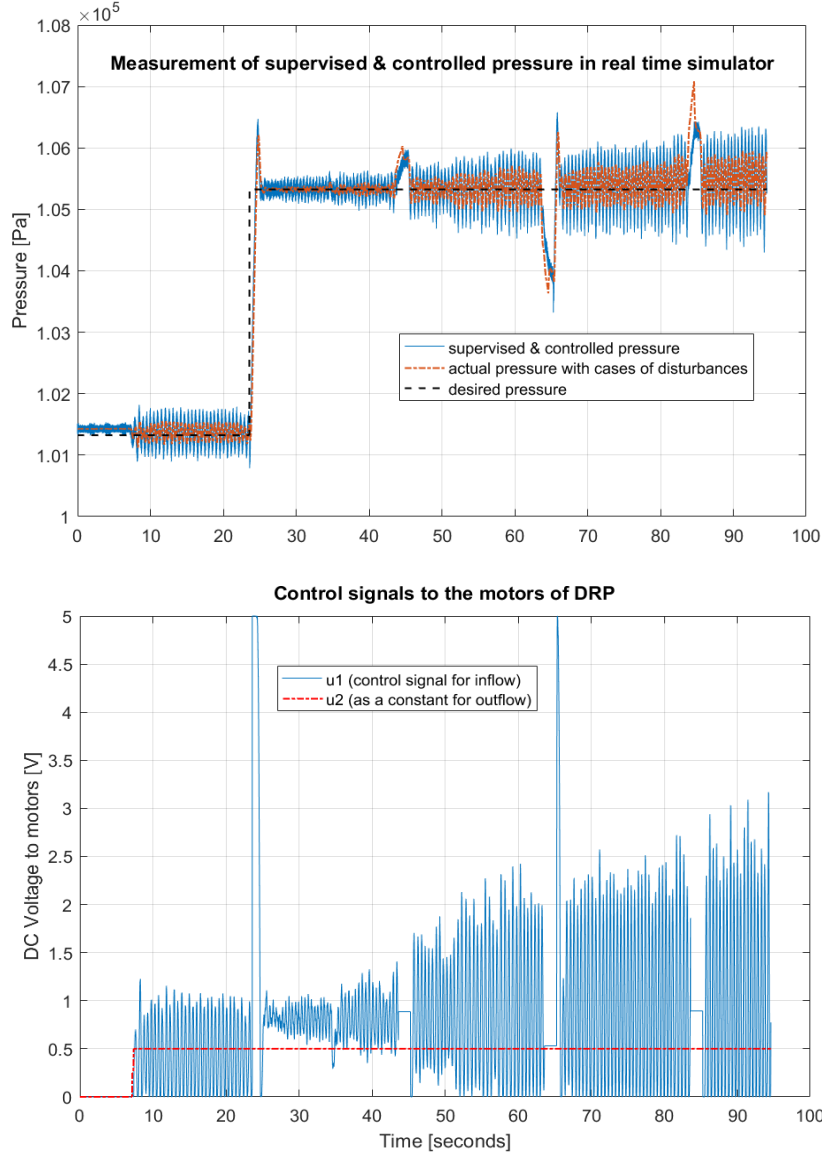


*Fig. A.10 Case of controller with disturbances and supervision ( $PM = 37^\circ$ )*

#### ***A.2.2.2 Case of phase margin $60^\circ$***

In this case of controlling and supervising, two types of knee angle disturbances ( $-30^\circ$  and  $60^\circ$ ) were tested. Time of disturbances were in 44s and 64s relatively (in dark yellow signal). The result is presented in Fig. A.11. The response of supervised and controlled pressure is indicated (in blue) on the upper panel of the figure. It looks better than the result in the case of  $37^\circ$  phase margin from Fig. A.10 .

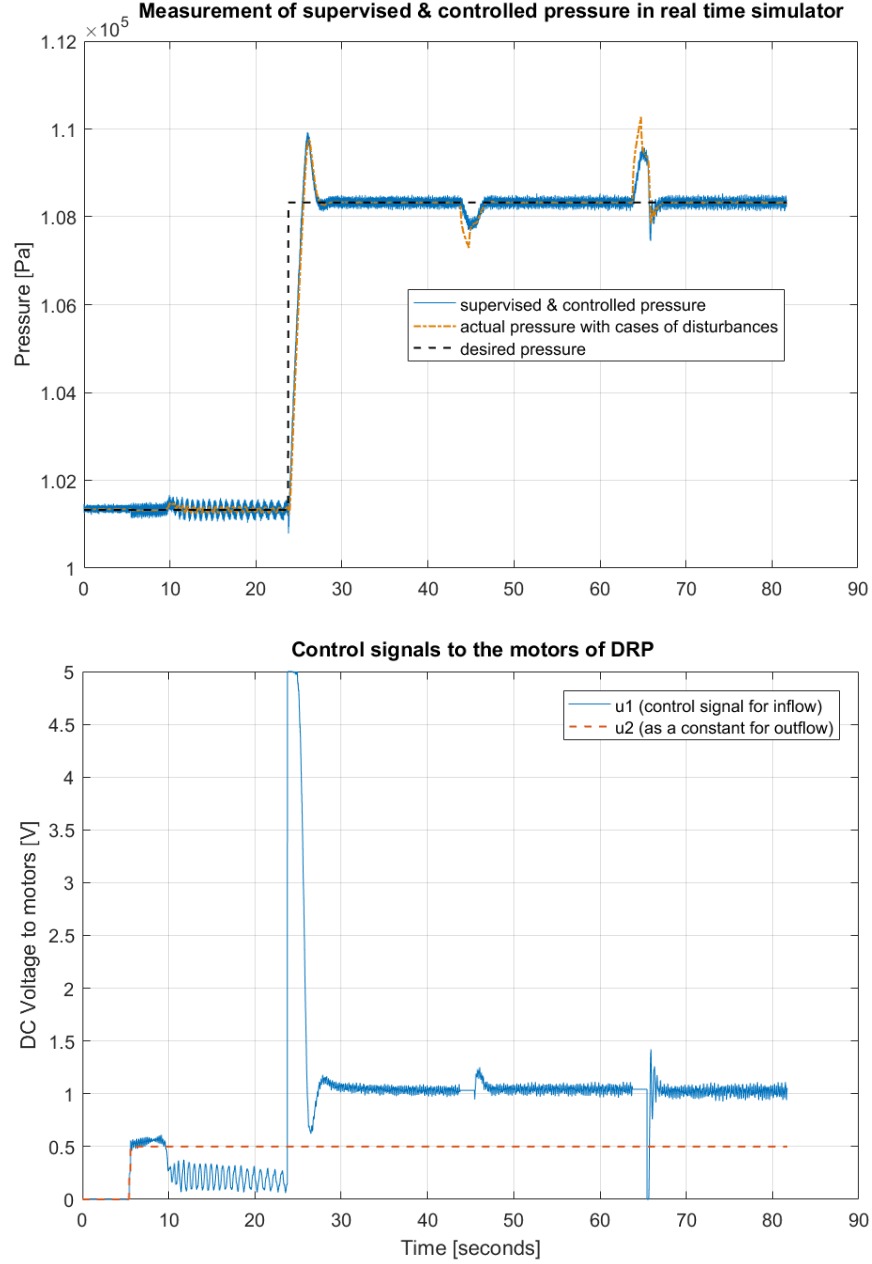
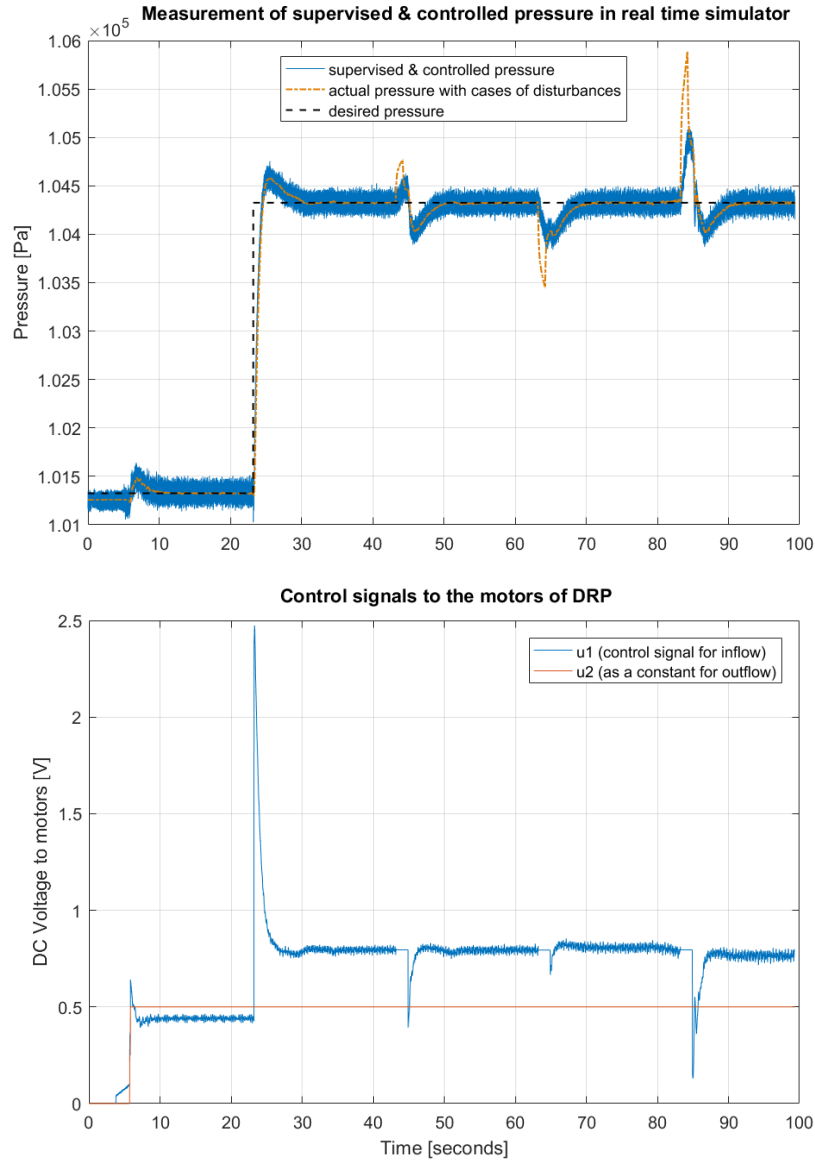


Fig. A.11 Case of controller with disturbances and supervision ( $PM = 60^\circ$ )

### A.2.2.3 Case of phase margin $78^\circ$

As mentioned in Section A.1.2.3 (at the same case of phase margin in Simulink), it is obvious that the result in this case of real-time experiment is also smoother than the other cases with the reduced overshoot percentage, although there has been a little bit longer time in transition period. This is shown in Fig. A.12. From the lower plot of the figure, there existed some difference between the signal  $u_2$  (for the outflow) and the control signal  $u_1$  (for the inflow). This might come from some loss of gas or flows for the expansion in the OA during MIS.



*Fig. A.12 Case of controller with disturbances and supervision ( $PM = 78^\circ$ )*



## LIST OF FIGURES

Fig. 1.1 An overview of the knee arthroscopy [10] .....	2
Fig. 1.2 A simple schematic representaion of the knee arthroscopy [11] .....	2
Fig. 1.3 Graph of pressure-volume relationship with the knee flexion angles 15°, 60°, 80° [16]..	5
Fig. 1.4 An overview of the whole controlled system .....	7
Fig. 2.1 An example of the knee arthroscopy in minimally invasive surgery [18] .....	12
Fig. 2.2 An overview of the system in minimally invasive surgery [7], [14] .....	12
Fig. 2.3 Block diagram and signals for modelling of process in minimally invasive surgery .....	15
Fig. 2.4 Overview of the brushed DC motor GR63-55 .....	15
Fig. 2.5 Response of revolution regarding to the input voltage .....	16
Fig. 2.6 Dynamic response of the motor .....	17
Fig. 2.7 Basic function of a peristaltic pump for flowing fluid [23] .....	18
Fig. 2.8 Overview of the DRP: 1. Motor; 2. Roller wheel; 3. Plastic tube; 4. Pressure sensor ....	18
Fig. 2.9 Relationship between the motor speed $n_i$ and the flow at the pump $Q_{pi}$ .....	18
Fig. 2.10 The tube for fluid transfer: 1. Trocar; 2. Pressure sensor; 3. Flexible part .....	19
Fig. 2.11 The pressure drop through the operation area depending on the flow at the pump .....	20
Fig. 2.12 The flow in the tube (close to the operation area) regarding to the motor speed .....	20
Fig. 2.13 Block diagram for modelling of the tubes in MIS .....	22
Fig. 2.14 The reservoir is used for the simulation of the operation area with some trocars .....	22
Fig. 2.15 Simple description of laminar and turbulent flows [24] .....	25
Fig. 2.16 Friction factor and Moody diagram (Note in figure: $D = D_i$ , $\lambda = \lambda_f$ ) [24] .....	25
Fig. 2.17 Pressure - injected volume relationship in cases of flexions 0-30° .....	27
Fig. 2.18 Pressure - injected volume relationship in case of flexion around 60° .....	27
Fig. 2.19 Pressure-injected volume relationship in case of flexion around 80° .....	28
Fig. 2.20 I/O interface connection between the development computer and physical devices ....	31
Fig. 2.21 Simplified description of the HIL-Simulator in MIS [7] .....	33
Fig. 2.22 Signal and states in the HIL-Simulator [7] .....	34

Fig. 2.23 Configuration of the air pump actuator of the HIL-Simulator [7].....	35
Fig. 2.24 Actuators with electric valve and air compressor of the HIL-Simulator.....	39
Fig. 3.1 Controller and supervisor strategy for the desired pressure in MIS .....	42
Fig. 3.2 Step response of pressure in the knee model (modelling and real-time).....	43
Fig. 3.3 Basic structure of PID controller [30] .....	44
Fig. 3.4 Simplified structure of the open loop controlled process .....	45
Fig. 3.5 Frequency response of the linearized process of $G_p(j\omega)$ .....	46
Fig. 3.6 Responses of a close-loop second order system regarding to various values of $\zeta$ [30] ..	47
Fig. 3.7 Frequency response of the open loop controlled process $G_{OL}(j\omega)$ with $\varphi_R = 37^\circ$ .....	48
Fig. 3.8 Frequency response of the open loop controlled process $G_{OL}(j\omega)$ with $\varphi_R = 60^\circ$ .....	49
Fig. 3.9 Frequency response of the open loop controlled process $G_{OL}(j\omega)$ with $\varphi_R = 78^\circ$ .....	50
Fig. 3.10 Frequency responses of the open loop controlled process $G_{OL}(j\omega)$ in 3 cases.....	51
Fig. 3.11 Conditional integration algorithm integrated in PI controller .....	53
Fig. 3.12 Anti-windup tracking by integrating time in PI controller .....	53
Fig. 3.13 Type of incremental algorithm of anti-windup integrated to the PI controller .....	54
Fig. 3.14 Structure of the inner disturbance controller for the knee flexion.....	55
Fig. 3.15 Response of system with the controller in the case of phase margin $PM = 72^\circ$ .....	56
Fig. 3.16 Case of controller with disturbances supervisory ( $PM = 72^\circ$ ) .....	57
Fig. 3.17 Case of controller without disturbances and supervision ( $PM = 72^\circ$ ).....	58
Fig. 3.18 Case of controller with disturbances and supervision ( $PM = 72^\circ$ ).....	59
Fig. 4.1 Role of an observer as an estimator in controlled system [37].....	62
Fig. 4.2 General description of the observer in the controlled process of MIS [38] .....	62
Fig. 4.3 A typical description of an observer in state space (in dashed block) [30] .....	63
Fig. 4.4 Response of the Luenberger observer in different values of gain selections .....	65
Fig. 4.5 Functional structure of the Kalman filter in MIS .....	67
Fig. 4.6 Recursive loop description of a Kalman filter.....	73
Fig. 4.7 Description of an estimated trajectory with extended Kalman filter [40] .....	74
Fig. 4.8 Recursive loop operation of extended Kalman filter [38] .....	75
Fig. 4.9 Cases of pressure estimation in different parameters of Luenberger observer gain (L) .	76

Fig. 4.10 Comparison between two cases of estimation parameters: $L = 10$ and $L = 50$ .....	77
Fig. 4.11 Luenberger responses while controlling valve for elimination of disturbances .....	77
Fig. 4.12 Response of pressure estimation with two cases of Kalman filter. ....	78
Fig. 4.13 Response of Kalman filter with the state $pknee$ and the observation $p1$ .....	79
Fig. 4.14 Response of Kalman filter cases during disturbance of the knee flexion.....	79
Fig. 4.15 Response of EKF estimation with two different cases .....	80
Fig. 4.16 Response of EKF estimation with disturbance of the knee bending at 50s.....	81
Fig. 4.17 Cases of pressure estimate in different parameters of EKF during time of disturbance	81
Fig. 4.18 Simulink results from the combination of 4 states EKF to the controlled system .....	82
Fig. 4.19 Experimental results of pressure estimation using Luenberger observer .....	83
Fig. 4.20 Experimental results of pressure estimation using Kalman filter.....	84
Fig. 4.21 Experimental results of pressure estimation using extended Kalman filter .....	85
Fig. 4.22 Result from using estimated state connecting to the controlled process in real-time ...	86
Fig. 5.1 An interpretation of iterative optimization algorithm in minimally invasive surgery [1]	91
Fig. A.1 Response of system with the controller in the case of phase margin $PM = 37^\circ$ .....	94
Fig. A.2 Response of system with the controller in the case of phase margin $PM = 60^\circ$ .....	94
Fig. A.3 Response of system with the controller in the case of phase margin $PM = 78^\circ$ .....	95
Fig. A.4a Case of controller with supervised disturbances ( $PM = 37^\circ$ ) .....	96
Fig. A.4b Description of disturbance period “Zoom block” from Fig. A.4a.....	96
Fig. A.5a Case of controller with supervised disturbances ( $PM = 60^\circ$ ) .....	97
Fig. A.5b Description of disturbance of the “Zoom block” from Fig. A.5a.....	97
Fig. A.6 Case of controller with disturbances supervisory ( $PM = 78^\circ$ ) .....	98
Fig. A.7 Case of controller without disturbances and supervision ( $PM = 37^\circ$ ).....	99
Fig. A.8 Case of controller without disturbances and supervision ( $PM = 60^\circ$ ).....	100
Fig. A.9 Case of controller without disturbances and supervision ( $PM = 78^\circ$ ).....	101
Fig. A.10 Case of controller with disturbances and supervision ( $PM = 37^\circ$ ).....	102
Fig. A.11 Case of controller with disturbances and supervision ( $PM = 60^\circ$ ).....	103
Fig. A.12 Case of controller with disturbances and supervision ( $PM = 78^\circ$ ).....	104



## **LIST OF TABLES**

Table 2.1 Proposed pressure level with and without tourniquet in various joints [5]. .....	14
Table 2.2 Parameters of the motor GR63-55 [22]. .....	16
Table 3.1 Parameters and results with the PI_SO controller .....	51



## REFERENCES

- [1] A. Benkmann, E. Smolinski, T. Jeinsch, P. Westerhoff, T. Wustrack, and H. Hommel, “Concept of iterative optimization of minimally invasive surgery,” in *2017 22nd International Conference on Methods and Models in Automation and Robotics (MMAR)*, Aug. 2017, pp. 443–446, doi: 10.1109/MMAR.2017.8046868.
- [2] Frank S. Tsai, Daniel Johnson, Cameron S. Francis, and Sung-Hwan Cho, “Fluidic lens laparoscopic zoom camera for minimally invasive surgery,” vol. 15, pp. 030504-15–3, 2010.
- [3] C. R. Molinas and P. R. Koninckx, “Hypoxaemia induced by CO(2) or helium pneumoperitoneum is a co-factor in adhesion formation in rabbits,” *Hum. Reprod.*, vol. 15, no. 8, pp. 1758–1763, Aug. 2000.
- [4] D. M. D. Özdemir-van Brunschot, K. C. J. H. M. van Laarhoven, G.-J. Scheffer, S. Pouwels, K. E. Wever, and M. C. Warlé, “What is the evidence for the use of low-pressure pneumoperitoneum? A systematic review,” *Surg Endosc*, vol. 30, no. 5, pp. 2049–2065, May 2016, doi: 10.1007/s00464-015-4454-9.
- [5] M. S. Hsiao, N. Kusnezov, R. N. Sieg, B. D. Owens, and J. P. Herzog, “Use of an Irrigation Pump System in Arthroscopic Procedures,” *Orthopedics*, vol. 39, no. 3, pp. e474-478, May 2016, doi: 10.3928/01477447-20160427-01.
- [6] T. Muellner, W. A. Menth-Chiari, R. Reihsner, J. Eberhardsteiner, and L. Engebretsen, “Accuracy of pressure and flow capacities of four arthroscopic fluid management systems,” *Arthroscopy*, vol. 17, no. 7, pp. 760–764, Sep. 2001, doi: 10.1053/jars.2001.25340.
- [7] E. Smolinski, A. Benkmann, P. Westerhoff, M. Van Nguyen, W. Drewelow, and T. Jeinsch, “A Hardware-In-The-Loop Simulator for the Development of Medical Therapy Devices,” *IFAC-PapersOnLine*, vol. 50, no. 1, pp. 15050–15055, Jul. 2017, doi: 10.1016/j.ifacol.2017.08.2517.
- [8] R. Bergstrom and J. Gillquist, “The use of an infusion pump in arthroscopy,” *Arthroscopy: The Journal of Arthroscopic & Related Surgery*, vol. 2, no. 1, pp. 41–45, Jan. 1986, doi: 10.1016/S0749-8063(86)80009-3.
- [9] “Knee Arthroscopy - OrthoInfo - AAOS.” <https://www.orthoinfo.org/en/treatment/knee-arthroscopy/> (accessed Mar. 31, 2019).
- [10] “Dr Peter Smith Orthopaedic Knee - Arthroscopy Procedures, Milnerton Medi-Clinic, Cape Town,” *Dr. Peter Smith | Orthopaedic Surgeon*. <https://www.orthosurgeon.co.za/dr-peter->

smith-orthopaedic-knee-arthroscopy-procedures-milnerton-medi-clinic-cape-town/  
(accessed Mar. 31, 2019).

- [11] J. W. Ewing, D. A. Noe, H. B. Kitaoka, and M. J. Askew, “Intra-Articular Pressures During Arthroscopic Knee Surgery,” p. 6.
- [12] D. J. Ogilvie-Harris and L. Weisleder, “Fluid pump systems for arthroscopy: A comparison of pressure control versus pressure and flow control,” *Arthroscopy: The Journal of Arthroscopic & Related Surgery*, vol. 11, no. 5, pp. 591–595, Oct. 1995, doi: 10.1016/0749-8063(95)90137-X.
- [13] V. M. Nguyen and T. Jeinsch, “Pressure Control in Minimally Invasive Surgery,” *International Symposium on Automatic Control*, Sep. 2017. [http://autsym.hs-wismar.de/?page\\_id=1405](http://autsym.hs-wismar.de/?page_id=1405) (accessed Sep. 10, 2018).
- [14] V.-M. Nguyen, E. C. Smolinski, A. Benkmann, W. Drewelow, and T. Jeinsch, “An application of pressure estimation in minimally invasive surgery,” in *4th International Conference on Green Technology and Sustainable Development (GTSD)*, Nov. 2018, pp. 658–662, doi: 10.1109/GTSD.2018.8595513.
- [15] M. Bauer and R. W. Jackson, “Intra-articular pressure in the knee during routine arthroscopy,” *Arthroscopy: The Journal of Arthroscopic & Related Surgery*, vol. 2, no. 3, pp. 198–199, Sep. 1986, doi: 10.1016/S0749-8063(86)80068-8.
- [16] D. A. Funk, F. R. Noyes, E. S. Grood, and S. D. Hoffman, “Effect of flexion angle on the pressure-volume of the human knee,” *Arthroscopy: The Journal of Arthroscopic & Related Surgery*, vol. 7, no. 1, pp. 86–90, Mar. 1991, doi: 10.1016/0749-8063(91)90084-B.
- [17] “Arthroscopic surgery - Answers on HealthTap.” <https://www.healthtap.com/topics/arthroscopic-surgery> (accessed Apr. 01, 2019).
- [18] “Knee Osteoarthritis: Is Arthroscopy Any Help?” <https://healamed.com/disease/43-arthritis-and-gout/343-knee-osteoarthritis-is-arthroscopy-any-help.html> (accessed Apr. 01, 2019).
- [19] D. S. Morrison, R. K. Schaefer, and R. L. Friedman, “The relationship between subacromial space pressure, blood pressure, and visual clarity during arthroscopic subacromial decompression,” *Arthroscopy: The Journal of Arthroscopic & Related Surgery*, vol. 11, no. 5, pp. 557–560, Oct. 1995, doi: 10.1016/0749-8063(95)90131-0.
- [20] G. Arangio and K. E. Kostelnik, “Intraarticular pressures in a gravity-fed arthroscopy fluid delivery system,” *Arthroscopy: The Journal of Arthroscopic & Related Surgery*, vol. 8, no. 3, pp. 341–344, Sep. 1992, doi: 10.1016/0749-8063(92)90065-J.
- [21] B. C. Bomberg, P. E. Hurley, C. A. Clark, and C. S. McLaughlin, “Complications associated with the use of an infusion pump during knee arthroscopy,” *Arthroscopy: The Journal of*



- Arthroscopic & Related Surgery*, vol. 8, no. 2, pp. 224–228, Jun. 1992, doi: 10.1016/0749-8063(92)90040-I.
- [22] D. GmbH, “GR/G | Brushed DC Motors,” *Dunkermotoren GmbH*, Jan. 30, 2019. <https://www.dunkermotoren.com/en/products/brushed-dc-motors/detail/8844201270/> (accessed Apr. 29, 2019).
- [23] “Peristaltic pump,” *Wikipedia*. Apr. 09, 2019, Accessed: Apr. 30, 2019. [Online]. Available: [https://en.wikipedia.org/w/index.php?title=Peristaltic\\_pump&oldid=891654646](https://en.wikipedia.org/w/index.php?title=Peristaltic_pump&oldid=891654646).
- [24] D. Han, *Concise Hydraulics*, 1st edition. 2008.
- [25] A. A. Olufemi, “Effect of Turbulence Flow on Pressure Drop in a Single Phase Vertical Pipe,” *The Open Petroleum Engineering Journal*, vol. 4, no. 1, pp. 1–8, Jan. 2011, doi: 10.2174/1874834101104010001.
- [26] F. M. White, *Fluid Mechanics*, 6th ed. McGraw-Hill, 2008.
- [27] J. Klespitz and L. Kovacs, “Peristaltic pumps - A review on working and control possibilities,” in *2014 IEEE 12th International Symposium on Applied Machine Intelligence and Informatics (SAMI)*, Herl’any, Slovakia, Jan. 2014, pp. 191–194, doi: 10.1109/SAMI.2014.6822404.
- [28] “Kalman filtering for positioning and heading control of ships and offshore rigs,” *IEEE Control Systems*, vol. 29, no. 6, pp. 32–46, Dec. 2009, doi: 10.1109/MCS.2009.934408.
- [29] “MicroLabBox\_Product-information\_190128\_E.pdf.” [https://www.dspace.com/shared/data/pdf/2019/MicroLabBox\\_Product-information\\_190128\\_E.pdf](https://www.dspace.com/shared/data/pdf/2019/MicroLabBox_Product-information_190128_E.pdf) (accessed May 13, 2019).
- [30] “PID controller,” *Wikipedia*. Apr. 14, 2019, Accessed: Apr. 15, 2019. [Online]. Available: [https://en.wikipedia.org/w/index.php?title=PID\\_controller&oldid=950864163](https://en.wikipedia.org/w/index.php?title=PID_controller&oldid=950864163).
- [31] K. Ogata, *Modern control engineering*, 5th ed. Boston: Prentice-Hall, 2010.
- [32] K. J. Aström and T. Hagglund, *PID controllers: Theory, Design, and Tuning*, 2nd Edition. Instrument Society of America, 1995.
- [33] K. J. Aström and T. Hagglund, *Advanced PID Control*. ISA - Instrumentation, Systems, and Automation Society, 2006.
- [34] H. Lutz and W. Wendt, *Taschenbuch der Regelungstechnik: mit MATLAB und Simulink*, 10., ergänzte Aufl. Haan-Gruiten: Verl. Europa-Lehrmittel, Nourney, Vollmer, 2014.
- [35] S. Isaka and A. V. Sebald, “Control strategies for arterial blood pressure regulation,” *IEEE Transactions on Biomedical Engineering*, vol. 40, no. 4, pp. 353–363, Apr. 1993, doi: 10.1109/10.222328.

- [36] The Analytic Sciences Corporation and A. Gelb, Eds., *Applied optimal estimation*. Cambridge, Mass: M.I.T. Press, 1974.
- [37] G. Ellis, “The Luenberger Observer: Correcting Sensor Problems,” in *Observers in Control Systems*, Elsevier, 2002, pp. 67–96.
- [38] G. Ellis, “Introduction to Observers in Control Systems,” in *Control System Design Guide*, Elsevier, 2012, pp. 185–212.
- [39] V.-M. Nguyen, E. C. Smolinski, A. Benkmann, W. Drewelow, and T. Jeinsch, “An Application of Extended Kalman Filter for the Pressure Estimation in Minimally Invasive Surgery,” in *Advances in Neuroergonomics and Cognitive Engineering*, vol. 953, H. Ayaz, Ed. Cham: Springer International Publishing, 2020, pp. 331–343.
- [40] B. D. O. Anderson and J. B. Moore, *Linear Optimal Control*. U.S.A: Prentice-Hall, Inc., Englewood Cliffs, N.J., 1971.
- [41] R. G. Brown and P. Y. C. Hwang, *Introduction to Random Signals and Applied Kalman Filtering*, Fourth Edition. United States of America: John Wiley & Sons, Inc., 2012.
- [42] S. M. M, N. Naik, R. M. O. Gemson, and M. R. Ananthasayanam, “Introduction to the Kalman Filter and Tuning its Statistics for Near Optimal Estimates and Cramer Rao Bound,” *arXiv:1503.04313 [stat]*, Mar. 2015, Accessed: Oct. 24, 2018. [Online]. Available: <http://arxiv.org/abs/1503.04313>.
- [43] C. K. Chui and G. Chen, *Kalman filtering with real-time applications*, 4th Edition. Berlin; New York: Springer, 2009.
- [44] F. Auger, M. Hilairet, J. M. Guerrero, E. Monmasson, T. Orlowska-Kowalska, and S. Katsura, “Industrial Applications of the Kalman Filter: A Review,” *IEEE Transactions on Industrial Electronics*, vol. 60, no. 12, pp. 5458–5471, Dec. 2013, doi: 10.1109/TIE.2012.2236994.
- [45] Y. H. Xie, “Kalman Filter for Dynamic Positioning Ships Using Position and Acceleration Feedback,” *Applied Mechanics and Materials*, vol. 543–547, pp. 2362–2367, Mar. 2014, doi: 10.4028/www.scientific.net/AMM.543-547.2362.
- [46] B. M. Bell and F. W. Cathey, “The iterated Kalman filter update as a Gauss-Newton method,” *IEEE Transactions on Automatic Control*, vol. 38, no. 2, pp. 294–297, Feb. 1993, doi: 10.1109/9.250476.
- [47] T. Vaispacher, R. Andoga, R. Breda, and F. Adamcik, “Application of linearized Kalman filter in integration of navigation systems,” in *2015 16th IEEE International Symposium on Computational Intelligence and Informatics (CINTI)*, Budapest, Hungary, Nov. 2015, pp. 79–84, doi: 10.1109/CINTI.2015.7382898.

- [48] Mohd. A. Eleffendi and C. M. Johnson, "Application of Kalman Filter to Estimate Junction Temperature in IGBT Power Modules," *IEEE Transactions on Power Electronics*, vol. 31, no. 2, pp. 1576–1587, Feb. 2016, doi: 10.1109/TPEL.2015.2418711.
- [49] R. E. Kalman, "A New Approach to Linear Filtering and Prediction Problems," *Transactions of the ASME - Journal of Basic Engineering*, vol. 82, pp. 35–45, Mar. 1960.
- [50] C. F. Van Loan and N. Pitsianis, "Approximation with Kronecker Products," in *Linear Algebra for Large Scale and Real-Time Applications*, M. S. Moonen, G. H. Golub, and B. L. R. De Moor, Eds. Dordrecht: Springer Netherlands, 1993, pp. 293–314.
- [51] C. F. Van Loan, "Computing Integrals Involving the Matrix Exponential," *IEEE Transactions on Automatic Control*, vol. AC-23 (3), pp. 395–404, Jun. 1978.
- [52] M. S. Grewal and A. P. Andrews, *Kalman Filtering*. Somerset: Wiley, 2001.
- [53] M. T. Nasri and W. Kinsner, "Extended and unscented Kalman filters for the identification of uncertainties in a process," in *2013 IEEE 12th International Conference on Cognitive Informatics and Cognitive Computing*, New York, NY, USA, Jul. 2013, pp. 182–188, doi: 10.1109/ICCI-CC.2013.6622242.
- [54] J. McNames and M. Aboy, "Statistical Modeling of Cardiovascular Signals and Parameter Estimation Based on the Extended Kalman Filter," *IEEE Transactions on Biomedical Engineering*, vol. 55, no. 1, pp. 119–129, Jan. 2008, doi: 10.1109/TBME.2007.910648.
- [55] J. A. Burns, E. M. Cliff, and T. L. Herdman, "Parameter Estimation of a Thermal Fluid System," in *2018 Annual American Control Conference (ACC)*, Milwaukee, WI, Jun. 2018, pp. 122–127, doi: 10.23919/ACC.2018.8431435.
- [56] Frederick E. Daum, "Beyond Kalman filters: practical design of nonlinear filters," 1995, vol. 2561, pp. 2561–11, [Online]. Available: <https://doi.org/10.1117/12.217702>.
- [57] G. Anagnostou and B. C. Pal, "Derivative-Free Kalman Filtering Based Approaches to Dynamic State Estimation for Power Systems With Unknown Inputs," *IEEE Transactions on Power Systems*, vol. 33, no. 1, pp. 116–130, Jan. 2018, doi: 10.1109/TPWRS.2017.2663107.
- [58] A. R. Lyons, A. Gerry, K. A. Kramer, F. Vanderstiggel, and S. C. Stubberud, "Control of inverted pendulum system using a neural extended Kalman filter," in *2009 4th International Conference on Autonomous Robots and Agents*, Wellington, New Zealand, Feb. 2000, pp. 210–215, doi: 10.1109/ICARA.2000.4803978.
- [59] T. J. Vyncke, R. K. Boel, and J. A. A. Melkebeek, "On Extended Kalman Filters with augmented state vectors for the stator flux estimation in SPMSMs," in *2010 Twenty-Fifth Annual IEEE Applied Power Electronics Conference and Exposition (APEC)*, Palm Springs, CA, USA, Feb. 2010, pp. 1711–1718, doi: 10.1109/APEC.2010.5433462.

- [60] J. Li and G. Xia, “The application of an extended Kalman filter in the dynamic positioning system,” in *2016 12th International Conference on Natural Computation, Fuzzy Systems and Knowledge Discovery (ICNC-FSKD)*, Changsha, China, Aug. 2016, pp. 1945–1949, doi: 10.1109/FSKD.2016.7603477.
- [61] J. Adamy, *Nichtlineare Systeme und Regelungen*, 3. aktualisierte Auflage. Berlin: Springer Vieweg, 2018.
- [62] S. Romaniuk, L. Ambroziak, Z. Gosiewski, and P. Isto, “Real time localization system with Extended Kalman Filter for indoor applications,” in *2016 21st International Conference on Methods and Models in Automation and Robotics (MMAR)*, Miedzydroje, Poland, Aug. 2016, pp. 42–47, doi: 10.1109/MMAR.2016.7575085.

## THESES

- Fundamentals of minimally invasive surgery (MIS) and related procedures were investigated. Mathematical equations in theory for modelling process of MIS with the usage of medical therapy device DRP in flowing fluid were established. These are required concepts to develop methods of pressure control and estimation in the operation area.
- The process of the knee arthroscopy for rinsing fluid was modelled and simulated on MATLAB/Simulink. This is necessary in the stage of control design.
- While doing experiment on the real patient is not allowed in the stage of verification and evaluation, an alternative real-time device simulator of the knee arthroscopy process was constructed and implemented. A Hardware-in-the-Loop (HIL) Simulator was concreted with a physical interface and a software model for the realization of physiological states of the human body.
- Input/Output hardware interface module for the communication between the computerized programs and the actuators of the HIL-Simulator was also set up.
- The process of the knee arthroscopy was identified and linearized for controller design strategy. This is really helpful in pressure control during MIS. Due to the identified process, the PI controller was proposed to design based on symmetric optimum method (PI\_SO controller).
- Some possibilities of pressure disturbances from the knee flexions were considered to identify and simulate some effects of disturbance into the process. Those are useful information for supervisory algorithm integrated to the control strategy of the whole system.
- The problem of windup phenomenon in nonlinear process was solved with the anti-windup algorithm integrated in the PI\_SO controller. The designed controller was implemented successfully in the closed loop controlled system with a stable pressure in the operation area.
- Some different phase margin cases implemented in PI\_SO controller were analyzed to decide the optimal parameters for the controlled pressure stability in the knee model during arthroscopy.

- Cases of the knee flexion disturbances of the process were applied in supervision strategy integrated to the controller effectively. The supervisory algorithm for the elimination of the pressure disturbance can be applied with another separated PI\_SO controller integrated. However, with a small volume injected to the knee model as usual applied in the real patient, the pressure changes from angle knee actions response in a linear area (around or smaller 10ml/s). Therefore the simple empirical proportional controller was implemented for the elimination of pressure disturbance effectively.
- Another limitation that needs to be solved during MIS is how to get a feedback data for pressure control without using pressure sensor in the operational area. This solution is the implementation of the observer method. Three observer methods of Luenberger, basic Kalman filter, and extended Kalman filter (EKF) were implemented in pressure estimation for evaluating the quality of estimated pressure in the knee arthroscopy among methods.
- The whole controlled system working with the observers was established and simulated on MATLAB/ Simulink. The system was also executed in real-time with the HIL-simulator efficiently.
- During experiments in real-time simulator as well as in MATLAB/Simulink, the results in chapter 3 presented the stability of pressure control in the knee joint model within some disturbances. In addition, the results of pressure estimate in chapter 4 showed that the extended Kalman filter gave more accurate in estimated state than the other implemented observers in this research. Therefore, it would be better to choose the EKF instead of using pressure sensor at the operation area interconnecting to the closed loop controlled system. And the EKF worked effectively in this case. Those results in this thesis offered a contribution of pressure control and estimate in minimally invasive surgery.

## LIST OF PUBLICATIONS

1. **Van Muot Nguyen**, Eike Smolinski, Alexander Benkmann, Wolfgang Drewelow, Torsten Jeinsch; ***A Hardware-in-the-Loop Simulator Concept for the Minimally Invasive Surgery***; was presented and published on International workshop of Automation & Medicine (AUTOMED); ISBN 978 3 942100 441; Wismar 2016.
2. Eike Smolinski, Alexander Benkmann, Peter Westerhoff, **Muot Van Nguyen**, Wolfgang Drewelow, Torsten Jeinsch; ***A Hardware-In-The-Loop Simulator for the Development of Medical Therapy Devices***; was presented and published on 20th International Federation of Automatic Control World Congress, Toulouse - France, pp. 15050 - 15055, July 9–14, 2017.
3. **Van Muot Nguyen**, Torsten Jeinsch; ***Pressure Control in Minimally Invasive Surgery***; was presented and published on the 8th International Symposium on Automatic control (AUTSYM-2017); Wismar; September 21-22th, 2017.
4. **Nguyen, V.-M.**, Smolinski, E. C., Benkmann, A., Drewelow, W. Jeinsch, T.; ***An application of pressure estimation in minimally invasive surgery***; was presented and published on the Proceeding of the 4th International Conference on Green Technology and Sustainable Development (GTSD-2018); Ho Chi Minh city; November 23-24<sup>th</sup>, 2018; pp. 658 - 662; IEEE 2018.
5. **Nguyen, V.-M.**, Smolinski, E. C., Benkmann, A., Drewelow, W., Jeinsch, T.; ***An application of Extended Kalman Filter for pressure estimation in minimally invasive surgery***; was presented and published on the 10<sup>th</sup> International Conference on Applied Human Factors and Ergonomics (AHFE-2019) in Washington D.C.; July 24<sup>th</sup> - 28<sup>th</sup>, 2019; AISC 953, pp. 331-343, Springer Nature 2020.





## **BIOGRAPHY**

### **PERSONAL INFORMATION**

Full name: NGUYEN, VAN MUOT

Date of birth: January 05<sup>th</sup>, 1975

Place of birth: Dong Thap Province, Vietnam

Nationality: Vietnamese

Address: Khoa Cong nghe, Truong Dai hoc Can Tho.

Khu II, duong 3/2, P. Xuan Khanh, Q. Ninh Kieu, TP. Can Tho, Vietnam.

Telephone: +84 292 383 4267; Fax: +84 292 383 1151

E-mail: nguyenvanmuot@yahoo.com; nvmuot@ctu.edu.vn



### **EDUCATION**

1980 - 1992: Elementary, Secondary, and High school in Dong Thap province, Vietnam.

1993 - 1998: Bachelor degree in Electronics, College of Information Technology, Can Tho University, Vietnam.

2006 - 2009: Master degree in Automation Engineering, Electrical - Electronics Department, Ho Chi Minh City University of Transport, Vietnam.

2015 - 2019: Ph.D. candidate in Medical engineering and control at the Institute of Automation, Faculty of Computer Science and Electrical Engineering, University of Rostock, Germany.

### **PROFESSIONAL EXPERIENCES**

1998 - 2007: Teaching assistant at the Department of Telecommunication & Control Engineering, College of Information Technology, Can Tho University, Vietnam.

2009 - 2015: Lecturer at the Department of Automation Technology, College of Engineering Technology, Can Tho University, Vietnam.



## **DECLARATION**

I herewith declare that the dissertation for this submission of doctorate degree has been performed and written by my own work independently. The contents have no any of other resources or publications previously without the citations listed in references. The results in this thesis have been provided and organized by myself without any outside assistance. And I also state that I have not previously submitted any other doctoral dissertation at the University of Rostock nor at any other universities in Germany as well as in other nations.

Rostock, 19-Dec-2019

Van Muot Nguyen